THE TEMPORAL VARIATION OF VERTICAL MICROMETEOROLOGICAL PROFILES IN A LOWER MONTANE TROPICAL FOREST

A Thesis

by

RYAN S. ANDREWS

Submitted to the Office of Graduate and Professional Studies of
Texas A&M University
in partial fulfillment of the requirements for the degree of

MASTER OF SCIENCE

Chair of Committee,	Gretchen Miller
Committee Members,	Anthony Cahill
	Georgianne Moore
	Kevin McInnes
Head of Department,	Robin Autenrieth

May 2016

Major Subject: Civil Engineering

ABSTRACT

Earth system models recently began to implement a multilevel canopy modeling approach to represent vertical variation in biophysical and microclimate parameters. To inform such modeling efforts, this study seeks to characterize the variability and causal relationships between vertical sub-canopy profiles of meteorological variables in a tropical montane forest. Variability of CO_2 and H_2O concentrations, photosynthetically active radiation (PAR), leaf wetness percentage, temperature, and vapor pressure deficit was analyzed over a range of time scales using one year of continuously collected data. Seasonal, monthly, diurnal, and individual precipitation event time scales were all used to determine how patterns in vertical profile variability change with time scale. Additionally, consideration was given to trace gas transport mechanisms as eddy flux, vertical advection, and storage fluxes were used to determine diurnal average net transfers.

Variations in CO_2 concentration (382 and 372 μmol mol^{-1}) profiles between two months with similar PAR (64.0±1.5 and 60.9±1.7 μmol m^{-2} s^{-1}) suggest that plant stomata may limit water loss in the dry season despite continuous water availability. The maximum diurnal PAR value of 263 μmol m^{-2} s^{-1}, occurring at 10:00, indicates that slope aspect strongly influences the light regime in a montane forest sub-canopy. Rainfall and subsequent leaf wetness were also shown to affect most micrometeorological processes at the site, such as causing an increase in CO_2 concentration (3.35 μmol mol^{-1} mean increase) with canopy wetting. These results indicate that significant error in modeled

precipitation, even at sub-daily time steps, could change magnitude and direction of trace gas movements. The data presented should be a valuable tool for validation of existing multilevel canopy models and aid in development of future model improvements.

ACKNOWLEDGEMENTS

I would like to thank my committee chair, Dr. Gretchen Miller, and my committee members, Dr. Anthony Cahill, Dr. Georgianne Moore, and Dr. Kevin McInnes, for their guidance and support throughout the course of this research.

Thanks also go to Dr. Eugenio Gonzalez and the rest of the staff at the Soltis Center for Research and Education for providing logistics and support on our field campaigns. I also want to extend my gratitude to the Office of Science (BER) U.S. Department of Energy (DE-FOA-0000749) for funding this research.

Finally, thanks to my wife Bethany for showing me patience and grace throughout the course of this work.

NOMENCLATURE

CO_2	Carbon dioxide
LE	Latent energy
ET	Evapotranspiration
VPD	Vapor pressure deficit
EC	Eddy covariance
PAR	Photosynthetically active radiation
H_2O	Water vapor
e^*	Saturation vapor pressure
T	Ambient air temperature
e_a	Ambient vapor pressure
T_{st}	Steam-point temperature
e_{st}^*	Vapor pressure at the steam-point temperature
χ_v	Mole fraction of water vapor
P_a	Ambient air pressure
LAI	Leaf area index
Adv	Vertical advection (+ indicates transport away from ground)
V_a	Molar volume of dry air
w	Vertical wind speed
h	Specifies the height of the top of the control volume
c	Dry mole fraction of CO_2

z	Variable height in the sub-canopy from ground
S_c	Carbon dioxide storage flux (+ flux indicates CO_2 added to air)
t	Time
Q_a	Sensible heat storage flux (+ flux indicates temperature rise)
ρ	Air density
C_p	Specific heat of air
Q_w	Latent energy storage flux (+ flux indicates H_2O added to air)
Γ	Psychrometric constant
u	Horizontal wind speed
met	Specifies an instrument located on the meteorological tower
σ	Standard deviation
CLM	Community Land Model

TABLE OF CONTENTS

Page

LIST OF FIGURES

Page

LIST OF TABLES

Page

CHAPTER I

INTRODUCTION AND REVIEW OF LITERATURE

1.1 Overview

Studying ecosystem-climate interactions in tall, dense forest ecosystems is complex because of meteorological variation that exists from canopy top to forest floor. Vertical profiles of micrometeorological variables taken inside the canopies of such forests can give invaluable information about these ecosystems (Kumagai et al., 2001). Variable microclimate exists in tall forests because successive layers of vegetation restrict transmission of energy and light from the sun, as well as controlling interception of precipitation and the flow dynamics of wind. At the stand scale, the variation of these and other related micrometeorological variables within a forest canopy can have a profound effect on transport of trace gases through processes such as transpiration (Ohkubo et al., 2008; Roberts et al., 1993). Researchers of meteorology and climate are very interested in furthering the understanding of trace gas exchange between biosphere and atmosphere because of the sharp rise in atmospheric carbon dioxide over the last 150 years. The scientific community derives much of its understanding of and future predictions of global climate through modeling efforts (Bonan, 2008). To improve such models, it is necessary to understand how ecosystem gas exchange varies across different biome types and how the meteorological and physiological factors of these biomes cause the gas exchange variations.

Of the various forest biome types, tropical forests warrant additional research because they are studied relatively infrequently and play such a significant role in the global exchange of carbon and water. Tropical forests also vary in terms of tree species composition, elevation, and rainfall, presenting a need to study many different types of tropical forests. Many of these forest types feature a canopy structure and height such that vertical profiles of micrometeorological variables could help to enhance our understanding of the relationship between microclimate and plant physiology. As such, we seek to characterize the degree to which tropical forest sub-canopy microclimate variability affects ecosystem gas exchange. The remainder of this chapter will cover gas exchange between the biosphere and the atmosphere, micrometeorological variables that enhance our understanding of observed gas exchange patterns, analytical models that predict micrometeorological gradients in forests, and a description of the study site for this project. The second chapter is a manuscript focusing on variability and relationships between vertical sub-canopy profiles of micrometeorological variables, while the third and final chapter will cover conclusions and recommendations for future work.

1.2 Trace Gas Fluxes

Due in large part to human activities, atmospheric carbon dioxide has risen substantially over the last 150 years. Because of this increase and its link to rising global temperatures, efforts in the scientific community to better understand and quantify carbon dioxide transport between the biosphere and atmosphere have also increased dramatically. It was this effort to better understand carbon fluxes that led to the creation of FLUXNET, a worldwide network of towers that measure CO_2 fluxes, as well as other

fluxes and meteorological variables (Baldocchi et al., 2001). This network allows for the exchange of CO_2 to be monitored and quantified across different biomes, climates, and time scales. The role of plants in the larger scheme of carbon flux exchange is unique because they both take in CO_2 through photosynthesis and release CO_2 through respiration.

In addition to measuring fluxes of CO_2, FLUXNET sites typically also measure the exchange of water vapor and sensible heat, in the form of an energy balance. While sensible heat is an expression to represent the flow of energy needed to change the temperature of air in the biosphere, water vapor fluxes can also be represented by the latent energy (LE) flux. The available energy in an ecosystem is the net radiation it receives from the sun, minus losses into the soil, and can be used for sensible or latent heat fluxes. All of these different types of fluxes are controlled by myriad meteorological and biophysical factors and processes. Because the relationships between these factors and fluxes is highly variable across different ecosystems, it is important to have studies range a multitude of biome types and geographic locations to get a clear picture of global sums and trends in biosphere to atmosphere flux exchange. By studying natural ecosystem processes over a range of biome types, models can be generated and calibrated to represent these processes correctly for each biome.

Tropical forests play an important role in the earth's gas exchange scheme as they have a remarkable ability to store carbon. They are currently estimated to contain 25% of the carbon in the terrestrial biosphere (Bonan, 2008). With rising levels of atmospheric carbon dioxide, these forests could also potentially mitigate the warming of

the earth's climate by providing high levels of evaporative cooling (Bonan, 2008). Furthermore, tropical forests are responsible for 34% of global gross primary production, which is both the highest percentage and largest amount per unit area of any biome type (Beer et al., 2010). Fluxes of water vapor from tropical forests are also noteworthy, as tropical forests are the leading contributor of LE fluxes to the atmosphere (Choudhury et al., 1998; Zhang et al., 2010). These large fluxes of water between tropical forests and the atmosphere impact both the global water cycle (Werth and Avissar, 2004) and global atmospheric circulation patterns (Numaguti, 1993).

1.3 Transpiration and Evapotranspiration

To more fully understand ecosystem scale fluxes of water vapor from the land surface, it is necessary to understand the processes that cause evaporation and transpiration, the vaporization of liquid water from free surfaces and from vegetation respectively. Over the land surface the two are most tractably estimated as one quantity, termed evapotranspiration (ET), that is the sum of evaporation and transpiration. To understand each individual process better, ET measurements need to be partitioned into evaporation and transpiration using either supplementary measurements or analytical estimates. Partitioning ET is especially important considering the relationship between ET fluxes and carbon dioxide intake. The two are related through plant water use efficiency, the ratio of the rate of CO_2 assimilation to the transpiration rate. However, when water evaporates off the free surface of a leaf, there is no associated carbon flux as the stomata remain closed. Where vegetation exists it can also be helpful to further partition evaporation into evaporation from soil and that from rainfall intercepted by the

canopy. In tropical forests this further partitioning of evaporation can be important as dense canopies and frequent rainfall cause relatively high values of interception evaporation (Kang et al., 2012).

Tropical forests are also unique in the variables that drive ET. In these ecosystems, ET is largely independent of precipitation as trees rarely experience soil moisture deficits (Juárez et al., 2007). This phenomenon does not occur in most other ecosystem types, where precipitation and ET are tightly coupled (Porporato et al., 2002). Many studies have concluded that net radiation is the primary driver of ET in tropical forests (e.g. Fisher et al., 2009; Hasler and Avissar, 2007; Juárez et al., 2007; Loescher et al., 2005). Additionally, vapor pressure deficit (VPD) was commonly found to be a secondary driver of ET in tropical forests (e.g. Fisher et al., 2009; Juárez et al., 2007; cf. Loescher et al., 2005). Furthermore, Giambelluca et al. (2009) found that tropical forest ET is strongly correlated with the wetness of the canopy. In contrast, VPD tends to be the strongest driver of ET in most other ecosystem types (Hogg et al., 1997).

Modeling studies that have been done using flux data illustrate the overall lack of tropical field data that is available. Zhang et al. (2010) used data from 82 different FLUXNET sites to parameterize and validate a model of global ET. Only four of the 82 sites used were located at tropical latitudes, and only two of these were tropical forest sites. Because of the significance of tropical forests to global ET, and the variation that exists between different types of tropical forests, more tropical field site datasets are needed to allow for increased representation in such studies. Fisher et al. (2008) also did a study on global fluxes of ET across different types of ecosystems. They found that

their modeled and observed fluxes were very well correlated for all sites except for the single tropical rainforest site examined.

There are a number of techniques available to estimate transpiration and ET. The eddy covariance (EC) method can estimate fluxes of CO_2, sensible heat, and LE flux. This method uses a fast response 3-D anemometer to measure wind speeds and an infrared gas analyzer to compute trace gas concentrations. The covariance of the gas concentration (or sonic temperature in the case of sensible heat) with the vertical wind velocity component gives the flux value. This method is computationally intensive, but is widely considered to provide the best estimate of flux exchange at the ecosystem scale (Baldocchi et al., 2001; Wilson et al., 2002). As such, it is the method employed by FLUXNET tower sites (Baldocchi et al., 2001). The EC method was initially developed for ideal conditions, including homogeneous canopy structure, flat terrain, and steady values of measured variables such as wind, temperature and gas concentrations (Baldocchi, 2003). To estimate fluxes in areas where these conditions do not hold, it can be helpful to employ a variety of methods to estimate ET or transpiration.

The sap flux method is another commonly used technique to measure fluxes of water on an ecosystem scale. This method involves estimating the rate of sap flow in individual trees, and then scaling those values to estimate transpiration for the forest stand. One of the techniques commonly used to employ the sap flux method is the heat dissipation method (Granier, 1987). This method involves two needles inserted into a tree and separated by about 40 mm (Allen et al., 2011), one of which provides a constant heat source. Convective transport of the heat along the sap flow path causes a

temperature gradient between the two needles. This temperature gradient is measured and used in empirical equations (Granier, 1987) to estimate sap flux density (Allen et al., 2011). Even with accurate measurements of sap flux density from many trees in a study plot, several researchers have noted the difficulty of scaling up these measurements to accurate estimations of stand scale transpiration. Various ages and species of trees within a forest stand (Williams et al., 2004; Wilson et al., 2001) and variations in incident radiation and aerodynamic turbulence present at different levels in the canopy (Allen et al., 2011) were both cited as reasons that scaling up to transpiration can be challenging. To overcome some of these challenges, it is crucial to select trees in the study plot that are a representative sample of the larger forest stand (Smith and Allen, 1996).

Sap flux measurements have often been used to complement EC estimates (e.g. Hogg et al., 1997) by giving an independent estimate of transpiration. These measurements can provide an estimate of nighttime transpiration (e.g. Fisher et al., 2007; Moore et al., 2008), allowing them to make up for the EC method's weakness in estimating turbulent fluxes under stable conditions. In addition to providing a check on EC measurements, sap flux measurements also allow for ET to be partitioned into evaporation and transpiration.

1.4 Introduction to In-Canopy Micrometeorology

As climate models have become more refined, researchers have begun to give more consideration of vertical heterogeneity of micrometeorological variables within forest canopies (e.g., Bonan et al., 2012; Drewry et al., 2010; Flerchinger et al., 2015; Pyles et al., 2000; Staudt et al., 2011). The benefits of such an approach can be

illustrated by the example of canopy light exposure modeling in the Community Land Model (Bonan et al., 2012). They show that using a two leaf approach to modeling canopy light exposure has led to disagreement between modeled and measured flux data because of a failure to adequately resolve photosynthetic traits of leaves with canopy height. A multi-layer model of canopy light absorption at different levels within the canopy yielded modeled gross primary production that were an improvement over the two leaf model. Furthermore, Bonan et al. (2012) concluded that field measurements of within-canopy profiles of photosynthetic capacity would provide important information to further refine such models. Because fluxes of carbon and water depend on many micrometeorological variables, within-canopy vertical profiles of several of these variables could lead to important insights about how forest microclimate impacts canopy gas exchange.

This type of research is particularly needed in tropical forests as vertical profiles of meteorological variables are relatively sparse. In a review of tropical forest's response to changing climatic conditions, Clark (2007) concluded that more comprehensive datasets of environmental variables were needed at tropical forest research sites and that a better understanding of sensitivities of plant processes to atmospheric factors at the stand scale was needed. Furthermore, Motzer (2005) concludes that the microclimate in tropical montane forests is significantly different from the microclimate in tropical lowland forests, so studies are needed in both.

Although work on tropical forest micrometeorology has been done in the past, this work largely has either been for short time scales spanning a few days or weeks (e.g.

Kumagai et al., 2001; Roberts et al., 1993; Yasuda et al., 2003), or the focus has been on single leaf scale physiology (Kenzo et al., 2015; Kosugi et al., 2012; Lloyd et al., 2010). Other studies have considered vertical profiles of single variables or just a few variables in tropical forests. Motzer (2005) studied vertical profiles within and above a tropical forest canopy of photosynthetically active radiation (PAR), temperature, humidity, and wind, but did not compare these observations to any flux measurements. Dietz et al. (2007) did an in-depth study on leaf wetness variation with canopy height and Ohkubo et al. (2008) looked at CO_2, H_2O, and air temperature profiles over several years to estimate storage fluxes. Aparecido et al. (in review) found that canopy wetness altered the correlation between sap flux and VPD, as well as that between sap flux and PAR. The following sections will outline the variables measured in this study in an attempt to have a long-term, comprehensive micrometeorological dataset, with emphasis on possible implications on fluxes and modeling efforts.

1.5 Fundamental Scalars: Temperature, CO_2, and Water Vapor

Scalar values of temperature, carbon dioxide, and water vapor are the some of the most fundamentally important variables in micrometeorology as changes in these variables represent transfers of mass and energy that are the primary outputs of flux network measurements and land surface modeling schemes. Vertical profiles of temperature are found in the literature for a soybean canopy (Baldocchi, 1992), temperate forests (e.g., Lee and Black, 1993; Shuttleworth et al., 1989; Webb, 1970), boreal forest (Mahrt et al., 2000), and tropical forest (Shuttleworth et al., 1989). Vertical profiles of CO_2 have been reported for a soybean canopy (Baldocchi, 1992), alfalfa and

corn canopies (Buchmann and Ehleringer, 1998), modeling studies (e.g., Katul et al., 1997; Lai et al., 2000), in a boreal forest (Baldocchi et al., 1997), a tropical forest (Ohkubo et al., 2008), and in many temperate forests (e.g., Katul et al., 1997; Katul and Chang, 1999; Lai et al., 2000). Vertical profiles of water vapor or humidity are less common in the literature, but have been given by Xiao et al. (2006) for a maize crop and Shuttleworth et al. (1989) for temperate and tropical forest types.

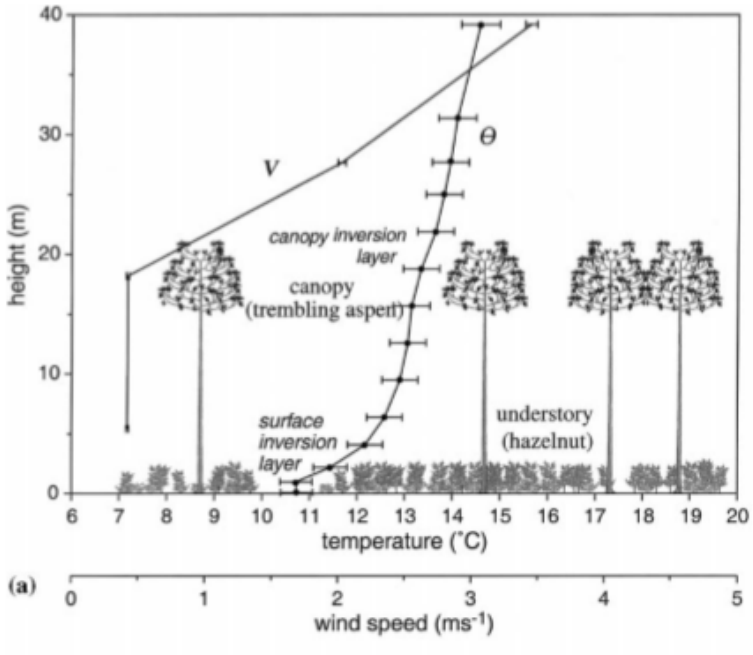

Figure 1: Nocturnal vertical variation of wind speed (V) and potential temperature (θ) in and above a boreal forest canopy, from Mahrt et al., 2000.

Profiles of temperature tend to generally increase with height in the canopy and experience the sharpest gradients near the ground where the air is least mixed. The profiles of temperature in Figure 1 and the daytime of Figure 2 are a typical shape for forests, although variations in shape can occur in different climates. This can be seen by

comparing the Figure 1 boreal nighttime temperature profile to the nighttime tropical temperature profile in Figure 2. CO_2 profiles like those shown in Figure 3 for corn are typical of many canopy types. Most notable for this profile is the sharp gradient that exists near the ground where soil respiration causes increased CO_2 concentrations. At heights near the top of the canopy, the CO_2 profile may remain vertical as with the corn profile, or may begin to increase again slightly as with the alfalfa profile (Figure 3). The plots of Shuttleworth et al. (1989) (Figure 2) show how water vapor concentration typically decreases with height in a tropical forest canopy, though this effect is more prominent in the daytime.

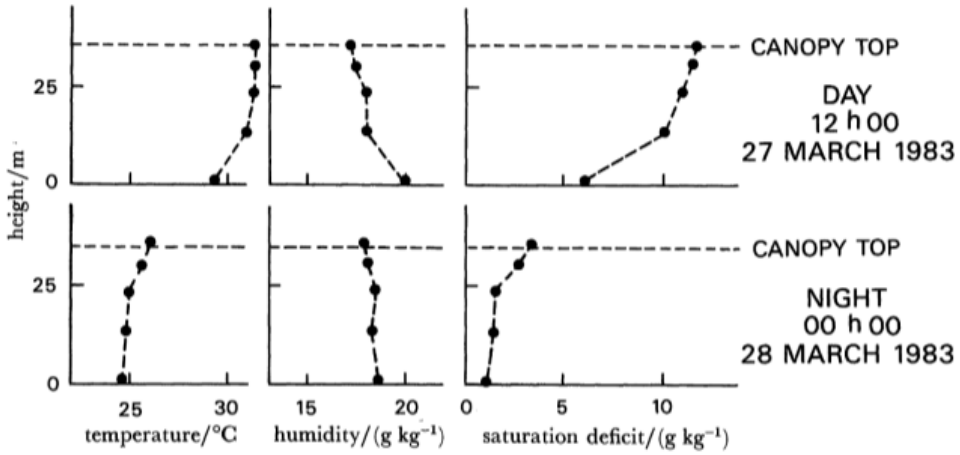

Figure 2: Vertical variation of air temperature, atmospheric specific humidity, and water vapor saturation deficit with height in the sub-canopy of a tropical rain forest in the middle of the day and the middle of the night, from Shuttleworth et al., 1989.

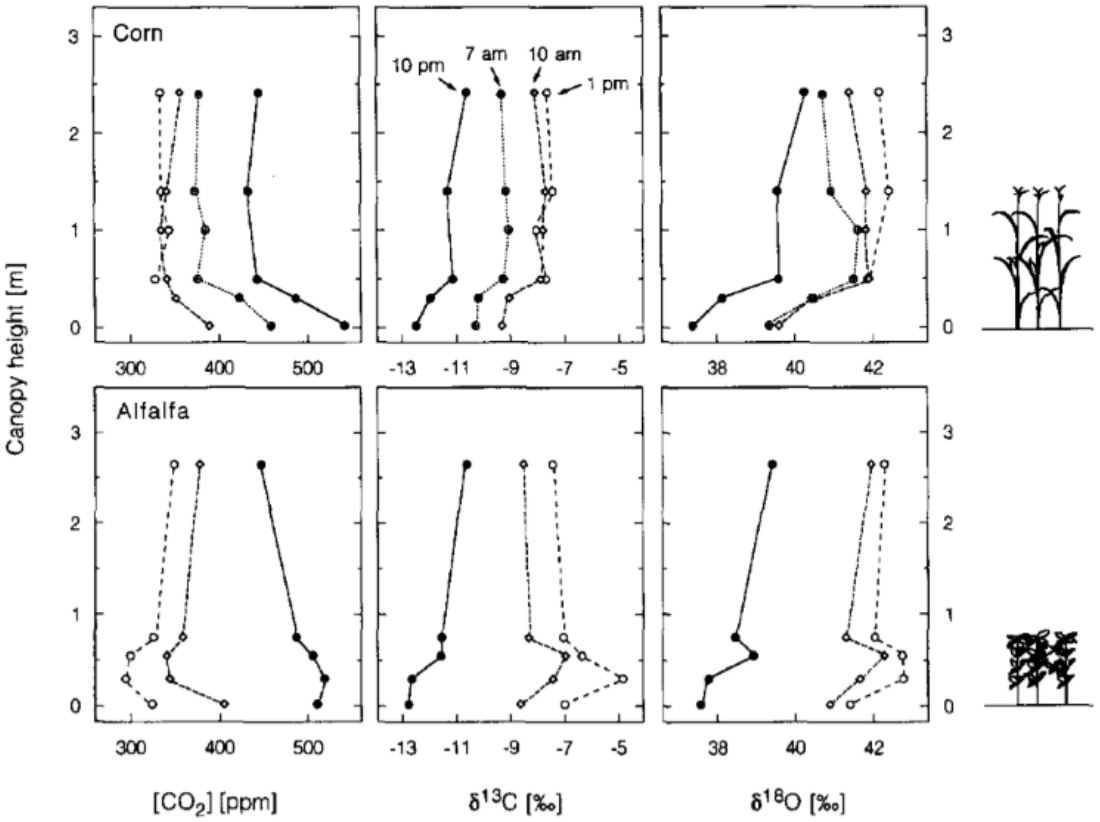

Figure 3: Vertical variation of CO_2 concentration, $\delta^{13}C$, and $\delta^{18}O$ of canopy air with height in and above canopies of corn and alfalfa for several different times of day, from Buchmann and Ehleringer, 1998.

1.6 Wind

Wind is a critically important component of micrometeorology as turbulent and advective movement of air acts as a major transport mechanism for other important variables such as CO_2. Vertical profiles of horizontal wind speed are particularly important because wind facilitates the transfer of heat and water between vegetation and the air and because wind magnitude varies significantly with height. The ground acts as a boundary layer to wind flows causing wind velocity to generally increase as distance from the ground increases. The presence of trees or other obstructions acts as a

roughness layer, impeding fluid flow, which creates variable and complex vertical profiles of wind. Many studies have sought to quantify the vertical variation in horizontal wind speed and have spanned wind tunnel studies using various roughness elements (e.g., Brunet et al., 1994; Macdonald, 2000), modeled flow regimes in and above vegetated canopies (e.g., Shaw and Schumann, 1992; Shen and Leclerc, 1997; Wang and Yi, 2012), and flow studies in various forest types (e.g., Daikoku et al., 2007; Lee and Black, 1993; Mahrt et al., 2000; Oliver, 1971; Webb, 1970). The review of Raupach et al. (1996) shows that all vertical profiles of wind tend to take a similar shape regardless of canopy type (Figure 4). The modeled vertical profile of Shaw and Schumann (1992) (Figure 5) shows more specifically what the typical forest canopy flow looks like, showing an increase in wind speed as height increases from the ground to the trunkspace. As height continues to increase, there is a slight decrease in wind as the lower part of the canopy is reached before a sharp increase that continues through the top of the canopy and into the roughness sublayer above the canopy. A wind decrease from trunkspace to the lower part of the midstory is especially pronounced in tropical forests (Figure 6), where forest canopies tend to be farther away from the ground than in other forest types. In addition to canopy type, factors such as time of day (Mahrt et al., 2000), wind direction (Daikoku et al., 2007), and spatial location on a hill (Wang and Yi, 2012) can all affect wind profile shapes.

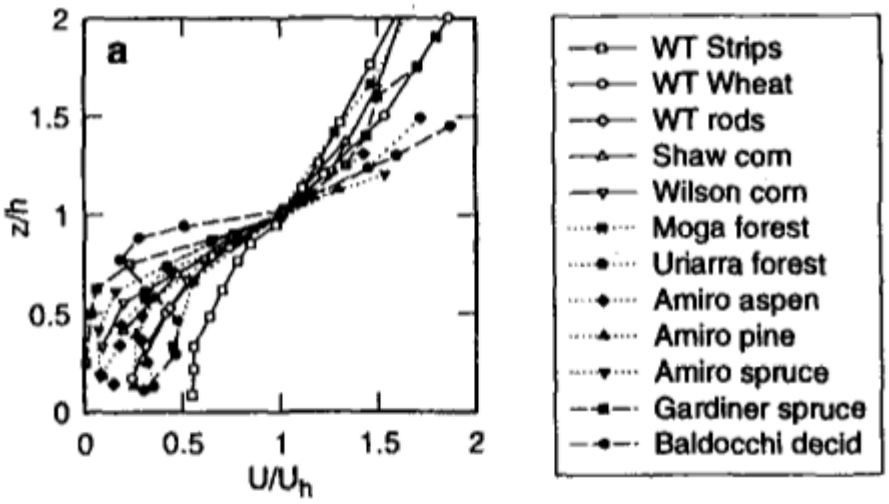

Figure 4: Vertical variation of normalized horizontal wind speed with normalized height in and above a vegetated canopy for many different measured and modeled canopy types, modified from Raupach et al., 1996.

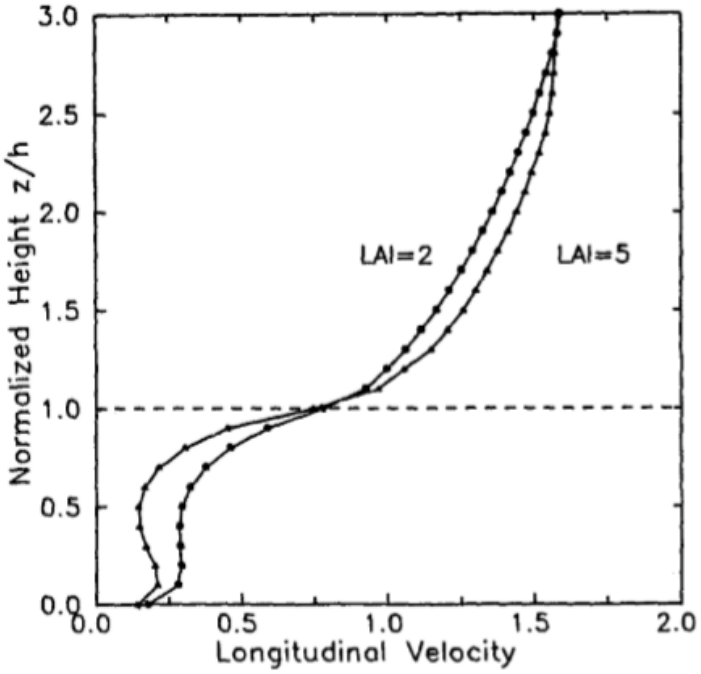

Figure 5: Modeled vertical variation of horizontal wind speed with normalized height in and above a vegetated canopy for two different values of LAI under weakly unstable conditions, from Shaw and Schumann, 1992.

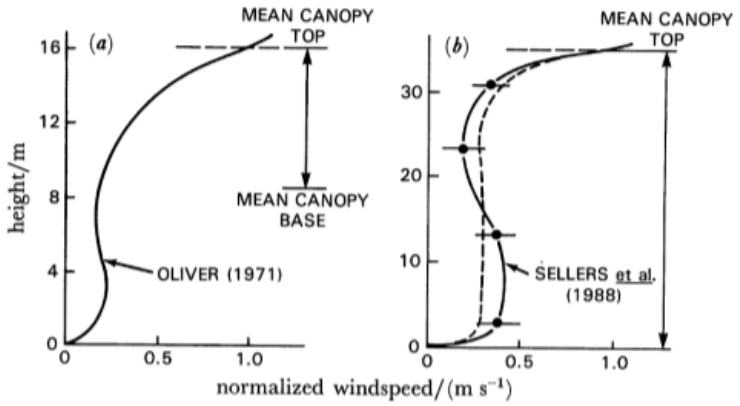

Figure 6: Vertical variation of normalized horizontal wind speed with height in the sub-canopy at a) temperate forest of Scots pine and b) tropical rain forest sites, from Shuttleworth et al., 1989.

1.7 Vapor Pressure Deficit

Vapor pressure deficit (VPD), a useful expression of moisture content of the air in pressure terms, is tightly linked to fluxes of water vapor and the processes that cause them. VPD is the difference between the actual vapor pressure of the air, and the saturation vapor pressure at the current air temperature. As such, VPD is strongly correlated to air temperature. High values of VPD indicate a low relative humidity and will cause high values of transpiration in plants assuming that they have adequate access to water in the soil. The opposite case of low VPD, which is more common in tropical forests, is characterized by high relative humidity and lower rates of transpiration. Because the variability in temperature and VPD is relatively small in tropical forests, available energy plays a larger role in tropical forests than it does in other biome types. Vertical profiles of VPD or vapor pressure in the literature (Baldocchi, 1992; Motzer, 2005; Shuttleworth et al., 1989) show that VPD increases with height from the ground and that the profiles change significantly with time of day (Motzer, 2005; Shuttleworth

et al., 1989) (Figure 2) and with cloud cover (Baldocchi, 1992). It should be noted that VPD profiles show a strong resemblance to temperature profiles (Motzer, 2005; Shuttleworth et al., 1989) (Figure 2).

VPD is not directly measured, but instead depends on measurements of air temperature, air pressure, and moisture content of the air. The first term in the VPD difference (Equation 1), saturation vapor pressure, is solely a function of air temperature, and is calculated from the Goff–Gratch formulation following List (1971):

1. $$VPD = e^*(T) - e_a$$

2. $$\log e^*(T) =$$

$$-7.90298\left(\frac{T_{st}}{T}-1\right)+5.02808\log\left(\frac{T_{st}}{T}\right)-1.3816\times10^{-7}\left(10^{11.344(1-T/T_{st})}-1\right)+$$

$$8.1328\times10^{-3}\left(10^{-3.19149(T_{st}/T-1)}-1\right)+\log e^*_{st}$$

where e^* is the saturation vapor pressure (kPa), T is ambient air temperature (K), e_a is actual vapor pressure (kPa), T_{st} is the steam-point temperature of 373.16 K, and e_{st}^* is the saturation vapor pressure at the steam-point temperature, 101.325 kPa. The actual vapor pressure is then calculated by multiplying the mole fraction of the water vapor in the air by the air pressure (Equation 3). The actual vapor pressure, e_a, is computed as:

3. $$e_a = \chi_v P_a$$

where χ_v is the mole fraction of H_2O (mol mol^{-1}) and P_a is the atmospheric pressure (kPa).

1.8 Canopy Wetness

It is important to consider the wetness state of the canopy in a tropical land surface study as canopy wetness will determine how ET is partitioned (Chu et al., 2014).

When the canopy is wet, evaporation of intercepted rainfall is the dominant ET process, while dry canopy ET is dominated by transpiration. Since transpiration indicates open plant stomata and subsequent fluxes of carbon dioxide, incorrect understanding and representation of canopy wetness and drying out processes could lead to poor representation in modeled carbon exchange between forest and atmosphere. Properly representing canopy wetness and its effects on gas exchange will require consideration of the transient processes of wetting and drying. As the canopy transitions from wet to dry after a period of precipitation, there will be a time when the canopy is only partially wet, as drying times vary with height in the canopy (Kang et al., 2012). Because of this, we will examine micrometeorological drivers and their interactions with trace gas fluxes at varying stages in the canopy wetting and drying processes.

To measure a vertical profile of canopy wetness, dielectric leaf wetness sensors can be installed at various heights within the canopy. Since the dielectric constants of water and air are more than an order of magnitude different, a millivolt output from the sensor will vary in magnitude based on the amount of water present on the sensor surface. The leaf wetness sensor manual (Decagon Devices, Pullman, Washington) recommends interpretation of these millivolt signals by establishing a Boolean threshold to determine times at which the sensor is either wet or not wet. From these binary designations, duration of leaf wetness can also be determined. Leaf wetness duration could potentially prove to be a significant contributor towards lower canopy flux values as long leaf wetness durations have been reported in tropical forest lower canopies. Kang et al. (2012) studied canopy wetness in nearby coniferous and deciduous forest sites in

South Korea and reported a mean drying time of 5 hours at the bottom of the canopy, with 10% of drying times exceeding 16 hours. Dietz et al. (2007) studied canopy wetness in an old-growth lower montane tropical forest with a closed canopy and reported maximum drying times as high as 22 hours in the lower canopy. Because of these variable drying times, it is expected that a vertical profile of leaf wetness would show decreasing average wetness with increasing height from the ground.

1.9 Radiation and Light Inputs from the Sun

A key factor in the drying times of wet leaves, as well as other important ecosystem functions, is the input of light and energy provided by the sun. Incoming radiation from the sun is often split into a longwave, or infrared component, and a shortwave component that includes visible, ultraviolet, and near-infrared light. These components are measured separately and interact differently with the vegetation they contact. Since incoming radiation can be absorbed, reflected, or transmitted, and all ecosystem matter emits radiation, it is important to consider both incoming and outgoing radiation from an ecosystem. The measurement of net radiation fulfills this purpose as it measures the incoming short and longwave radiation minus the outgoing short and longwave radiation. Thus, net radiation is often used synonymously with the term available energy. This available energy in an ecosystem can be used in four primary ways: to accomplish phase changes from liquid water to water vapor in a LE flux, to raise the temperature of the air as a sensible heat flux, to raise the temperature of biomass, or to raise the temperature of the soil as a ground heat flux. Available energy can also be negative which will result in the cooling of air and soil temperatures.

PAR is a particularly important solar input to the ecosystem because it only considers light that is useful for plant photosynthesis. PAR is most commonly defined as a measure of photon flux density, or the quantity of photons incident on a surface over a given time interval (McCree, 1981). The photon flux density considered in a measure of PAR is also limited by the wavelength of the light, and only considers wavelengths from 400 to 700 nm, roughly the same as the visible light spectrum. These wavelengths are included because the amount of photosynthetic activity that occurs per quanta of light received drops off sharply as these limits are approached (McCree, 1981). Motzer (2005) measured a within-canopy PAR profile in a tropical montane forest and found that the data was useful in calibrating the transmissivity of the HemiView solar model for their site, used to calculate the leaf area index from photographs. Dang et al. (1997) also measured profiles of PAR at five different boreal forest sites, showing that PAR profiles generally have a concave down pattern as they increase with height from the ground (Figure 7). It is also known that PAR correlates well to sap flux at our own study site (Aparecido et al., in review). Comparison of in-canopy profiles of PAR at the field site to light extinction models will be a valuable tool in refining and validating these models for tropical forests.

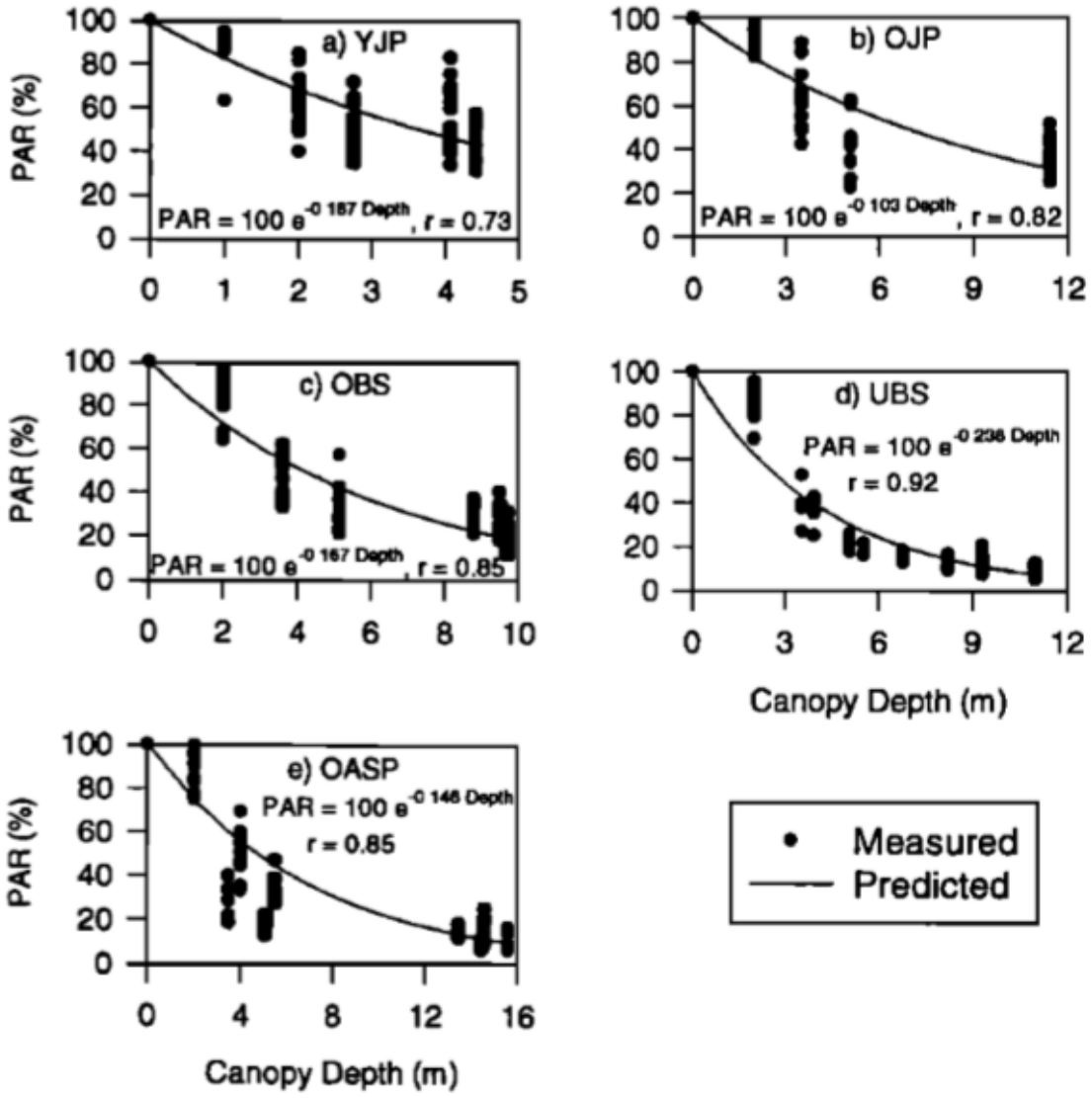

Figure 7: Vertical variation of photosynthetically active radiation (PAR) with height in the sub-canopy at five different boreal forest types, from Dang et al., 1997.

Closely related to PAR is another measurement commonly used to characterize canopy structure and how it relates to meteorological phenomena, leaf area index (LAI). LAI is a measure of leaf area per unit ground area, and gives information about how thick the canopy is on average. Several methods exist for estimating LAI, such as using

MODIS imagery (Myneni et al., 2002), or hemispherical photos and image processing techniques. Jonckheere et al. (2004) provides a thorough overview of commonly used methods to calculate LAI. Asner et al. (2003) notes that LAI data are an important input to terrestrial ecosystem and land-surface models. LAI data can be used to model various processes such as light penetration into the canopy or rainfall interception. LAI values may also provide information about how ET is partitioned in tropical forests. Giambelluca et al. (2009) found that the seasonal fraction of available energy used for ET was correlated to seasonal trends in LAI.

1.10 Field Site Description

All field data for this research has been collected at Texas A&M University's Soltis Center for Research and Education. The Soltis Center is located in San Isidro de Peñas Blancas, Costa Rica (10° 22' 55" N, 84° 37' 15" W), on the Caribbean slope of the Cordillera Tilarán, and has been in operation since 2009. The center contains 250 hectares of forested area. With elevations ranging from 400 – 715 m above sea level, this area would best be classified as a *lower montane forest*, in the transitional zone between *lowland rainforest* and *lower montane cloud forest* (Scatena et al., 2010). Due to selective logging in the area, which began in the 1950s and ended in the mid-1990s, the area consists of both primary and secondary forest. The study plot where the majority of the project field data was collected is located in a densely forested area that lies on a steep slope. The canopy top is at a height of approximately 28 m, with emergent trees extending up to 42 m above the ground surface. The in-canopy walk-up tower that contains much of the field site instrumentation is 39 m tall, and features a 10

m extension that can support limited instrumentation up above the emergent tree adjacent to the tower.

A meteorological station is located in a clearing just outside the forest and has been collecting data since the summer of 2010. This station measures precipitation, humidity and temperature at 3 and 10 m, incident solar radiation, air pressure, and wind speed. Mean monthly air temperatures for the site range between 20 – 25 °C with the warmest temperatures occurring in May and June, and the coolest occurring in December. Mean annual precipitation reaches nearly 4,200 mm, with a wet season lasting from May through December and a dry season from January through April. Prevailing winds at the site are primarily from the north with no significant contribution from other directions.

Due to differences in latitude and elevation, different tropical forests are exposed to different seasonal weather patterns and exhibit varying ecohydrologic responses as a result (e.g. Hasler and Avissar, 2007). For example, some tropical forests have short dry seasons of three months, while others have relatively intense dry seasons that can last up to six months (Juárez et al., 2007). Lowland rainforests regularly experience prolonged dry periods while cloud forests, located in mountainous regions, rarely dry out due to frequent cloud cover. Costa Rica represents a diverse range of tropical forest studies, as it is home to two other research sites that collect or have collected micrometeorological measurements. The Monteverde site (http://www.monteverde-institute.org/), located at an elevation of 1,440 m, represents the *cloud forest* ecosystem type. The La Selva research station (http://www.ots.ac.cr/) is located at an elevation of 103 m, and is

representative of the *lowland rainforest* type. A transitional forest classification, termed a *lower montane tropical forest*, exists at intermediate elevations between lowland rainforests and tropical montane cloud forests (Scatena et al., 2010) and is most applicable to our site. Lower montane tropical forests such as the site used in this study frequently transition from wet to dry states, and present an ecosystem type that is both more representative of a wider range of tropical forest types, and ideal to study such wetting and drying transitions.

1.11 Study Period

Monthly averaged weather data for the site has been collected continually since 2010 at the meteorological tower just outside the forest. Data from instruments on the in-canopy walk-up tower and from surrounding sap flux and soil instrumentation spans from August 2014 through the end of 2015. When directly comparing dry season to wet season results, the 2014 data will be excluded so that there is one dry season and one wet season being considered. Measurements made by the AP200 gas profile system (Campbell Scientific, Logan, UT) were taken on thirty minute averaging intervals while sap flux data was taken on ten minute averaging intervals. All other measurements were taken at five minute averaging intervals except where otherwise indicated. For a more thorough discussion of project methodology, see the Methods section of Chapter 2.

CHAPTER II

MANUSCRIPT

2.1 Introduction

Vertical profiles of meteorological variables taken within the canopies of dense, tall forests provide a deeper understanding of the physiological responses to climate in these forest ecosystems (Kumagai et al., 2001). A variable microclimate exists in tall forests because successive layers of vegetation restrict transmission of solar energy and throughfall of precipitation to lower heights within the forest stand. This vertical heterogeneity of meteorological variables has a profound impact on the functioning of the ecosystem as a whole because water and energy availability affect the physiological processes that drive gas exchange between ecosystems and the atmosphere. Unfortunately, stand scale vertical variation in tropical forest microclimate is seldom studied, despite their importance in global gas exchange scheme, providing carbon storage that could potentially mitigate warming of the earth's climate (Bonan, 2008).

Recent studies that have been done in tropical forest micrometeorology tend to either focus on leaf scale physiology (Kenzo et al., 2015; Kosugi et al., 2012; Lloyd et al., 2010) or cover short time scales such that temporal variations cannot be assessed in depth (e.g., Kumagai et al., 2001; Roberts et al., 1993; Yasuda et al., 2003). Other studies have considered vertical profiles of just a few variables in tropical forests for a specific purpose, such as Ohkubo et al. (2008), whose study looked at storage fluxes and Motzer (2005), who characterized spatio-temporal patterns of wind and light.

Some studies hint that canopy wetness should be considered a key micrometeorological variable in wet, tropical forest ecosystems. Leaf wetness fundamentally alters the processes of transpiration and photosynthesis that drive ecosystem gas exchange because a wet leaf surface can cause plant stomata to remain closed. Since tropical forest canopies are frequently wet, leaf wetness has been identified both as a variable that is strongly correlated to evapotranspiration (ET) (Giambelluca et al., 2009) and as a variable that will determine how ET is partitioned (Chu et al., 2014). However, consideration of leaf wetness and its relation to physiological processes in the forest sub-canopy is complicated by the fact that tropical forest canopies have been shown to have widely variable drying times (Dietz et al., 2007; Kang et al., 2012). Furthermore, Aparecido et al. (in review) specifically linked canopy wetness to altered correlations between sap flux and vapor pressure deficit (VPD), and between sap flux and photosynthetically active radiation (PAR). But it is not only canopy wetness that has an effect on micrometeorological profiles. Several of these variables such as PAR and VPD influence the drying time of the canopy but the nature of this influence has not been quantified. Further study of the stand scale variation of a full range of meteorological variables is needed to characterize the cause and effect relationships of different biophysical and climatic factors.

The objective of this study was to examine the variability and interrelationships between vertical profiles of micrometeorological variables in a wet tropical lower montane forest. Wind speed, VPD, PAR, and concentrations of H_2O and CO_2 were analyzed at several different time scales and canopy wetness states. By looking at

individual precipitation events, as well as daily, monthly, and seasonal variations, we characterize to what extent canopy wetness causes and is affected by micrometeorological gradients. Data collection and analysis will support the creation and refinement of models of individual sub-canopy gradients and processes. Furthermore, the results will also aid in modeling systems of ecosystem scale land-atmosphere interactions in tropical forests.

2.2 Methods

All field data for this research were collected at the Soltis Center for Research and Education, located in San Isidro de Peñas Blancas, Costa Rica (10° 22' 55" N, 84° 37' 15" W) (Figure 8) on the Caribbean slope of the Cordillera Tilarán. With elevations ranging from 400 to 715 m above sea level, the forested land at the center would best be classified as a *lower montane forest*, in the transitional zone between *lowland rainforest* and *lower montane cloud forest* (Scatena et al., 2010). Due to selective logging in the area throughout much of the 20th century, the land at the center consists of both primary and secondary forest. A 2200 m^2 plot was designated for the study (Aparecido et al., in review) in a densely forested area that is situated on an ENE facing slope that ranges from 12° to 55° (Teale et al., 2014). The canopy top is at a height of approximately 28 m, with emergent trees extending up to 42 m above the ground surface. The in-canopy walk-up tower at the center of the study plot is 39 m tall, and features a 10 m extension that can support limited instrumentation above the emergent tree adjacent to the tower. All vertical profile instrumentation is installed on this canopy tower.

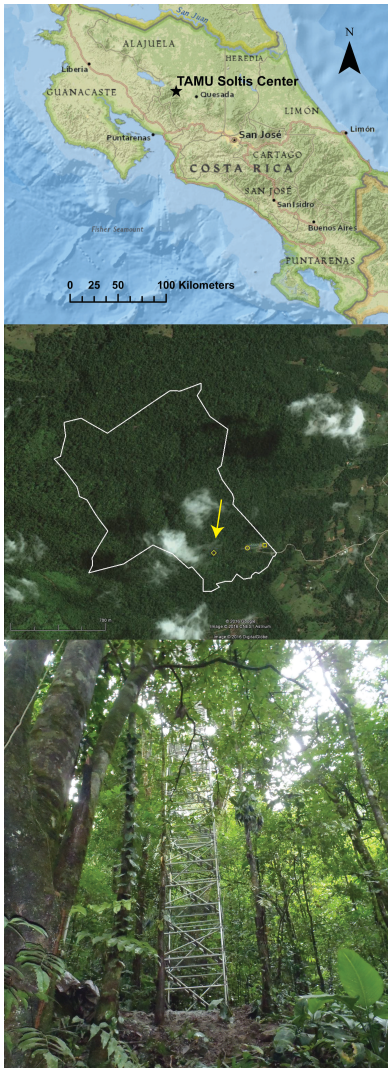

Figure 8: Top – Site location in Costa Rica. Sources: National Geographic, Esri, DeLorme, HERE, UNEP-WCMC, USGS, NASA, ESA, METI, NRCAN, GEBCO, NOAA, increment P Corp.
Middle – Soltis Center site map, image source: Google Earth; thick white line = property boundaries, square = center, circle = met tower, diamond = canopy tower, arrow shows predominant wind direction.
Bottom – Canopy tower located at study plot.

Weather data has been collected at the site since the summer of 2010 on a standard meteorological tower located in a forest clearing near the study plot. This station measures precipitation, incident solar radiation, air pressure, wind velocity, and humidity and temperature (at 3 and 10 m). Mean monthly air temperatures for the site

range between 20 – 25 °C with the warmest temperatures occurring in May and June and the coolest occurring in December (Figure 9). Mean annual precipitation reaches nearly 4,200 mm, with a wet season lasting from May through December and a relatively dry season from January to April (Figure 9). Annual mean values for five minute averaged wind speed and peak wind speed are 0.95 and 1.9 m s^{-1} respectively. Prevailing winds at the site are primarily from the north with no significant contribution from other directions (Figure 10). Wind only comes directly upslope (WSW) or downslope (ENE) for approximately 5% of data records (Figure 10).

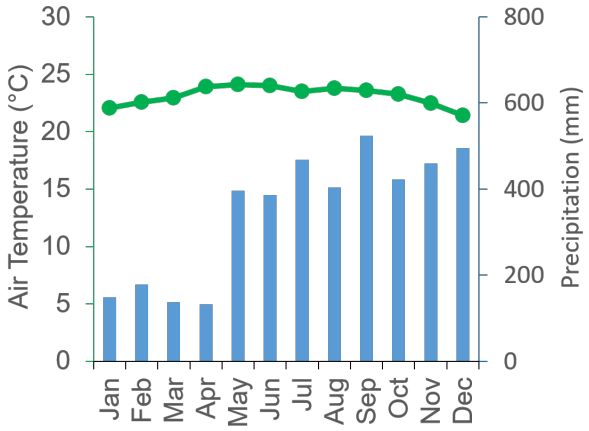

Figure 9: Mean monthly air temperature and precipitation measured at the site from 2010-2015.

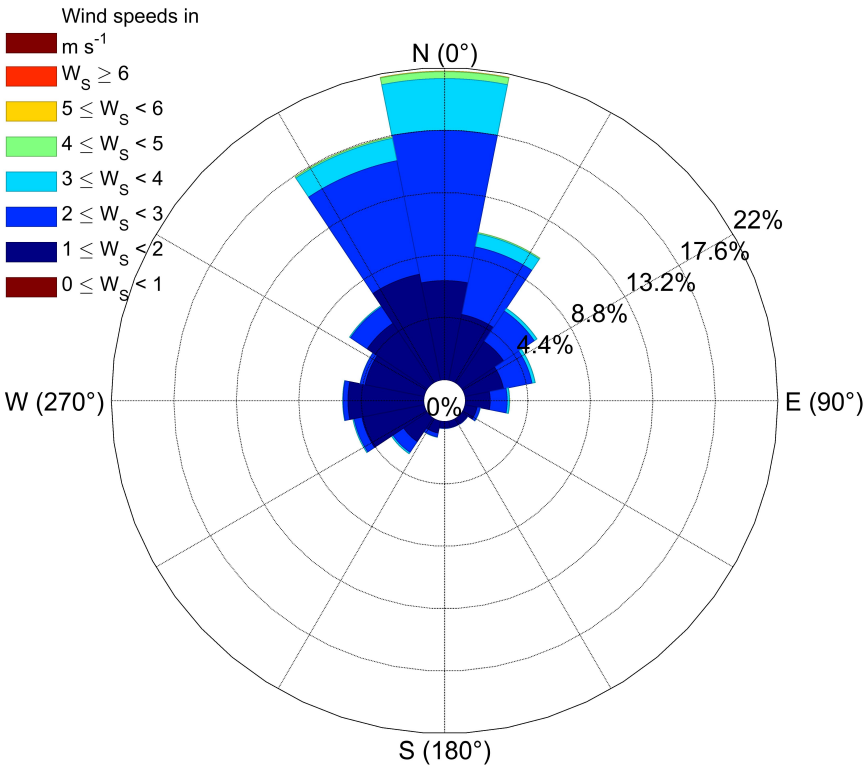

Figure 10: Wind rose showing predominant wind directions at the meteorological tower.

Forest micrometeorological profiles were measured within the forest between August 2014 and July 2015. The vertical profile dataset includes measures of CO_2 and H_2O gas concentration, temperature, VPD, PAR, horizontal wind velocity, and leaf wetness. The placement of the canopy tower relative to the surrounding canopy structure leads to unique profiles because a tall emergent tree shades the highest levels on the tower for much of the day. Therefore, the tower heights just below the highest level tend to receive the most light as there is a gap between the lower crown of the emergent tree and the top of the midstory level tree crowns (Figure 11).

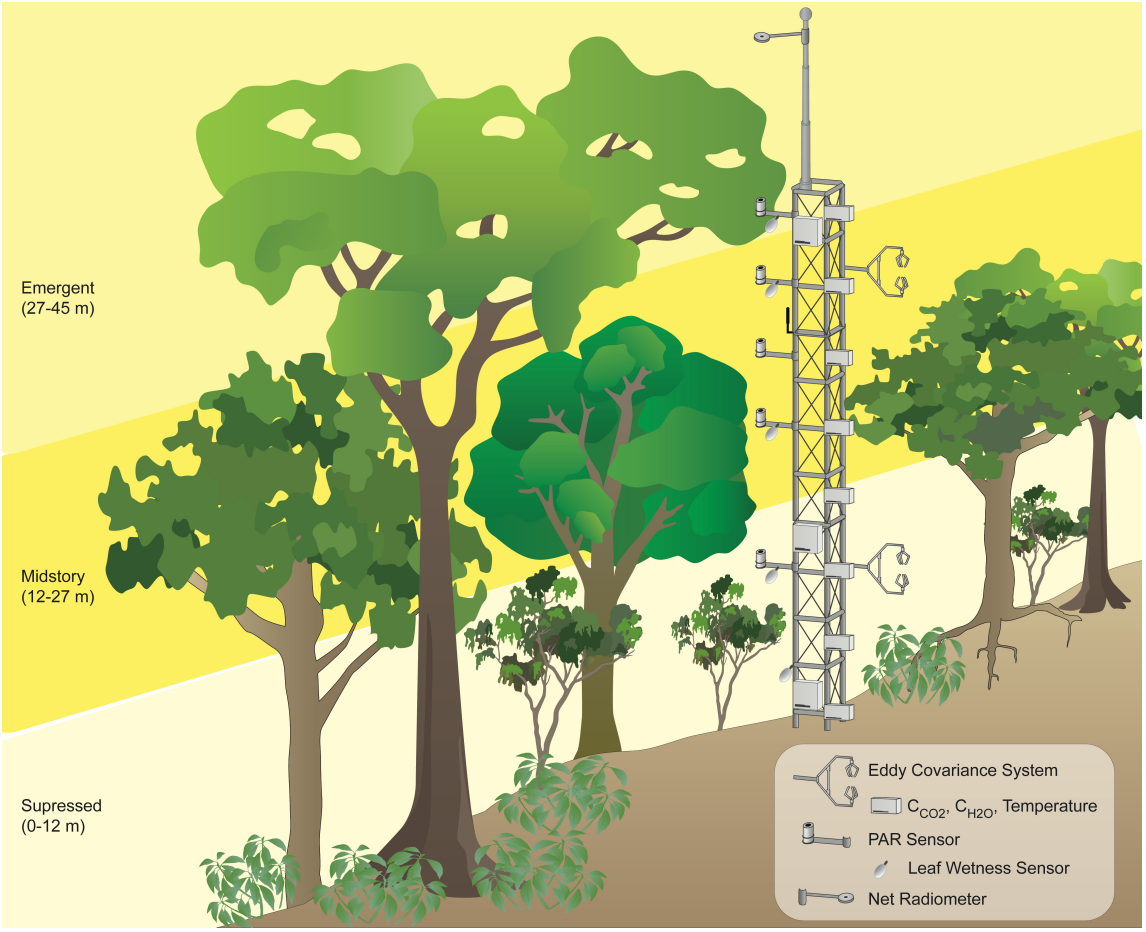

Figure 11: Study plot vegetation layers and canopy tower instrumentation. The intensity of yellow shading represents approximate light extinction at a given height in the canopy. Predominant wind direction is into the page. Symbols from library courtesy of the Integration and Application Network, University of Maryland Center for Environmental Science (ian.umces.edu/symbols/).

CO_2 and H_2O gas mole fractions were measured by an automated gas concentration profile system (AP200, Campbell Scientific, Logan, Utah). This system measures the mole fraction of each trace gas at eight different heights in the canopy by sampling air from one inlet at a time through an infrared gas analyzer (LI-840, LI-COR, Lincoln, Nebraska). The gas concentration profile data was collected using a thirty minute averaging interval, consisting of fifteen two minute cycles during which each of

the eight heights are sampled for fifteen seconds. The eight sensors are spaced evenly throughout the canopy with three located in the understory, three in the midstory, and two in the upper canopy (Table 1).

Table 1: Instrumentation on the canopy tower.

Sensor	Model	Quantity	Vertical Level (m)	Measured Variables[a]
Three-dimensional Sonic Anemometer	CSAT3[b]	2	11 and 33	U,V,W,P_{air},T_{sonic}
CO_2/H_2O Gas Analyzer	LI-7200[c]	2	11 and 33	CO_2,H_2O
CO_2/H_2O Atmospheric Profile System	AP200[b]	1	1,5,11,16,22,27,33,38	CO_2,H_2O
Temperature	107[b]	8	1,5,11,16,22,27,33,38	T_{air}
Dielectric Leaf Wetness Sensor	LWS[d]	5	3,11,22,33,38	LW
Pyranometer	LI-190SB[c]	5	10,21,27,32,38	PAR

[a] U, V, and W = x, y, and z components of wind velocity, P_{air} = air pressure, T_{sonic} = air temperature derived from speed of sound, CO_2 = concentration of carbon dioxide, H_2O = concentration of water vapor, T_{air} = air temperature, LW = leaf wetness, PAR = photosynthetically active radiation, R_{net} = net radiation, T_{leaf} = leaf temperature
[b] Campbell Scientific, Logan, Utah, USA
[c] LI-COR Biosciences, Lincoln, Nebraska, USA
[d] Decagon Devices, Pullman, Washington, USA
[e] Kipp & Zonen, Delft, The Netherlands

Dry mole fraction of CO_2 and H_2O (LI-7200, LI-COR, Lincoln, Nebraska) and three-dimensional wind speed (CSAT3, Campbell Scientific, Logan, Utah) were measured at 10 Hz for eddy flux calculations. Instrumentation for the eddy covariance measurements as well as the vertical profile gas analyzer were calibrated against AmeriFlux standards. Data processing of the eddy covariance data was done in EddyPro (LI-COR, Lincoln, Nebraska). Vertical advection calculations used the vertical component of the 3-D wind speed measurements and the vertical trace gas profile measurements, and were calculated following Aubinet et al. (2005):

$$Adv = \frac{1}{V_a}\overline{w}_h\left(\bar{c}_h - \frac{1}{h}\int_0^h \bar{c}(z)dz\right)$$

where Adv is the vertical advection of CO_2 (μmol m^{-2} s^{-1}), V_a is the molar volume of dry air (m^3 mol^{-1}), w is vertical wind speed (m s^{-1}), c is the dry mole fraction of CO_2 (μmol mol^{-1}), and h is the height (m) of the top of the vertical profile. Vertical advection of water vapor was calculated with the same formulation and converted to energy units (W m^{-2}). Storage fluxes of CO_2, sensible heat, and LE were also computed following Ohkubo et al. (2008):

$$S_c = \int_0^h \frac{1}{V_a}\left(\frac{\delta c}{\delta t}\right)dz$$

$$Q_a = \int_0^h \rho C_p\left(\frac{\delta T}{\delta t}\right)dz$$

$$Q_w = \int_0^h \left(\frac{\rho C_p}{\Gamma}\right)\left(\frac{\delta e_a}{\delta t}\right)dz$$

where S_c, Q_a, and Q_w are the CO_2 storage flux (μmol m^{-2} s^{-1}), sensible heat storage flux (W m^{-2}), and LE storage flux (W m^{-2}) respectively. The variables ρ, C_p, e_a, Γ, and T are air density (kg m^{-3}), specific heat (J kg^{-1} K^{-1}), water vapor pressure (kPa), the psychrometric constant (kPa K^{-1}), and ambient air temperature (K) respectively. Positive fluxes indicate an increase in stored CO_2, temperature, or stored H_2O, while negative fluxes indicate a decrease in the same respective quantities.

Temperature probes (107, Campbell Scientific, Logan, Utah) are located next to the AP200 inlets, with data collected at a thirty minute averaging interval. This temperature data, along with air pressure and water vapor concentration data were used

to calculate VPD. Saturation vapor pressure, a function of air temperature, was calculated from the Goff–Gratch formulation following List (1971):

$$\log e^*(T) =$$

$$-7.90298\left(\frac{T_{st}}{T}-1\right)+5.02808\log\left(\frac{T_{st}}{T}\right)-1.3816\times10^{-7}\left(10^{11.344(1-T/T_{st})}-1\right)+$$

$$8.1328\times10^{-3}\left(10^{-3.19149(T_{st}/T-1)}-1\right)+\log e^*_{st}$$

where e^* is the saturation vapor pressure (kPa), T is ambient air temperature (K), e_a is actual vapor pressure (kPa), T_{st} is the steam-point temperature of 373.16 K, and e_{st}^* is the saturation vapor pressure at the steam-point temperature, 101.325 kPa. Actual vapor pressure was calculated as the product of the mole fraction of water vapor and the ambient air pressure.

Additionally, two types of PAR measurements were made to characterize the vertical profile of light transmission into the canopy. The long-term PAR profiles were from five LI-190SB (LI-COR, Lincoln, Nebraska) pyranometers, concentrated towards the upper canopy, that were averaged on five minute intervals (Table 1). Handheld measurements were made over several days in January and February of 2016 during the daytime at 2-m height increments on the canopy tower with the LI-191 (LI-COR, Lincoln, Nebraska) line quantum sensor. These measurements were used to characterize light extinction in the canopy.

The wind instrumentation was relatively limited over period of this study; however, a new installation made in January of 2016 allowed the gathering of data to do a short term profile analysis on the wind data. In addition to the anemometer on the meteorological tower giving site wind conditions unaffected by the vegetation, long term

measurements include the two 3-D sonic anemometers (CSAT3, Campbell Scientific, Logan, Utah) as part of the eddy covariance systems. A more extensive vertical array of 2-D wind instruments (DS-2, Decagon Devices, Pullman, Washington) was used to evaluate the vertical variation of horizontal wind flow in the canopy.

The final vertical profile measurement included is the leaf wetness profile, measured by five leaf wetness sensors (Decagon Devices, Pullman, WA) spaced evenly throughout the canopy. Raw leaf wetness data, averaged over a five minute interval, was used to develop calculated leaf wetness percentages, classify the entire canopy or specific parts of the canopy by one of several wetness classifications, and to calculate drying times to correlate against variables that affect time to dry. The sensors were oriented horizontally over the entire study period.

Because the Decagon leaf wetness sensors measure the dielectric constant just above the sensor, they are able to supply more information about the wetness of the leaf surface than just a Boolean designation of wet or dry. To capture the changing canopy wetness at a finer scale, a calibration algorithm was developed to take the raw voltage signals from the Decagon sensors and convert them to percentage wetness measures. These percentage wetness measures are specific to each individual sensor and represent approximately the percentage of water present on the leaf relative to its maximum water storage capacity. Due to the drift over time associated with the leaf wetness sensors, and the variability between different instruments, the algorithm was applied to develop a percentage range of leaf wetness for each sensor each week. For a given week and sensor, the wettest and driest 10% of the dataset respectively were used to calculate an

average and standard deviation for the wet and dry subsets of data. The 0% wetness and 100% wetness values for the week were assigned to the dry average plus one standard deviation and the wet average minus one standard deviation respectively. Values falling below the 0% threshold or above the 100% threshold were assigned to these respective thresholds, and intermediate values were linearly interpolated. In this paper we apply the terminology of *fully dry*, *partially wet*, and *fully wet* to either describe an individual sensor or the canopy as a whole when specific wetness percentage criteria are met (Table 2).

Table 2: Wetness percentage criteria that must be met for the three wetness classifications to be assigned at either the single instrument or entire canopy scale.

Wetness Class	Single Instrument	Whole Canopy
Fully Dry	< 10%	< 10% at all levels
Partially Wet	10% - 50%	Fully dry and wet criteria not met
Fully Wet	> 50%	> 50% at all levels

Several criteria were used to guide the selection of the wetting and drying events used for analysis of vertical profile variation as canopy wetness changed. It was important to consider only those wetting or drying events that represented a "smooth" transition from dry to wet or from wet to dry. Two conditions had to be met for the transition to be considered smooth. Firstly, the canopy had to both start and end at a fully dry or wet state, meaning that all sensors must have been dry at the beginning of a

wetting transition or at the end of a drying transition. Similarly, the canopy had to be fully wet at all heights at the end of a wetting transition or the beginning of a drying transition. The second condition was that no intermittent drying could occur during a wetting event and no rewetting of the canopy could occur during a drying event. The two records selected for each wetness transition event represent the first or last timestamp when the canopy was either fully wet or fully dry. In total, 83 drying events and 77 wetting events were identified for analysis, covering all twelve months of the period of study and all times of day.

2.3 Results

2.3.1 Overview and Seasonal Weather Patterns

Over the twelve month study period, rainfall was slightly greater than the mean amount, measuring 4413 mm. The dry season months were wetter than average, receiving 247 mm mo^{-1}, 67% more than an average dry season month. January and February in particular were atypical as the rainfall in these months was more than double the average. The wet season months had more typical rainfall amounts, and received 428 mm mo^{-1} which is 96% of the average rainfall during those months. These precipitation trends translated into canopy wetness durations that were significantly longer in the wet season. During the wet season the upper canopy was wet for 35% of all records; by contrast, the lower canopy was wet for 52% of all records. During the dry season, the upper and lower canopy were wet for 12% and 17% of records collected respectively.

2.3.2 Monthly Profile Plots

Sub-canopy vertical profile monthly averages are presented for temperature, PAR, leaf wetness percentage, CO_2 concentration, H_2O concentration, and VPD (Figures 12-17) and tabular monthly averages are shown for sixteen variables (Table 3). The canopy was wettest during the months of June and December and driest during March and April (Figure 12). September was not significantly wet overall but the sensor in the lower canopy did record high wetness readings (Figure 12).

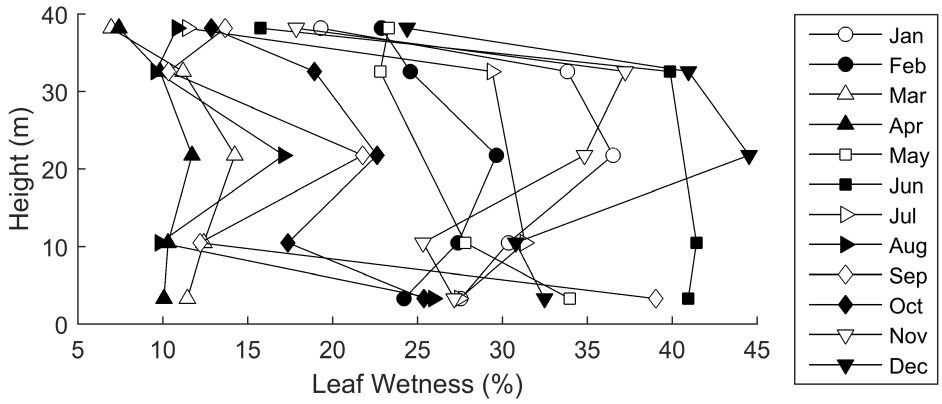

Figure 12: Monthly average vertical sub-canopy profiles of percentage leaf wetness.

The PAR profiles display the highest values in the mid to upper canopy with some month-to-month variability in regard to which level displays the highest PAR value (Figure 13). PAR values from ground level to twenty meters are much lower than those seen in the upper canopy, particularly during peak months of April and August. PAR values show less variability with height for months with lower average incident PAR, such as in June and December.

Table 3: Monthly and annual averages of meteorological variables. The 33 m height was used for all profile variables.

	2014						2015											
	A	**S**	**O**	**N**	**D**	**J**	**F**	**M**	**A**	**M**	**J**	**J**	**Annual**	**Std. Err.**
Precip (mm)	341	558	404	547	515	288	441	108	149	232	574	255	4413	-
T_{air} (°C)	23.7	23.5	23.4	22.6	21.6	21.5	21.7	22.7	23.7	23.3	23.7	23.1	22.9	0.013
VPD (kPa)	0.705	0.813	0.804	0.706	0.645	0.593	0.677	0.891	0.841	0.710	0.602	0.633	0.718	0.0025
LW (%)	9.6	10.3	18.9	37.2	41.0	33.8	24.6	11.2	9.8	22.8	39.9	29.4	23.7	0.102
PAR (µmol m^{-2} s^{-1})	54.5	47.4	49.3	35.0	30.2	32.9	-	-	-	-	16.4	36.0	39.7	0.350
CO_2 (µmol mol^{-1})	372	372	374	375	378	381	382	381	382	381	378	375	377	0.046
H_2O (mmol mol^{-1})	22.4	22.2	22.0	21.4	20.5	20.9	20.5	19.8	22.2	22.9	24.3	23.2	21.8	0.017
F_{CO2} (µmol m^{-2} s^{-1})	-4.04	-5.36	-4.02	-2.67	-2.12	-1.80	-2.63	-3.42	-3.74	-1.94	-0.41	-3.40	-2.91	0.063
F_{LE} (W m^{-2})	59.3	62.8	50.9	37.1	24.2	29.0	41.1	56.2	53.6	15.5	7.7	38.0	39.5	0.7
adv_{CO2} (µmol m^{-2} s^{-1})	1.99	0.169	1.54	1.91	2.78	2.68	1.71	1.96	2.16	1.18	1.10	0.899	1.75	0.0612
adv_{LE} (W m^{-2})	6.39	4.75	10.5	11.2	18.9	23.4	19.8	21.8	36.7	27.2	13.6	49.4	21.5	0.645
S_c (µmol m^{-2} s^{-1})	0.0074	0.0104	0.0080	0.0039	-0.0016	0.0049	0.0069	0.0020	-0.0198	0.0044	0.0074	-0.0027	0.0021	0.0109
Q_a (W m^{-2})	0.0434	-0.0042	-0.0457	0.0096	-0.0208	0.0123	-0.0352	-0.0346	0.0271	-0.0385	-0.0705	-0.0055	-0.0133	0.0566
Q_w (W m^{-2})	-0.021	-0.012	-0.195	0.066	0.000	-0.068	-0.012	-0.101	-0.004	0.181	-0.029	-0.095	-0.023	0.0935
u_{canopy} (m s^{-1})	0.81	0.49	0.50	0.84	0.97	1.5	1.2	1.3	1.1	0.54	0.81	1.1	0.96	0.0052
u_{met} (m s^{-1})	0.94	0.79	0.59	1.0	1.1	1.5	1.1	0.88	0.82	0.87	0.93	1.1	0.95	0.0022

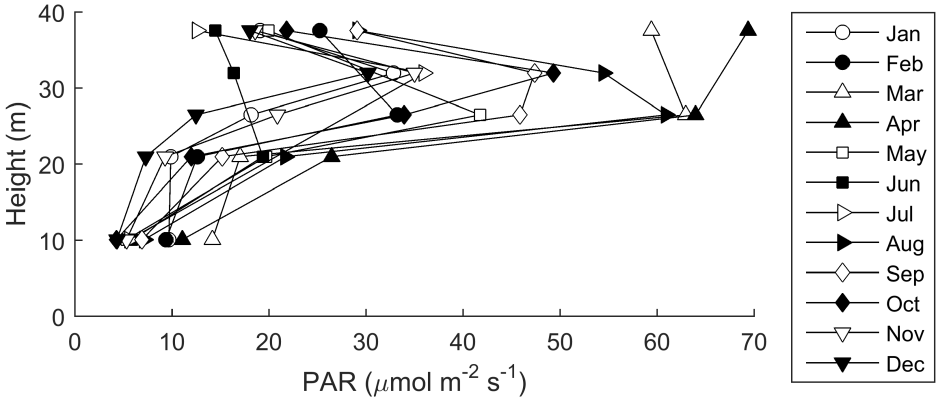

Figure 13: Monthly average vertical sub-canopy profiles of photosynthetically active radiation (PAR).

The two gas concentration measurements (H_2O and CO_2) both have a distinct vertical profile shape that exists during all months of the year. At the lowest measurement point, around 1 m from the forest floor, gas concentrations are substantially higher than at all other heights in the canopy (Figures 14-15). The monthly CO_2 profiles and the H_2O profiles follow a unimodal pattern from month to month. The CO_2 data show maximum and minimum values in April and August respectively, while H_2O maximum and minimum values occur in June and March respectively.

The monthly temperature profiles following a vertical pattern that is nearly identical for all twelve months, showing a steady increase in temperature with height from the ground (Figure 16). Seasonal differences in temperature are clearly present, with December and January being the coldest months, and April and June being the warmest; however, the overall variation in average temperatures does not exceed 2 °C, consistent with the site's proximity to the equator.

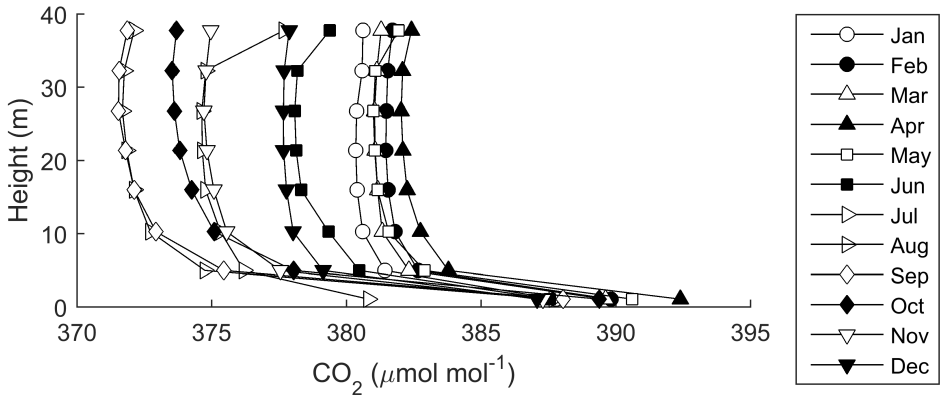

Figure 14: Monthly average vertical sub-canopy profiles of CO_2 concentration.

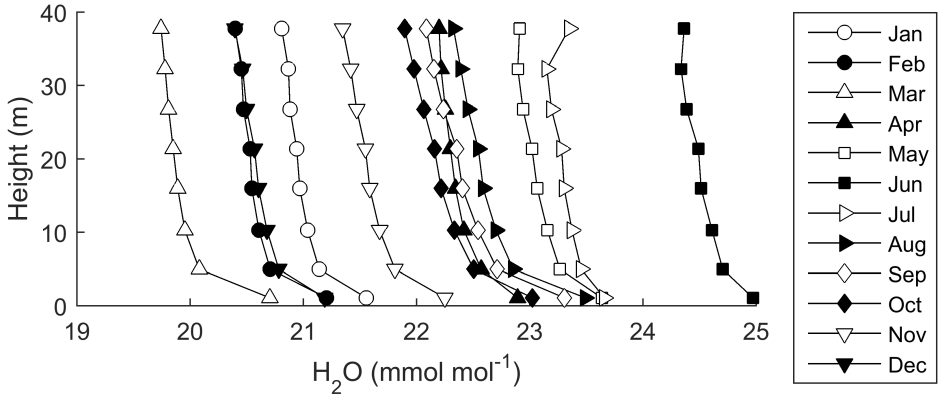

Figure 15: Monthly average vertical sub-canopy profiles of H_2O concentration.

The VPD profiles show an increase in value as height from the ground increases across all twelve months (Figure 17). The gradients for this increase are sharpest at the bottom of the canopy while VPD values in the upper canopy show little change from one height to the next. Peak monthly values of VPD occur in March and September with minimum values occurring in June and January.

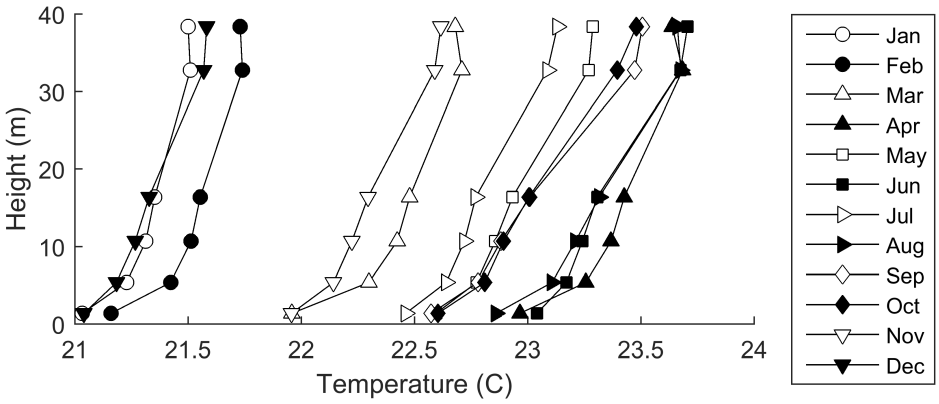

Figure 16: Monthly average vertical sub-canopy profiles of ambient air temperature.

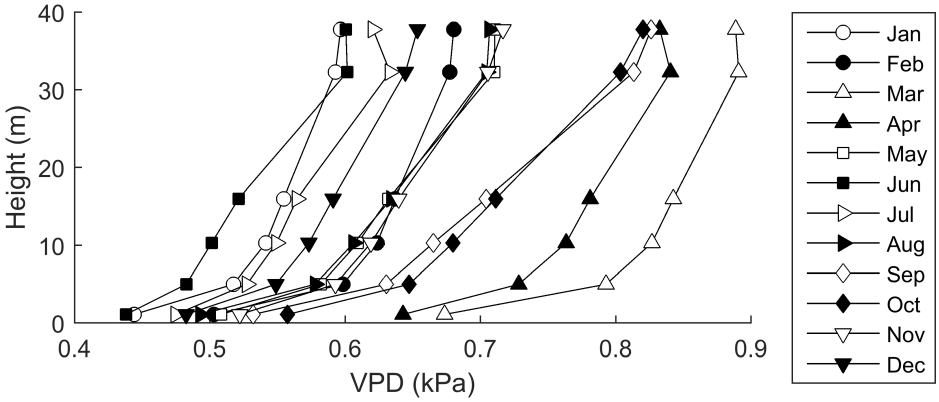

Figure 17: Monthly average vertical sub-canopy profiles of vapor pressure deficit (VPD).

2.3.3 Diurnal Profile Plots

Diurnal vertical profiles are given for the same six variables as for the monthly plots in addition to diurnal plots of storage fluxes for sensible heat, latent heat, and CO_2 storage (Figures 18-23) that were not included in the monthly plots. The average leaf wetness diurnal profiles have multiple sets of peaks (Figure 18). The absolute maximum and minimum peaks occur in the evening (18:00-18:30) and at midday (11:30-13:30) respectively, with the precise time of peak changing slightly with height in canopy. The

morning hours of leaf wetness data are characterized by tremendous variability as three sets of smaller peaks occur, the relative maximum values at 01:30, 04:30, and 08:00. The PAR profile data display one high peak at approximately 10:00 with no distinct time at which a minimum value occurs as PAR is zero for many hours of the day (Figure 19).

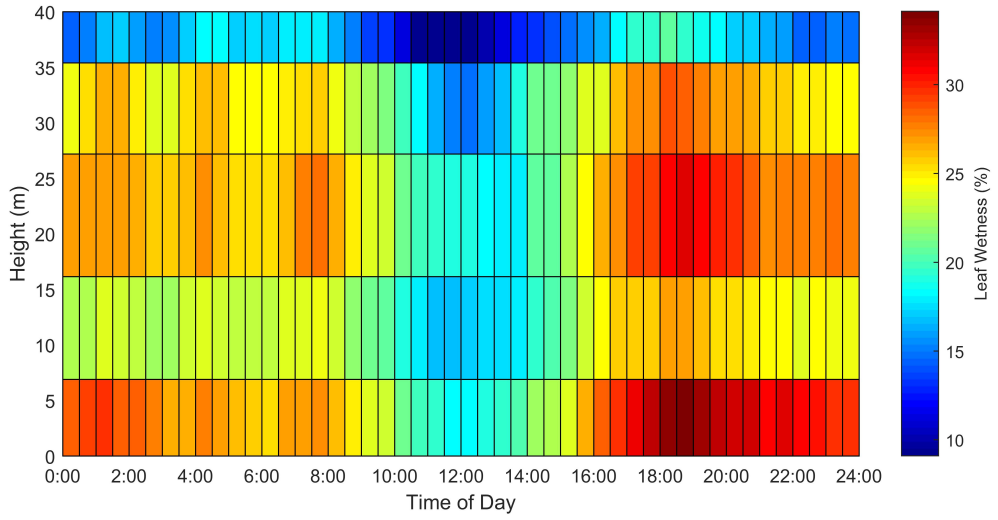

Figure 18: Diurnal average vertical sub-canopy profiles of percentage leaf wetness.

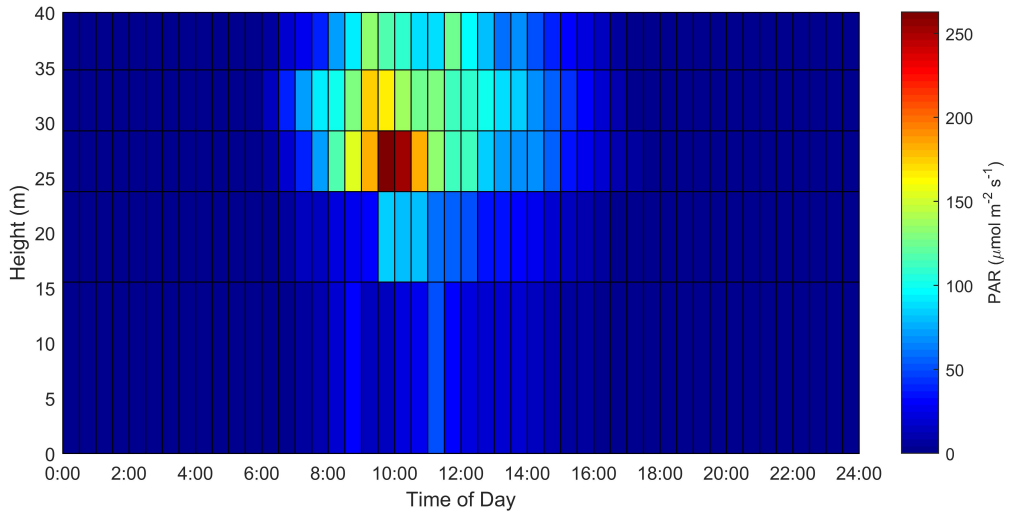

Figure 19: Diurnal average vertical sub-canopy profiles of photosynthetically active radiation (PAR).

The diurnal CO_2 data show only one set of peaks with gas concentration maximums and minimums occurring at 05:00 and 14:30 respectively, while CO_2 storage flux peaks at 17:30 and reaches its minimum at 08:30 (Figure 20). The profile again has sharp gradient in the lower part of the canopy, which persists throughout the diurnal cycle. The H_2O data also show a sharp gradient in the lower canopy throughout the day, but the time of day when the water vapor concentration reaches its peak values changes with height in the canopy (Figure 21). The H_2O data displays two sets of peaks, with the absolute minimum and maximum values occurring at 05:30 and at midday. The precise timing of the maximum peak is 11:30 at the top of the canopy and transitions to a peak time of 13:00 in the understory. The LE storage flux (Figure 21) has peak values at 01:00 and 07:30, with relative minimum and maximum peaks occurring in the evening as is observed in the H_2O concentration data.

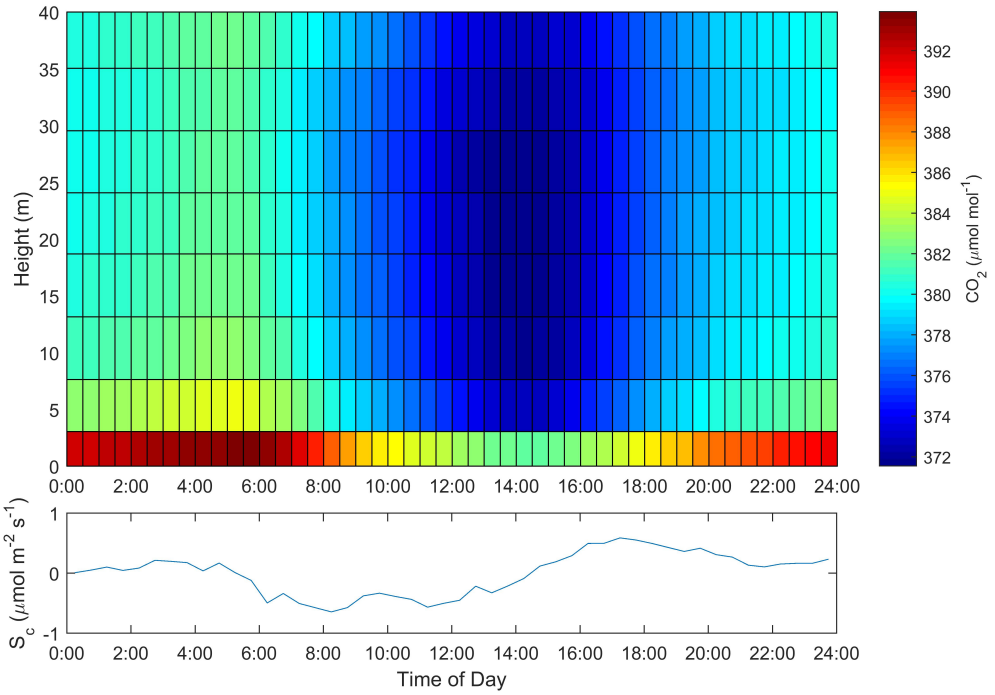

Figure 20: Diurnal average vertical sub-canopy profiles of CO_2 concentration and diurnal sub-canopy CO_2 storage flux.

The temperature and VPD diurnal profiles look similar to one another, each with a maximum peak occurring at 13:30 (Figures 22 and 23). The temperature data display a clear minimum peak in the morning (06:00) while the VPD data remains constant throughout the night and does not display a clear minimum peak at a specific time. Another difference between the two plots is the sharp gradient that can be seen in the VPD data in the lower canopy that is not present in the temperature data. Annual mean values of VPD at 10 m, 5 m, and 1 m are 0.633±0.002 kPa, 0.605±0.002 kPa, and 0.525±0.001 kPa respectively.

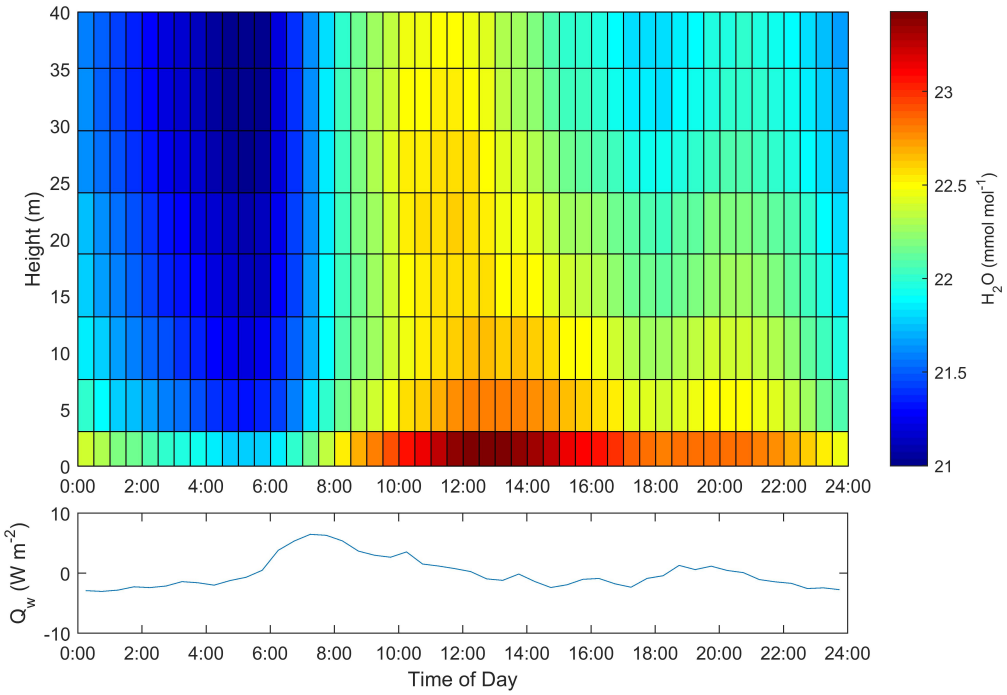

Figure 21: Diurnal average vertical sub-canopy profiles of H_2O concentration and diurnal sub-canopy latent energy (LE) storage flux.

Additionally, diurnal plots of wind (Figure 24) both at the meteorological tower (u_{met}) and at 33 m in the canopy (u_{canopy}) further inform diurnal patterns at the site. Wind speed reaches its minimum diurnal values (0.76 m s^{-1}) at approximately 05:00, before rapid increase as energy begins to come into the ecosystem. Average daily wind speeds peak at noon at 1.1 m s^{-1} in the canopy and 1.2 m s^{-1} at the meteorological tower. The diurnal wind data also displays a second smaller peak (1.1 m s^{-1} and 1.0 m s^{-1}) in the evening at approximately 19:00 before it continues to decrease for the remainder of the night.

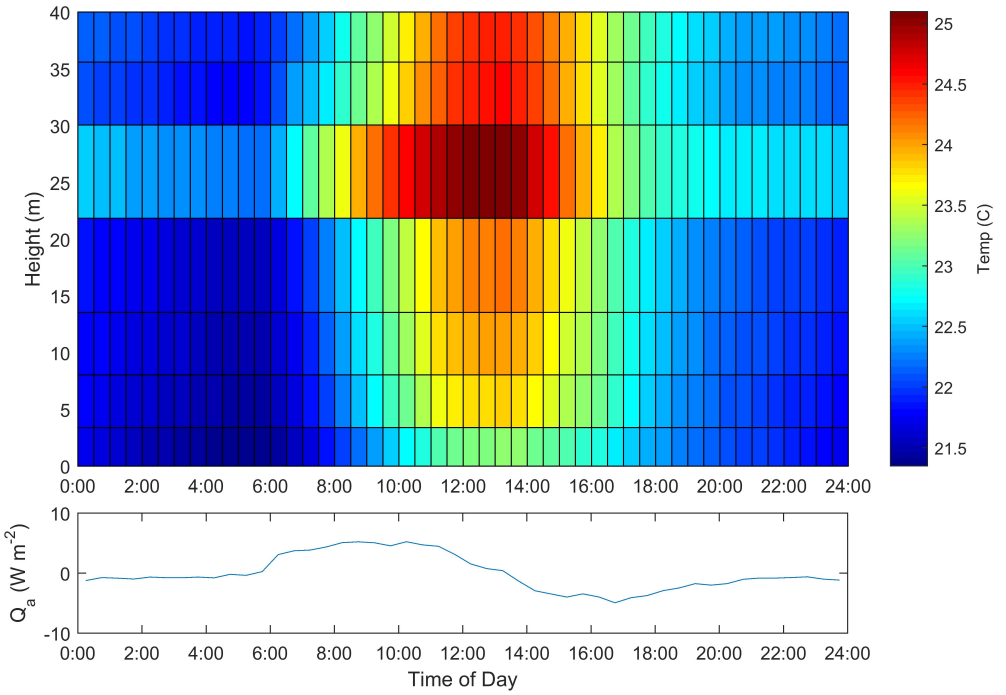

Figure 22: Diurnal average vertical sub-canopy profiles of ambient air temperature and diurnal sub-canopy sensible heat storage flux.

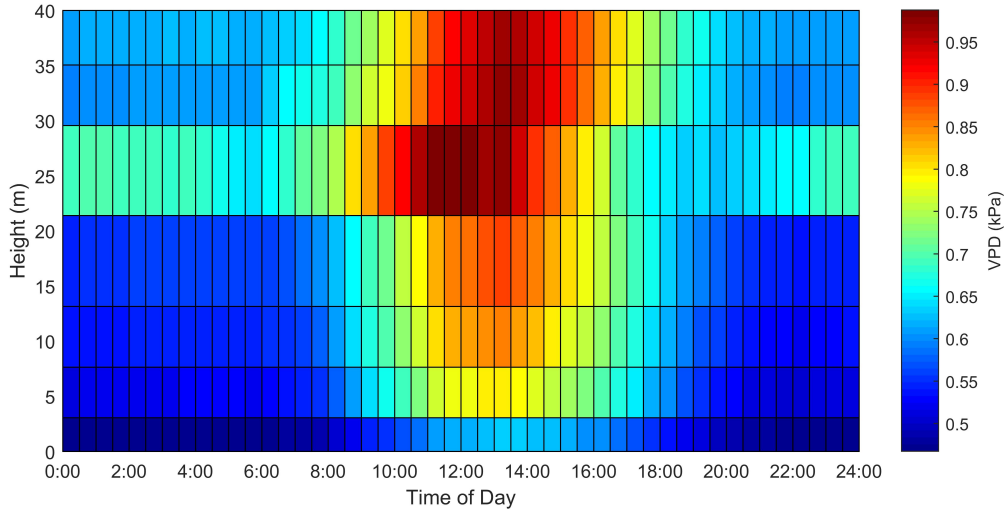

Figure 23: Diurnal average vertical sub-canopy profiles of vapor pressure deficit (VPD).

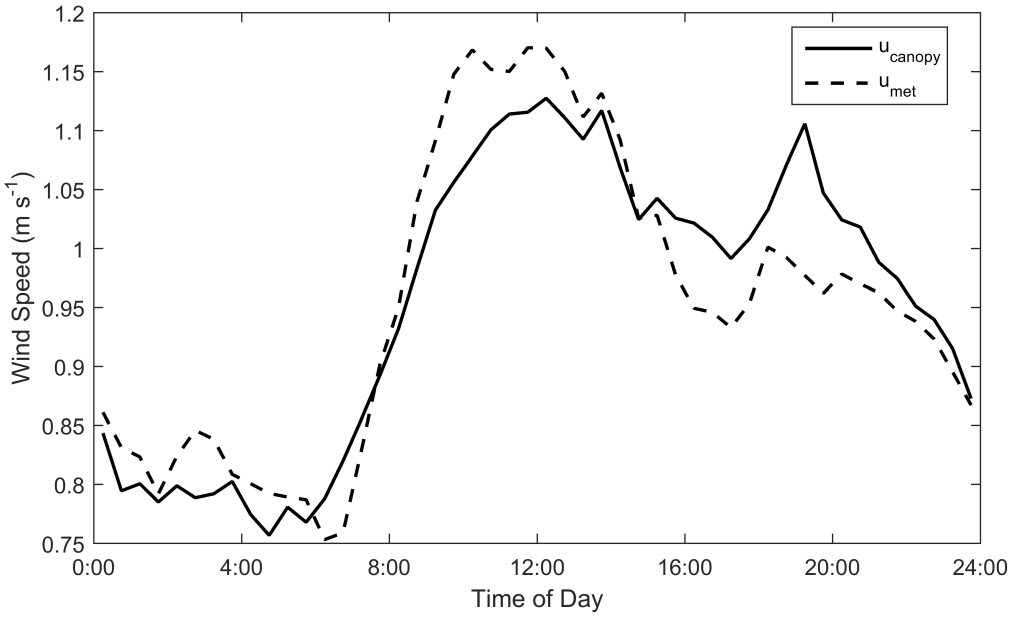

Figure 24: Diurnal average values of horizontal wind speed at 33 m from the ground between the midstory and emergent tree layers in the canopy (u_{canopy}) and at the meteorological tower (u_{met}) in a clearing near the study plot.

2.3.4 Trace Gas Advection, Storage, and Flux

Vertical advection and eddy flux transport of both CO_2 and H_2O are the dominant terms in the trace gas budgets, rendering the storage fluxes almost negligible (Figure 25). The vertical advection of CO_2 follows the same general trend as the CO_2 storage flux, except that maximum and minimum values are almost ±6 μmol m^{-2} s^{-1} whereas the peak and low storage flux values are an order of magnitude lower (Figure 25.a). The CO_2 eddy flux is even more influential as a transport mechanism for carbon uptake during the day, with a low value of –12.6±0.4 μmol m^{-2} s^{-1} occurring at 11:30. Summing all three rates of carbon uptake during this peak time of uptake gives a net flux of –18.4±0.7 μmol

m^{-2} s^{-1}. The maximum net rate of carbon ejection is 7.25±0.37 μmol m^{-2} s^{-1}, occurring at 03:30 and largely dominated by vertical advection.

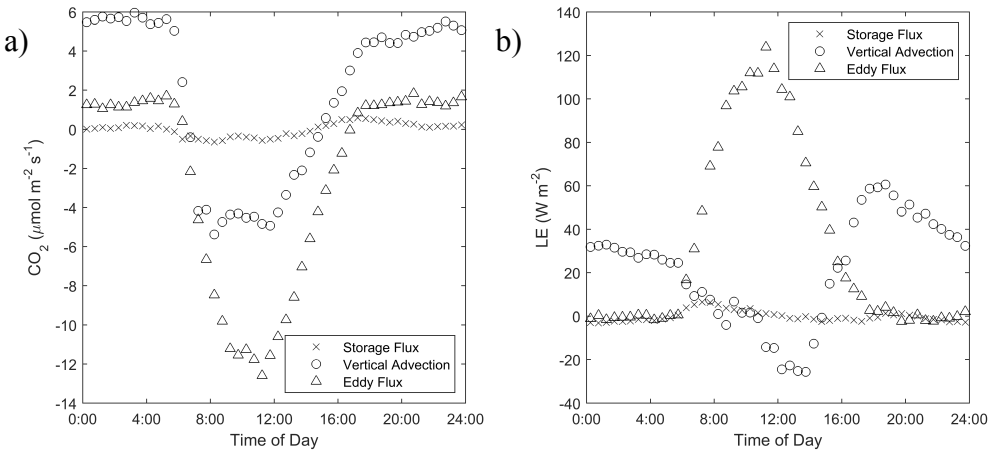

Figure 25: Diurnal average values of: a) CO_2 storage flux, vertical CO_2 advection, and eddy flux, b) latent energy (LE) storage flux, vertical advection of water vapor, and LE eddy flux. Positive vertical advection and eddy flux indicate movement away from the ground.

The vertical advection for the water vapor data (Figure 25.b), conversely, does not follow the trend of either the storage flux of eddy flux of LE. The eddy flux of LE is inversely related to the eddy flux of CO_2, exhibiting a peak average value of 124±6 W m^{-2} at 11:30. Vertical advection of H_2O, however, is negative throughout much of the daylight hours, reaching an average minimum value of –25.6±5.5 W m^{-2} at 14:00. In the evening hours, vertical advection becomes the dominant process, reaching a peak value of 60.6±4.7 W m^{-2} at 19:00, when eddy and storage fluxes of LE are negligible.

2.3.5 Single Wetness Event Delta Profile Plots

Figures 26-29 display the average delta profiles for all the smooth wetting and drying events identified in the dataset, sorted by the time of day during which they

occurred (Table 4). The delta profiles represent the difference between the initial and final profiles of a variable, i.e., when the canopy is last wet and first fully dry for drying events and last dry and first fully wet for wetting events. The delta profiles for CO_2 display a similar shape across all times for the subset of drying events and the subset of wetting events with one key difference between drying and wetting events (Figure 26). Both the drying and wetting profiles are vertical through the middle and upper canopy but the difference occurs at the lowest level in the canopy. For the drying events, the lowest level always has a higher delta value while the lowest level for the wetting events displays the lowest delta value of all the heights. The profiles are negative in the morning and midday for drying events, and positive for evening and nighttime, as well as for all times for the wetting events (3.35 μmol mol^{-1} mean increase). Midday and nighttime display the most variability in drying events (σ = 5.96 and 5.65 μmol mol^{-1}) while the morning is when wetting events experience the most variability (σ = 5.57 μmol mol^{-1}) for CO_2.

Table 4: Drying and wetting event statistics *used to calculate delta profiles in Fig. 5. Each event is assigned a time by its median time and times are classified as: Morning = 05:00-09:30, Midday = 09:30-14:30, Evening = 14:30-19:00, Night = 19:00-05:00*

	Drying Events		**Wetting Events**	
Time of Day	**No. of Events**	**Avg. Duration**	**No. of Events**	**Avg. Duration**
Morning	18	5 hr	9	26 min
Midday	23	3.6 hr	12	14 min
Evening	13	4.7 hr	32	21 min
Night	29	7.9 hr	24	30 min

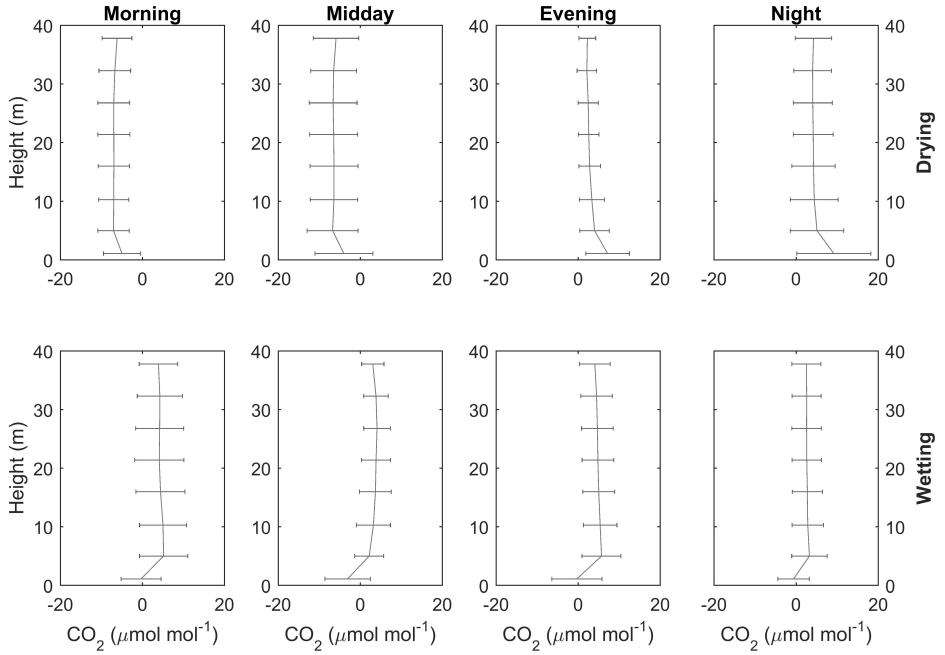

Figure 26: The average change in vertical profile across all drying and wetting events, sorted by time of day for CO_2 concentration. Horizontal bars represent one standard deviation to each side of the vertical distribution.

The delta profiles for H_2O drying events (Figure 27) are very similar to the CO_2 drying event profiles, with the delta profile magnitudes being inversely related. Unlike the CO_2 profiles however, the H_2O profiles do vary with time of day for wetting events. During morning and nighttime the H_2O wetting delta profiles are near zero while the midday and evening profiles both show a decrease in vapor concentration (–1.22 and –0.435 mmol mol^{-1} mean change) as the canopy is wetted. Variability in the H_2O profiles is highest at night (σ = 1.75 mmol mol^{-1}) in the drying profiles and highest at midday and evening (σ = 1.66 and 1.38 mmol mol^{-1}) for the wetting delta profiles.

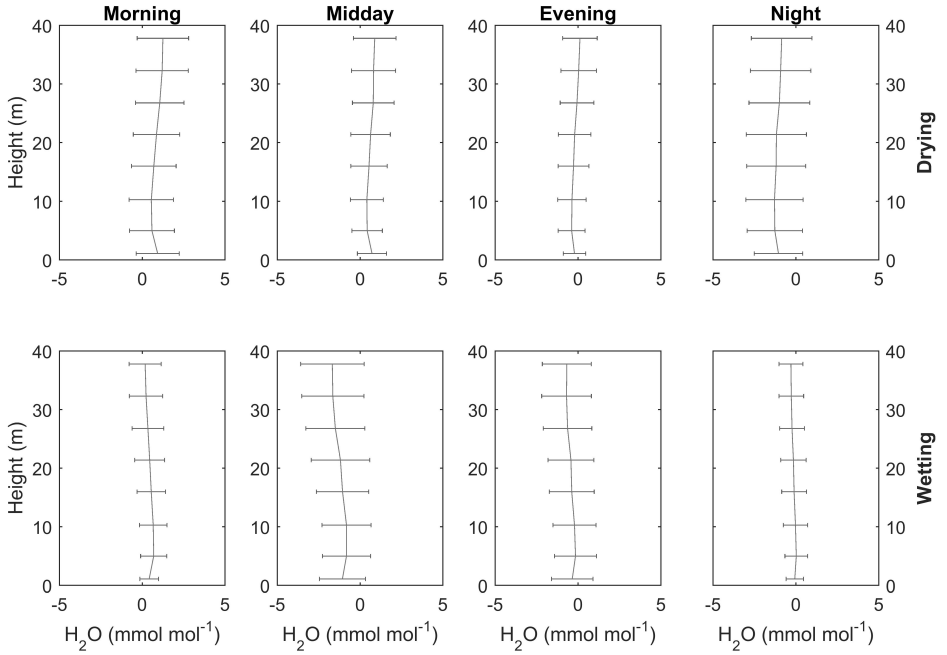

Figure 27: The average change in vertical profile across all drying and wetting events, sorted by time of day for H_2O concentration. Horizontal bars represent one standard deviation to each side of the vertical distribution.

The delta profiles for temperature and VPD are nearly identical in shape, magnitude, variability, and trend with time of day (Figures 28-29). For each set of drying profiles, values of temperature and VPD are positive (1.62 °C and 0.253 kPa mean increase at 33 m) for all times of day and closer to zero at the lowest height. The greatest increase in temperature and VPD is seen during drying events in the morning (2.27 °C and 0.304 kPa mean increase) and midday (2.11 °C and 0.295 kPa mean increase), and the lowest variability occurs in the evening (σ = 0.768 °C and 0.118 kPa). Wetting events cause the opposite effect, where temperature and VPD decrease as a wetting event ensues. As is the case with the drying events, this trend is less pronounced near the forest floor as the lowest height remains closest to a change of zero. Midday and evening

are the times of day when the temperature decrease (–2.88 and –2.33 °C mean) has the greatest magnitude and also are the times when the greatest variability (σ = 1.22 and 1.40 °C) is present.

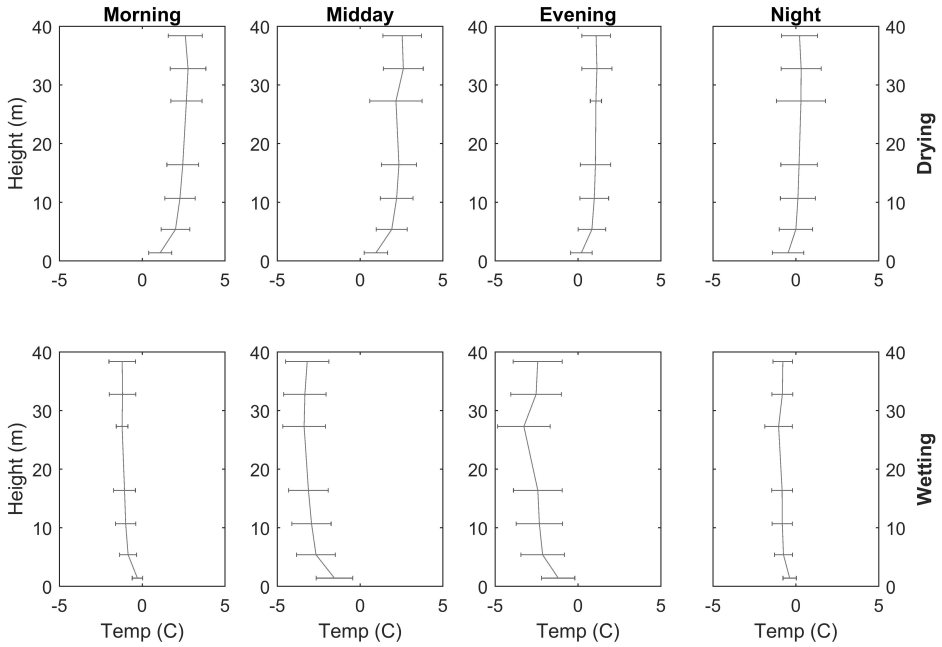

Figure 28: The average change in vertical profile across all drying and wetting events, sorted by time of day for ambient air temperature. Horizontal bars represent one standard deviation to each side of the vertical distribution.

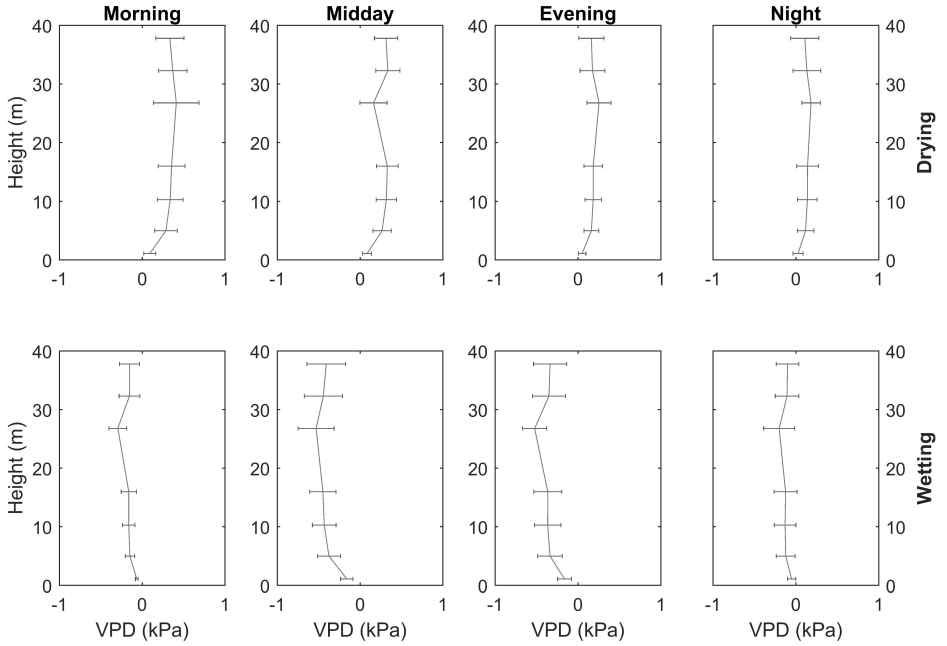

Figure 29: The average change in vertical profile across all drying and wetting events, sorted by time of day for vapor pressure deficit (VPD). Horizontal bars represent one standard deviation to each side of the vertical distribution.

2.4 Discussion

2.4.1 Dry Season Stomatal Control

The difference in monthly average trends between the CO_2 (Figure 14) and the PAR (Figure 13) data indicate that, despite the lack of water stress at this extraordinarily wet site, stomatal control limits water loss in the dry season. Recall that the typical dry season in this region lasts from January to April, and that the study period included an uncharacteristically wet January and February. Thus, March and April were the two months in the study period most representative of typical dry season conditions. The monthly diurnal leaf wetness data (Figure 12) validates this point, showing that these

two months were the two driest months of the twelve month period. It follows then that April ought to have been the month in which the ecosystem was most water limited.

August is another month in the data that will help to illustrate the stomatal control exhibited in the dry season. Although it occurs in the middle of the wet season, August was the third driest month (Figure 12) during the study period. Because frequent precipitation brings cloud cover with it, the driest months of March, April, and August are also the months that experience the highest rates of PAR (Figure 13). Because PAR is a primary driver of photosynthesis and high rates of photosynthesis should lead to a decrease in CO_2 concentrations, low levels of CO_2 were expected in these months with high PAR.

Interestingly, April and August are the two months during which the CO_2 concentration reaches its maximum and minimum values (382 and 372 μmol mol^{-1} at 33 m) respectively. The pattern between PAR and CO_2 concentration in August is what was expected: a relatively dry and cloudless August led to high values of average PAR which drove high levels of photosynthesis. The high rates of photosynthesis took carbon dioxide out of the air, leading to the lowest concentrations of CO_2 of the year. But the trend in April is the complete opposite: despite relatively high levels of PAR (64.0±1.5 μmol m^{-2} s^{-1} mean at 27 m), CO_2 concentrations reach their maximum value for the year, indicating that there might have been relatively little photosynthetic activity.

The difference between the two months seems to be a matter of water limitation. Although August itself was relatively dry, it followed several months of wet conditions. During a water limited April, however, presumably low rates of photosynthesis indicate

that stomatal control was likely limiting water loss. Two alternate possibilities could also contribute to the high levels of CO_2 in April: lower wind speeds that reduced air mixing and relatively low VPD to limit transpiration. Both of these explanations are countered by the results displayed in Table 3, however, showing that wind speeds were average in April (1.1 m s^{-1}) and VPD was slightly above (0.841 kPa) the annual average (0.718 kPa).

Even during a wet year in a wet environment, it seems that the plant response was still to conserve water when supplies were lower than normal for the ecosystem. This is contrary to what is often assumed about wet tropical environments: that access to water year-round means that plants do not need to regulate water loss. Hasler and Avissar (2007) note that water stress can occur in Amazonian forests located farther from the equator, which tend to be much drier than our site. They also mention that modeled tropical forest water stress is often overestimated. Additionally, Malhi et al. (2002) report water stress in Manaus during a particularly dry season.

2.4.2 Slope Aspect and Carbon Dioxide

The site's slope aspect appears to strongly influence the biophysical function of the forest. Because the slope at the study site faces east-northeast, the sun's light is transmitted into the lower canopy best as the sun is rising from the east (Figure 19). Conversely, by solar noon, much of the canopy is shaded by vegetation upslope. While the aforementioned frequent afternoon rainfall may be the cause of some of the reduced afternoon PAR values, we posit that slope aspect is the primary contributor to the peak timing of the diurnal PAR profiles. The opposite trend was found by Motzer (2005), who

reported highest levels of lower canopy PAR from 15:00 – 17:00 for a north-northwest oriented slope located in the southern hemisphere.

As the peak time of PAR seems to be strongly related to the minimum value of CO_2 storage flux (Figure 20) and the maximum of sensible heat storage flux (Figure 22), which both occur at the same time, the slope aspect could strongly influence ecosystem energy and gas exchange. Potential effects of slope aspect and energy availability may also influence the diurnal patterns of wind (Figure 24). Although the peak of the diurnal wind data is approximately at noon, wind speed approaches its maximum value by 09:00 and reaches somewhat of a plateau for several hours (Figure 24). During this time period from 09:00 to 12:00, eddy fluxes of both CO_2 and LE (Figure 25) are at their highest values as well. As a result, considering a site's slope aspect could increase model accuracy of predicting land-atmosphere gas and energy exchange.

2.4.3 Response of Trace Gases to Precipitation, Wetting, and Drying Events

Frequent precipitation events are shown to have synergistic effects on gas exchange patterns at the site, with different combinations of gases, processes, and time scales leading to different effects. Diurnal variations in H_2O concentration considered against leaf wetness show how transpiration and evaporation of intercepted rainfall dominate vapor transfer at different times of day. Wetting events cause an increase in carbon dioxide concentrations regardless of the time of day, indicating that wetting has a stronger control on CO_2 than average diurnal fluctuation. Finally, change in water vapor concentrations with drying events was found to be less affected than hypothesized.

The two peak structure exhibited by the diurnal average H_2O data (Figure 21) shows two different influences that each increase water vapor concentration. The larger of the two peaks, occurring near midday, follows the same trend as the diurnal temperature data (Figure 22). As leaf wetness values tend to be lowest at midday (Figure 18), the increase in water vapor concentration is likely due to peak rates of transpiration that coincide with high levels of midday photosynthesis. This assertion follows the findings of Aparecido et al. (in review), who showed that sap flux at the site peaks at approximately noon and decreases substantially on days when the canopy is wet for much of the day. The sap flux data that they report do not explain the second peak in the H_2O data, however, which occurs in the evening at approximately 21:00 (Aparecido et al., in review). This peak is likely controlled primarily by evaporation of intercepted rainfall that frequently occurs in the afternoon. This pattern of afternoon wetting and then drying out can be seen from 15:00 to 21:00 in the diurnal leaf wetness plot (Figure 18).

It is interesting to note that the diurnal wind data (Figure 24) displays a similar two peak structure to that of the diurnal water vapor data. This similarity indicates the importance that wind speed plays in the transport of water vapor both through turbulent eddies and by advection. The wind speed data also helps to explain how the upper canopy is often able to dry out in the evening following a late afternoon or early evening wetting event. In the absence of available energy, wind is able to effectively dry the wet surfaces of these leaves higher up in the canopy, while the understory leaves tend to stay wet throughout the night.

The diurnal plots of the storage fluxes give us additional information about the diurnal profiles as the peaks and troughs in these plots inform us when the rate of change in the given variable reaches a maximum or minimum. The diurnal variations in each of the three storage fluxes (Figures 20-22) follow closely to the diurnal trends shown by Ohkubo et al. (2008) at a tropical forest site in Malaysia. The time of day when minimum and maximum values of both CO_2 concentration and CO_2 storage flux occur are the same between the Malaysia site and our observed data, even though the reported values of concentration and storage flux are greater in magnitude and variability (Ohkubo et al., 2008). Aubinet et al. (2005) note that storage fluxes can vary by an order of magnitude from site to site and report values of storage fluxes and vertical advection values that are comparable to those at our site (Figure 25.a), though the forests studied were not tropical.

These diurnal trends in the carbon data that appear both in Costa Rica and in Malaysia are significantly altered, however, by the onset of canopy wetness due to precipitation. CO_2 concentrations increased with canopy wetting across all times of day (Figure 26), even though the diurnal trend for carbon shows a decrease in concentration during morning and midday hours (Figure 20). From this deviation from the average pattern, we conclude that wetting events cause a rise in within-canopy CO_2 concentrations to the extent that wetting events are a stronger influence on hourly CO_2 values than the diurnal cycle is. Conversely, drying events do not seem to alter CO_2 concentration significantly from its average diurnal values.

The gain in CO_2 concentration with wetting indicates that photosynthesis must have decreased to the extent that plant respiration exceeded photosynthetic intake. This could be due to either the cloudy conditions brought on by a precipitation event or wet leaf surfaces causing stomata to close. Both this conclusion about CO_2 increasing with canopy wetting and the previous conclusion drawn about ET partitioning throughout the day point to the same modeling implication. Each of these observations note an ecosystem gas exchange phenomenon that is strongly influenced by the average timing of daily precipitation. For models that calculate rainfall sums on a monthly, weekly, or daily time step, varying effects of rainfall timing such as these cannot be captured. Similarly, if estimates of precise timing of precipitation are poor for a model with a smaller time step, these phenomena would be misrepresented as well. One possible solution would be to apply daily, weekly, or monthly average statistical distributions of precipitation occurrence to the precipitation sum for the time period, to randomly distribute rainfall over the period in a way that is representative of local conditions. To do this accurately, several years of precipitation data at a given location would be needed as input to the model.

2.4.4 Energy Availability, Humidity, and Their Effect on VPD

A comparison of the monthly patterns of VPD (Figure 17) to those of temperature (Figure 16) and H_2O concentration (Figure 15) is particularly noteworthy as the saturation vapor pressure component of VPD is a function of temperature and the actual vapor pressure is a function of moisture content in the air. Certain months, such as April and January, show similar patterns in VPD as they do in temperature, but other

months are completely different, with March, June, and August being the most notable (Figures 16-17). However, the pattern that exists from month to month in the VPD data is more similar to the H_2O data (Figures 15, 17). The water vapor concentrations are inversely related to VPD and both have their maximum and minimum peaks in March and June. The major difference, however, is that the H_2O monthly profiles only have one set of peaks, while the VPD monthly averages are bimodal. The VPD data follows the inverse trend of the H_2O data for all months except for September through January, where both sets of data decrease. During these months, the H_2O profiles decrease slightly while the temperature profiles decrease markedly and, thus, have a stronger effect on the VPD than does the water vapor concentration.

Temperature, VPD, and H_2O concentration, are also closely linked in the diurnal average data (Figures 21-23). Slightly before 06:00, H_2O, VPD, and temperature reach their daily minimums. As the morning progresses CO_2 concentration decreases as photosynthesis ensues while the other three quantities increase. At approximately 09:00, the associated storage fluxes with both CO_2 and H_2O reach their trough and peak, respectively, signaling the time of day when photosynthesis and subsequent transpiration is at a maximum. This occurs nearly an hour before the PAR and sensible heat storage fluxes hit their respective daily peaks, signaling the maximum light and energy inputs into the ecosystem. At approximately 13:00, temperature, VPD, and water vapor concentration reach their maximum daily values, with the CO_2 minimum following close behind at approximately 14:30. With the exception of a secondary peak in the H_2O

concentration profiles in the evening, the profiles return slowly to their pre-sunrise values.

The diurnal plots show a different picture than the monthly profile averages did concerning the relationship between temperature, H_2O, and VPD. While H_2O appeared more similar to VPD for the monthly plots, the temperature and VPD plots look almost identical in the diurnal profile data, suggesting that diurnal temperature variations play a larger role in determining diurnal VPD patterns than does H_2O concentration. Although H_2O concentration and VPD share the same peak and trough times in the diurnal data, the two are not inversely related like they were in the monthly data. An increase in H_2O concentration should cause a decrease in VPD so this is further evidence that daily fluctuations in VPD are controlled strongly by temperature and energy availability.

The temperature and VPD delta profiles (Figures 28-29), similarly to the temperature and VPD average diurnal profile plots, are almost identical in shape, variability, and trend versus time of day. Each set of profiles for these two variables show positive values at all heights for drying events in the morning, midday, and evening. This indicates that the change in available energy due to cloud cover going away during a drying event is a stronger influence on temperature and VPD than the evaporative cooling that occurs after a rain event. For nighttime events, however, we see that evaporative cooling does cause temperature changes to be negative while VPD changes are slightly positive due to sharp decreases in H_2O concentration (Figure 27).

These results, when taken together, suggest that H_2O concentration is the more dominant variable controlling VPD variation from month to month, whereas hourly VPD

is controlled more by temperature and available energy. Stated slightly differently, monthly average H_2O concentration is a better predictor of monthly VPD, while daily average temperature is a better predictor of daily VPD. This conclusion again leads to implication concerning time steps in the modeling scheme. When modeling fluxes of trace gases, influenced by VPD values, the best modeling scheme could depend on the time step. A monthly time step prediction of ecosystem exchange should be based more heavily on humidity, while a daily or weekly time step should be weighted more heavily towards energy availability.

2.5 Conclusions

The present study shows that the variability of and interrelationships between vertical profiles of micrometeorological variables in tropical forests provide insight on how to better model forest sub-canopy processes. The complex relationships that exist within the forest sub-canopy microclimate are further complicated when trying to couple in-canopy processes to processes that occur in the atmosphere or in the soil. Since land surface models are already being relied upon to provide accurate data concerning how soil, vegetation, and atmosphere interact, it is important to accurately represent the biophysical processes that are occurring by comparing modeled results to long-term sub-canopy microclimate data. The dataset presented here should be particularly useful for refining or validating land surface schemes that employ a multilevel canopy approach (e.g., Bonan et al., 2012; Drewry et al., 2010; Flerchinger et al., 2015; Pyles et al., 2000; Staudt et al., 2011).

Precipitation events, and the wet leaf surfaces and cloud cover that are inherently associated with them, have been shown to affect nearly every aspect of tropical forest micrometeorology. Rainfall amounts and timing are notoriously difficult to model because of the complex feedback systems that control rain events and the tremendous variability that exists in precipitation data at multiple time scales. Different patterns that emerged in the micrometeorological data between wet and dry months, as opposed to the patterns that emerged for single wetting and drying events, demonstrate that merely modeling accurate monthly rainfall sums is not sufficient to accurately model tropical forest microclimate. Modeled rainfall and related variables must be validated to ensure that diurnal average values are being represented as well.

Future work in tropical forest micrometeorology should include more studies that seek to couple soil gas exchange processes with lower canopy gas exchange because the sharpest gradients in the micrometeorological data tend to occur at the lowest heights in the profiles. Additionally, existing empirical models of meteorological variables need to be validated against long-term vertical profile data and new empirical models need to be developed for variables that do not have adequate models already. Long-term measurements in a variety of ecosystem types should be made going forward to inform these modeling efforts.

CHAPTER III

CONCLUSIONS

3.1 Summary of Findings

This study shows the degree to which micrometeorological variables in the sub-canopy of a tropical montane forest vary across multiple time scales and characterizes interrelationships between the different variables. Trends in the data were analyzed at seasonal, monthly, daily, and sub-daily scales to identify patterns that could lead to better understanding of and aid modeling efforts seeking to represent tropical forest microclimate processes. Rainfall and subsequent leaf wetness were shown to affect most micrometeorological processes at the site, indicating that significant error in modeled precipitation, even at sub-daily time steps, could change magnitude and direction of trace gas movements. Additionally, understory profile values closest to the forest floor showed the most extreme deviations from the rest of the profile, indicating that gas transport in the lower canopy is strongly linked to soil processes. Profile plots of all the variables studied maintained a similar shape across various times of day and months in the year. Because of this continuity, empirical equations could be fitted to the data to model sub-canopy profiles given certain weather conditions, or for data given at only one height in the canopy. Finally, slope aspect was shown to be an important characteristic of mountainous sites because PAR and CO_2 patterns seem to be affected by the different shading patterns that occur as a result of the direction the slope faces.

3.2 Directions for Future Research

Future areas of research for this field site could include analysis of both the eddy covariance and soil data that have been collected over the last 18 months in addition to the data that will be collected going forward. The eddy covariance data need to undergo a more sophisticated data processing routine and then can be further analyzed to build upon the results of this study. CO_2, LE, and sensible heat fluxes can be examined over multiple time scales and compared to selected datasets of eddy covariance data taken in the lower canopy and a nearby forest clearing. Sap flux data can be used in conjunction with the eddy covariance data to analyze ET partitioning, and these values can be compared to storage fluxes and calculated vertical advection.

Soil data analysis could include vertical soil profiles and spatial heterogeneity of temperature, volumetric water content, soil heat flux, and soil water potential. Additionally, soil respiration measurements have been taken in one location over several months as well as across over thirty locations at the study plot to characterize spatial heterogeneity and to give variation with elevation. These measurements could be analyzed alongside understory profile data and sap flux data to explore relationships between soil and understory processes. Other potential areas of study at the field site include: reorientation of intakes on the trace gas profile system to analyze horizontal gradients in CO_2 and H_2O concentrations, measurement of fog interception, and analysis of long-term variability in the vertical wind profile measurements.

In addition to study of more micrometeorological phenomena at the field site, modeling improvements should also be made. We aim to improve ET estimations in the

Community Land Model (CLM) land surface model by implementing observed tropical forest gas exchange patterns and by using data from the field site to do a preliminary calibration of the proposed model improvements. Some of the groundwork for this effort has already been completed, as the meteorological data to force the model has been organized and gap-filled. Additionally, a thorough review of how CLM currently models ET is provided in Appendix A. The results of this study in particular will be useful in the coming years to validate CLM model improvements that are currently underway in which a multi-level canopy modeling scheme is implemented (Bonan et al., 2012).

REFERENCES

Allen, R.G., Pereira, L.S., Howell, T.A. and Jensen, M.E., 2011. Evapotranspiration information reporting: I. Factors governing measurement accuracy. Agricultural Water Management, 98(6): 899-920, DOI: 10.1016/j.agwat.2010.12.015.

Aparecido, L.M.T., Miller, G.R., Cahill, A.T. and Moore, G.W., in review. Comparison of tree transpiration under wet and dry canopy conditions in a Costa Rican premontane tropical forest. Hydrological Processes.

Arya, P.S., 2001. Introduction to Micrometeorology, 79. Academic Press, San Diego, CA.

Asner, G.P., Scurlock, J.M. and A Hicke, J., 2003. Global synthesis of leaf area index observations: implications for ecological and remote sensing studies. Global Ecology and Biogeography, 12(3): 191-205, DOI: 10.1046/j.1466-822X.2003.00026.x.

Aubinet, M. et al., 2005. Comparing CO_2 storage and advection conditions at night at different CARBOEUROFLUX sites. Boundary-Layer Meteorol, 116(1): 63-93, DOI: 10.1007/s10546-004-7091-8.

Baldocchi, D., 1992. A Lagrangian random-walk model for simulating water vapor, CO_2 and sensible heat flux densities and scalar profiles over and within a soybean canopy. Boundary-Layer Meteorol, 61(1-2): 113-144, DOI: 10.1007/BF02033998.

Baldocchi, D. et al., 2001. FLUXNET: A new tool to study the temporal and spatial variability of ecosystem-scale carbon dioxide, water vapor, and energy flux densities. Bulletin of the American Meteorological Society, 82(11): 2415-2434, DOI: 10.1175/1520-0477(2001)082<2415:FANTTS>2.3.CO;2.

Baldocchi, D.D., 2003. Assessing the eddy covariance technique for evaluating carbon dioxide exchange rates of ecosystems: past, present and future. Global Change Biology, 9(4): 479-492, DOI: 10.1046/j.1365-2486.2003.00629.x.

Baldocchi, D.D., Vogel, C.A. and Hall, B., 1997. Seasonal variation of carbon dioxide exchange rates above and below a boreal jack pine forest. Agricultural and Forest Meteorology, 83(1): 147-170, DOI: 10.1007/BF00712525.

Beer, C. et al., 2010. Terrestrial gross carbon dioxide uptake: global distribution and covariation with climate. Science, 329(5993): 834-838, DOI: 10.1126/science.1184984.

Bonan, G.B., 2008. Forests and climate change: forcings, feedbacks, and the climate benefits of forests. Science, 320(5882): 1444-9, DOI: 10.1126/science.1155121.

Bonan, G.B., Oleson, K.W., Fisher, R.A., Lasslop, G. and Reichstein, M., 2012. Reconciling leaf physiological traits and canopy flux data: Use of the TRY and FLUXNET databases in the Community Land Model version 4. Journal of Geophysical Research: Biogeosciences (2005–2012), 117(G2), DOI: 10.1029/2011JG001913.

Brunet, Y., Finnigan, J. and Raupach, M., 1994. A wind tunnel study of air flow in waving wheat: single-point velocity statistics. Boundary-Layer Meteorol, 70(1-2): 95-132, DOI: 10.1007/BF00712525.

Buchmann, N. and Ehleringer, J.R., 1998. CO_2 concentration profiles, and carbon and oxygen isotopes in C 3 and C 4 crop canopies. Agricultural and Forest Meteorology, 89(1): 45-58, DOI: 10.1016/S0168-1923(97)00059-2.

Choudhury, B.J. et al., 1998. A biophysical process-based estimate of global land surface evaporation using satellite and ancillary data II. Regional and global patterns of seasonal and annual variations. Journal of Hydrology, 205(3–4): 186-204, DOI: 10.1016/S0022-1694(97)00147-9.

Chu, H.-S. et al., 2014. Does canopy wetness matter? Evapotranspiration from a subtropical montane cloud forest in Taiwan. Hydrological Processes, 28(3): 1190-1214, DOI: 10.1002/hyp.9662.

Clark, D.A., 2007. Detecting Tropical Forests' Responses to Global Climatic and Atmospheric Change: Current Challenges and a Way Forward. Biotropica, 39(1): 4-19, DOI: 10.1111/j.1744-7429.2006.00227.x.

Daikoku, K. et al., 2007. Impact of wind direction on diurnal and seasonal changes in wind profiles. Journal of Forest Research, 12(6): 452-466, DOI: 10.1007/s10310-007-0034-8.

Dang, Q.L. et al., 1997. Profiles of photosynthetically active radiation, nitrogen and photosynthetic capacity in the boreal forest: Implications for scaling from leaf to canopy. Journal of Geophysical Research: Atmospheres, 102(D24): 28845-28859, DOI: 10.1029/97JD00194.

Dietz, J., Leuschner, C., Hölscher, D. and Kreilein, H., 2007. Vertical patterns and duration of surface wetness in an old-growth tropical montane forest, Indonesia. Flora - Morphology, Distribution, Functional Ecology of Plants, 202(2): 111-117, DOI: 10.1016/j.flora.2006.03.004.

Drewry, D.T. et al., 2010. Ecohydrological responses of dense canopies to environmental variability: 1. Interplay between vertical structure and photosynthetic pathway. Journal of Geophysical Research. Biogeosciences, 115(4), DOI: 10.1029/2010JG001340.

Fisher, J.B., Baldocchi, D.D., Misson, L., Dawson, T.E. and Goldstein, A.H., 2007. What the towers don't see at night: nocturnal sap flow in trees and shrubs at two AmeriFlux sites in California. Tree Physiology, 27(4): 597-610, DOI: 10.1093/treephys/27.4.597.

Fisher, J.B. et al., 2009. The land–atmosphere water flux in the tropics. Global Change Biology, 15(11): 2694-2714, DOI: 10.1111/j.1365-2486.2008.01813.x.

Fisher, J.B., Tu, K.P. and Baldocchi, D.D., 2008. Global estimates of the land–atmosphere water flux based on monthly AVHRR and ISLSCP-II data, validated at 16 FLUXNET sites. Remote Sensing of Environment, 112(3): 901-919, DOI: 10.1016/j.rse.2007.06.025.

Flerchinger, G.N., Reba, M.L., Link, T.E. and Marks, D., 2015. Modeling temperature and humidity profiles within forest canopies. Agricultural and Forest Meteorology, 213: 251-262, DOI: 10.1016/j.agrformet.2015.07.007.

Giambelluca, T. et al., 2009. Evapotranspiration and energy balance of native wet montane cloud forest in Hawai‘i. Agricultural and Forest Meteorology, 149(2): 230-243, DOI: 10.1016/j.agrformet.2008.08.004.

Granier, A., 1987. Evaluation of transpiration in a Douglas-fir stand by means of sap flow measurements. Tree Physiology, 3(4): 309-320.

Hasler, N. and Avissar, R., 2007. What Controls Evapotranspiration in the Amazon Basin? Journal of Hydrometeorology, 8(3): 380-395, DOI: 10.1175/JHM587.1.

Hogg, E.H. et al., 1997. A comparison of sap flow and eddy fluxes of water vapor from a boreal deciduous forest. Journal of Geophysical Research, 102(D24): 28929, DOI: 10.1029/96jd03881.

Jonckheere, I. et al., 2004. Review of methods for in situ leaf area index determination: Part I. Theories, sensors and hemispherical photography. Agricultural and Forest Meteorology, 121(1): 19-35, DOI: 10.1016/j.agrformet.2003.08.027.

Juárez, R.I.N., Hodnett, M.G., Fu, R., Goulden, M.L. and von Randow, C., 2007. Control of Dry Season Evapotranspiration over the Amazonian Forest as Inferred from Observations at a Southern Amazon Forest Site. Journal of Climate, 20(12): 2827-2839, DOI: 10.1175/JCLI4184.1.

Kang, M., Kwon, H., Cheon, J.H. and Kim, J., 2012. On Estimating Wet Canopy Evaporation from Deciduous and Coniferous Forests in the Asian Monsoon Climate. Journal of Hydrometeorology, 13(3): 950-965, DOI: 10.1175/JHM-D-11-07.1.

Katul, G. et al., 1997. A Lagrangian dispersion model for predicting CO_2 sources, sinks, and fluxes in a uniform loblolly pine (Pinus taeda L.) stand. Journal of Geophysical Research: Atmospheres, 102(D8): 9309-9321, DOI: 10.1029/96JD03785.

Katul, G.G. and Chang, W.H., 1999. Principal length scales in second-order closure models for canopy turbulence. Journal of Applied Meteorology, 38(11): 1631-1643, DOI: 10.1175/1520-0450(1999)038<1631:PLSISO>2.0.CO;2.

Kenzo, T. et al., 2015. Height-related changes in leaf photosynthetic traits in diverse Bornean tropical rain forest trees. Oecologia, 177(1): 191-202, DOI: 10.1007/s00442-014-3126-0.

Kosugi, Y., Takanashi, S., Yokoyama, N., Philip, E. and Kamakura, M., 2012. Vertical variation in leaf gas exchange parameters for a Southeast Asian tropical rainforest in Peninsular Malaysia. Journal of Plant Research, 125(6): 735-748, DOI: 10.1007/s10265-012-0495-5.

Kumagai, T.O. et al., 2001. Vertical profiles of environmental factors within tropical rainforest, Lambir Hills National Park, Sarawak, Malaysia. Journal of Forest Research, 6(4): 257-264, DOI: 10.1007/BF02762466.

Lai, C.-T., Katul, G., Ellsworth, D. and Oren, R., 2000. Modelling vegetation-atmosphere CO_2 exchange by a coupled Eulerian-Langrangian approach. Boundary-Layer Meteorol, 95(1): 91-122, DOI: 10.1023/A:1002473906184.

Lawrence, P.J. and Chase, T.N., 2007. Representing a new MODIS consistent land surface in the Community Land Model (CLM 3.0). Journal of Geophysical Research: Biogeosciences (2005–2012), 112(G1), DOI: 10.1029/2006JG000168.

Lee, X. and Black, T.A., 1993. Atmospheric turbulence within and above a Douglas-fir stand. Part II: Eddy fluxes of sensible heat and water vapour. Boundary-Layer Meteorol, 64(4): 369-389, DOI: 10.1007/BF00711706.

List, R.J., 1971. Smithsonian Meteorological Tables. Smithsonian Institution Press, Washington DC.

Lloyd, J. et al., 2010. Optimisation of photosynthetic carbon gain and within-canopy gradients of associated foliar traits for Amazon forest trees. Biogeosciences, 7(6): 1833-1859, DOI: 10.5194/bg-7-1833-2010.

Loescher, H.W., Gholz, H.L., Jacobs, J.M. and Oberbauer, S.F., 2005. Energy dynamics and modeled evapotranspiration from a wet tropical forest in Costa Rica. Journal of Hydrology, 315(1–4): 274-294, DOI: 10.1016/j.jhydrol.2005.03.040.

Macdonald, R., 2000. Modelling the mean velocity profile in the urban canopy layer. Boundary-Layer Meteorol, 97(1): 25-45, DOI: 10.1023/A:1002785830512.

Mahrt, L., Lee, X., Black, A., Neumann, H. and Staebler, R., 2000. Nocturnal mixing in a forest subcanopy. Agricultural and Forest Meteorology, 101(1): 67-78, DOI: 10.1002/qj.49709640708.

Malhi, Y. et al., 2002. Energy and water dynamics of a central Amazonian rain forest. Journal of Geophysical Research: Atmospheres, 107(D20): LBA 45-1-LBA 45-17, DOI: 10.1029/2001JD000623.

McCree, K.J., 1981. Photosynthetically active radiation, Physiological Plant Ecology I. Springer, Berlin, Germany, pp. 41-55.

Moore, G.W., Cleverly, J.R. and Owens, M.K., 2008. Nocturnal transpiration in riparian Tamarix thickets authenticated by sap flux, eddy covariance and leaf gas exchange measurements. Tree Physiology, 28(4): 521-528, DOI: 10.1093/treephys/28.4.521.

Motzer, T., 2005. Micrometeorological aspects of a tropical mountain forest. Agricultural and Forest Meteorology, 135(1–4): 230-240, DOI: 10.1016/j.agrformet.2005.11.019.

Myneni, R. et al., 2002. Global products of vegetation leaf area and fraction absorbed PAR from year one of MODIS data. Remote Sensing of Environment, 83(1): 214-231, DOI: 10.1016/S0034-4257(02)00074-3.

Numaguti, A., 1993. Dynamics and Energy Balance of the Hadley Circulation and the Tropical Precipitation Zones: Significance of the Distribution of Evaporation. Journal of the Atmospheric Sciences, 50(13): 1874-1887, DOI: 10.1175/1520-0469(1993)050<1874:DAEBOT>2.0.CO;2.

Ohkubo, S. et al., 2008. Vertical profiles and storage fluxes of CO_2, heat and water in a tropical rainforest at Pasoh, Peninsular Malaysia. Tellus B, 60(4): 569-582, DOI: 10.1111/j.1600-0889.2008.00367.x.

Oleson, K. et al., 2013. Technical Description of version 4.5 of the Community Land Model (CLM). 420, DOI: 10.5065/D6RR1W7M.

Oliver, H., 1971. Wind profiles in and above a forest canopy. Quarterly Journal of the Royal Meteorological Society, 97(414): 548-553, DOI: 10.1002/qj.49709741414.

Porporato, A., D'Odorico, P., Laio, F., Ridolfi, L. and Rodriguez-Iturbe, I., 2002. Ecohydrology of water-controlled ecosystems. Advances in Water Resources, 25(8–12): 1335-1348, DOI: 10.1016/S0309-1708(02)00058-1.

Pyles, R.D., Weare, B.C. and Pawu, K.T., 2000. The UCD advanced canopy-atmosphere-soil algorithm: Comparisons with observations from different climate and vegetation regimes. Quarterly Journal of the Royal Meteorological Society, 126(569): 2951-2980, DOI: 10.1002/qj.49712656917.

Raupach, M.R., Finnigan, J. and Brunei, Y., 1996. Coherent eddies and turbulence in vegetation canopies: the mixing-layer analogy. Boundary-Layer Meteorol, 78(3-4): 351-382, DOI: 10.1007/BF00120941.

Roberts, J. et al., 1993. Transpiration from an Amazonian rainforest calculated from stomatal conductance measurements. Agricultural and Forest Meteorology, 65(3): 175-196, DOI: 10.1016/0168-1923(93)90003-Z.

Scatena, F.N., Bruijnzeel, L.A., Bubb, P. and Das, S., 2010. Setting the stage. In: L.A. Bruijnzeel, Scatena, F.N., Hamilton, L.S. (Eds.), Tropical Montane Cloud Forests: Science for Conservation and Management. International Hydrology Series. Cambridge University Press, Cambridge, UK.

Shaw, R.H. and Schumann, U., 1992. Large-eddy simulation of turbulent flow above and within a forest. Boundary-Layer Meteorol, 61(1-2): 47-64, DOI: 10.1007/BF02033994.

Shen, S. and Leclerc, M.Y., 1997. Modelling the turbulence structure in the canopy layer. Agricultural and Forest Meteorology, 87(1): 3-25, DOI: 10.1002/qj.49709640708.

Shuttleworth, W. et al., 1989. Micrometeorology of temperate and tropical forest [and discussion]. Philosophical Transactions of the Royal Society of London B: Biological Sciences, 324(1223): 299-334, DOI: 10.1098/rstb.1989.0050.

Smith, D. and Allen, S., 1996. Measurement of sap flow in plant stems. Journal of Experimental Botany, 47(12): 1833-1844, DOI: 10.1093/jxb/47.12.1833.

Staudt, K., Serafimovich, A., Siebicke, L., Pyles, R.D. and Falge, E., 2011. Vertical structure of evapotranspiration at a forest site (a case study). Agricultural and Forest Meteorology, 151(6): 709-729, DOI: 10.1016/j.agrformet.2010.10.009.

Teale, N.G. et al., 2014. Impacts of Vegetation and Precipitation on Throughfall Heterogeneity in a Tropical Pre-Montane Transitional Cloud Forest. Biotropica, 46(6): 667-676, DOI: 10.1111/btp.12166.

Wang, W. and Yi, C., 2012. A new nonlinear analytical model for canopy flow over a forested hill. Theoretical and Applied Climatology, 109(3-4): 549-563, DOI: 10.1007/s00704-012-0599-9.

Webb, E.K., 1970. Profile relationships: The log-linear range, and extension to strong stability. Quarterly Journal of the Royal Meteorological Society, 96(407): 67-90, DOI: 10.1002/qj.49709640708.

Werth, D. and Avissar, R., 2004. The Regional Evapotranspiration of the Amazon. Journal of Hydrometeorology, 5(1): 100-109, DOI: 10.1175/1525-7541(2004)005<0100:TREOTA>2.0.CO;2.

Williams, D. et al., 2004. Evapotranspiration components determined by stable isotope, sap flow and eddy covariance techniques. Agricultural and Forest Meteorology, 125(3): 241-258, DOI: 10.1016/j.agrformet.2004.04.008.

Wilson, K. et al., 2002. Energy balance closure at FLUXNET sites. Agricultural and Forest Meteorology, 113(1): 223-243, DOI: 10.1016/S0168-1923(02)00109-0.

Wilson, K.B., Hanson, P.J., Mulholland, P.J., Baldocchi, D.D. and Wullschleger, S.D., 2001. A comparison of methods for determining forest evapotranspiration and its components: sap-flow, soil water budget, eddy covariance and catchment water balance. Agricultural and forest Meteorology, 106(2): 153-168, DOI: 10.1016/S0168-1923(00)00199-4.

Xiao, W., Yu, Q., Flerchinger, G.N. and Zheng, Y., 2006. Evaluation of SHAW model in simulating energy balance, leaf temperature, and micrometeorological variables within a maize canopy. Agronomy Journal, 98(3): 722-729, DOI: 10.2134/agronj2005.0126.

Yasuda, Y. et al., 2003. Measurement of CO_2 flux above a tropical rain forest at Pasoh in Peninsular Malaysia. Agricultural and Forest Meteorology, 114(3): 235-244, DOI: 10.1016/S0168-1923(02)00198-3.

Zeng, X., Zhao, M. and Dickinson, R.E., 1998. Intercomparison of bulk aerodynamic algorithms for the computation of sea surface fluxes using TOGA COARE and TAO data. Journal of Climate, 11(10): 2628-2644, DOI: 10.1175/1520-0442(1998)011<2628:IOBAAF>2.0.CO;2.

Zhang, K., Kimball, J.S., Nemani, R.R. and Running, S.W., 2010. A continuous satellite-derived global record of land surface evapotranspiration from 1983 to 2006. Water Resources Research, 46(9), DOI: 10.1029/2009WR008800.

APPENDIX A

HOW CLM4.5 CALCULATES EVAPOTRANSPIRATION

Numerous equations and parameters play a role in the workflow that version 4.5 of the Community Land Model (CLM4.5 or CLM) uses to calculate evapotranspiration (ET). This appendix is provided to go through that workflow systematically, with emphasis on its application for tropical forests. Most of the information contained herein is summarized from the CLM4.5 Technical Description (Oleson et al., 2013). For a full methodology and list of equations describing the ET module, see Chapter 5 of the Technical Description.

Model Structure

Grid cells are the building blocks of CLM4.5 and are composed of land units. Land units can represent many different land types that may coexist in a particular grid cell, and can represent urban, agricultural, naturally vegetated, surface water, or bare land cover. Each land unit can contain multiple columns, which contain data that change with height, such as with depth in a lake or in the subsurface. Furthermore, columns within land units can also contain plant functional types (PFTs) representing broad categories of plants that are present at the location. Each PFT has a set of parameters that are used in equations when that particular PFT is present. The primary PFT that makes up tropical forests is Broadleaf Evergreen Tree (BET) – Tropical, and a selection of its parameters is given in Table A-1.

Table A-1: Tropical broadleaf evergreen forest PFT parameters in CLM4.5.

Parameter	Value
Height of Canopy Top, z_{top} (m)	35
Height of Canopy Bottom, z_{bot} (m)	1
Leaf Angle Distribution (χ_L) (1=horz, -1=vert)	0.1
Ratio of Momentum Roughness Length to Canopy Height, R_{z0m}	0.075
Ratio of Displacement Height to Canopy Height, R_d	0.67
Characteristic Dimension of Leaves in Direction of Wind Flow, d_{leaf} (m)	0.04
Parameter used to calculate stomatal resistance, *m*	9

In addition to canopy top height and canopy bottom height, which are PFT-dependent parameters, leaf area index (LAI) and stem area index (SAI) are also needed to define the vegetation structure in a land unit. Monthly LAI values that were developed from 1-km MODIS data as described in Lawrence and Chase (2007) form the basis for all LAI and SAI values used in the model. Percent PFT data over the Earth's land surface is also presented in the aforementioned paper.

Model Atmospheric Forcing and Initial Conditions

Atmospheric data drives or forces each module of the CLM4.5 model. Where the model gets this meteorological data can vary however. CLM can be coupled with the Community Earth System Model's (CESM) atmospheric model that can provide modeled forcing data. CESM also comes with two global meteorological data sets that can be used to force a CLM run. The final option is to supply the model with observed atmospheric data at the location to be modeled. This option gives the most accurate atmospheric forcing data and is the method that will be used for the model runs in this

project. In addition to atmospheric data, CLM also requires a set of initial conditions to begin a run. These can come from an arbitrary set of initial conditions stored in the code, a user supplied set of initial conditions, or from a continuation of another CLM run. The model may need to iterate over a long time period so that the parameters have time to equilibrate.

Parameters Supplied by Other CLM Modules

The portion of the model that calculates ET also relies on input from many other parts of the model to supply parameters used to solve its equations. The subsurface module (ch. 6 of Technical Description) provides humidity and temperature values at the ground surface as well as soil moisture "beta" parameters. The hydrology module (ch. 7 of Technical Description) supplies a parameter to specify what percentage of the canopy is wet at a given time as well as various parameters related to snow and surface water coverage. Sunlit and shaded leaf area indices come from the radiative fluxes module (ch. 4 of Technical Description). Finally, stomatal resistances for sunny and shaded conditions are calculated in the photosynthesis module (ch. 8 of Technical Desciption). Since each module iterates independently of the other modules at a given time step, parameters passed to the ET module from other modules may be from the previous time step.

State Variables and Heights

When considering evaporative fluxes in vegetated grid cells, CLM stores state variables for four different spatial locations. Temperature and humidity are the two state variables that are of primary importance at each of these locations. The first location is

at the vegetation, while the other three are specified as heights from the ground: atmosphere, canopy surface, and ground (Figure A-1). The atmospheric height is the height at which all variables from the atmospheric model or meteorological forcing data is considered to occur at. By default, this height is 30 m above the ground, although the height can be modified when using user-supplied forcing data. The canopy surface height is defined as the apparent sink for water vapor within the canopy. The canopy surface height, z_s, is equal to the sum of the vegetation displacement height, d, and roughness length, z_{0w}. Each of these two parameters is a function of canopy plant height and is adjusted for canopy density. The height for ground parameters is determined by another roughness length value. The three evaporative fluxes that the model calculates all occur between these four locations as shown in Figure A-1.

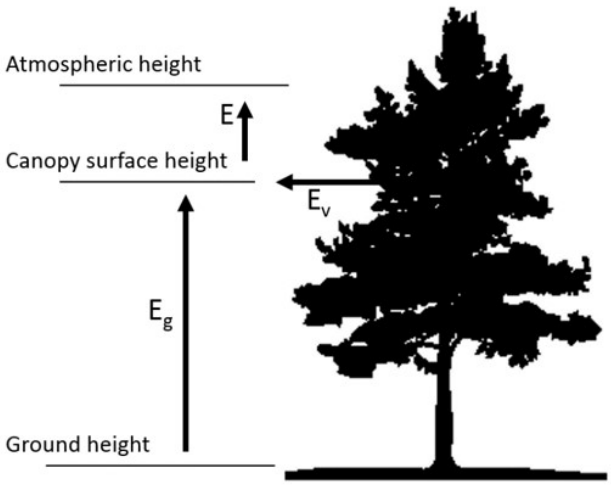

Figure A-1: Heights in the canopy as considered by CLM4.5.

Equations to Calculate Evapotranspiration

Since the air within the canopy is assumed by the model to have negligible capacity to store water, the three fluxes shown in Figure A-1 must balance one another:

$$E = E_v + E_g$$

In the above equation, E, E_v, and E_g are the water vapor fluxes (kg m^{-2} s^{-1}) between surface and atmosphere, vegetation and surface, and ground and surface respectively. Each of these evaporative fluxes is calculated using the same generalized equation:

$$E = -\rho_{atm} \frac{\Delta q}{r}$$

where ρ_{atm} is atmospheric air density (kg m^{-3}), Δq is a difference in specific humidity between two points, and r is a resistance value (s m^{-1}). Specific equations for each of the different evaporative fluxes will be given below, along with equations for each of the resistance values, once the resistance network has been explained in detail.

Monin-Obukhov Theory

In order to understand the resistance terms that will be presented in the following section, it is important to first develop some of the Monin-Obukhov Similarity Theory (MOST) that is prevalent in the resistance equations. MOST quantifies the effects of atmospheric stability in the atmospheric boundary layer, i.e. the density variations in the air as a function of height. The theory states that mean profiles of wind speed, temperature and humidity depend on unique functions of the dimensionless height variable, ζ, defined as:

$$\zeta = \frac{z - d}{L}$$

where z is height in the surface layer (m), d is displacement height (m), and L is the Obukhov length (m), a ratio of shear turbulence to convective turbulence. The Obukhov length is defined as:

$$L = \frac{u_*^2 \, mean(\theta_{v,atm})}{kg\theta_{v*}}$$

where $u*$ is the friction velocity (m s^{-1}), $\theta_{v,atm}$ is the reference virtual potential temperature (K) (, k is von Karman's constant (~ 0.4), g is gravitational acceleration (m s^{-2}), and θ_{v*} is the temperature scale (K). The unique function of ζ for the mean humidity profile, φ_w, is given as:

$$\frac{k\,(z - d)}{q_*}\,\frac{\partial q}{\partial z} = \Phi_w(\zeta)$$

where $q*$ is a moisture scale (kg kg^{-1}), and the partial derivative gives the gradient of specific humidity (kg kg^{-1}) with height. The moisture scale, $q*$, and the friction velocity, $u*$, are defined next:

$$q_* u_* = -\frac{E}{\rho_{atm}}$$

$$u_*^2 = \frac{|\tau|}{\rho_{atm}}$$

where τ is the shearing stress (kg m^{-1} s^{-2}). When integrated between two arbitrary heights in the surface layer – for our purposes we will choose the atmospheric and canopy surface heights, $z_{atm,w}$ and z_s, the differential equation for φ_w becomes:

$$q_{atm} - q_s = \frac{q_*}{k}\left[\ln\left(\frac{z_{atm,w} - d}{z_{0w}}\right) - \psi_w\left(\frac{z_{atm,w} - d}{L}\right) + \psi_w\left(\frac{z_{0w}}{L}\right)\right]$$

where q_{atm} and q_s give the specific humidity (kg kg^{-1}) at the atmospheric height and canopy surface height respectively, z_{0w} is the roughness length (m) for water vapor, and the function ψ_w is defined as:

$$\psi_w(\zeta) = \int_{z_{0w}/L}^{\zeta} \frac{[1 - \phi_w(x)]}{x} dx \, .$$

The model uses empirical flux gradient relationships from Zeng et al. (1998), that can be integrated to give specific humidity profiles for different stability conditions. Using the definitions of u^* and q^*, these equations can be iteratively solved for water vapor flux using surface and atmospheric values of specific humidity, except that the Obukhov length is also a function of u^* and q^*. The bulk Richardson number, related to ζ as in Arya (2001), is used to give a first guess for ζ and then L, beginning the iteration process. The numerical implementation of the MOST equations in the model will be further outlined below.

The Resistance Network

The resistance schematic given in the Technical Description details the resistance values used to calculate each of the three evaporation fluxes. This schematic will be examined at length by presenting the equations for each evaporative flux and resistance (Figure A-2).

When iteratively solving the specific humidity profile from MOST between canopy surface and atmospheric height, the result is evaporative flux in the general form as presented above:

$$E = -\rho_{atm} \frac{(q_{atm} - q_s)}{r_{aw}}$$

where r_{aw} is the aerodynamic resistance to water vapor transfer (s m^{-1}). This resistance term accounts for atmospheric stability and it is defined as:

$$r_{aw} = \frac{q_{atm} - q_s}{q_* u_*} = \frac{1}{k^2 V_a}\left[\ln\left(\frac{z_{atm,m} - d}{z_{0m}}\right) - \psi_m\left(\frac{z_{atm,m} - d}{L}\right) + \psi_m\left(\frac{z_{0m}}{L}\right)\right]$$
$$\left[\ln\left(\frac{z_{atm,w} - d}{z_{0w}}\right) - \psi_w\left(\frac{z_{atm,w} - d}{L}\right) + \psi_w\left(\frac{z_{0w}}{L}\right)\right]$$

where V_a is atmospheric wind speed (m s^{-1}), and the subscript *m* denotes parameters associated with momentum rather than water vapor (subscript *w*). A full set of the MOST equations, including those corresponding to momentum and temperature can be found in Section 5.1 of the Technical Description.

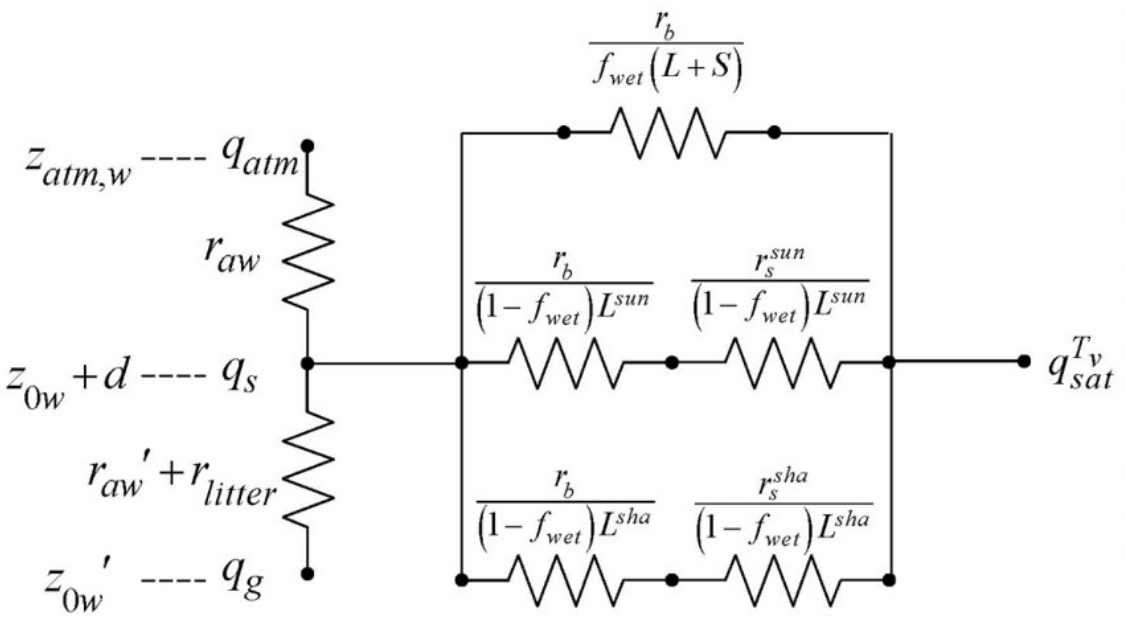

Figure A-2: Resistance model for water vapor fluxes from vegetated surfaces, from Oleson et al. (2013).

The next evaporative flux term to note is E_g, the ET from the ground surface to the canopy surface (between q_g and q_s). The resistance to this flux has a component accounting for aerodynamic resistance, r_{aw}', and a component accounting for resistance due to the litter layer, r_{litter}. The ground ET flux equation and both resistance terms are given as:

$$E_g = -\rho_{atm} \frac{\beta_{soi} (q_s - q_g)}{r_{aw}' + r_{litter}}$$

$$r_{aw}' = \frac{1}{C_s U_{av}}$$

$$r_{litter} = \frac{1}{0.004 u_*} \left(1 - e^{-L_{litter}^{eff}}\right)$$

where β_{soi} is a unitless parameter which can range from 0 – 1 that accounts for soil moisture, C_s is a turbulent transfer coefficient between the soil and the canopy air, U_{av} is the incident wind velocity on the leaf surface (m s^{-1}), and L^{eff}_{litter} is the effective litter index, set to 0.5 (m^2 m^{-2}) in the absence of snow.

The final flux depicted in the resistance network diagram is the evaporative flux from vegetation to canopy air. This flux represents both transpiration and evaporation from a wet surface in the canopy. The equation for this flux is:

$$E_v = -\rho_{atm} \frac{(q_s - q_{sat}^{T_v})}{r_{total}}$$

where q^{Tv}_{sat} is the saturated specific humidity (kg kg^{-1}) at the vegetation temperature, T_v, and r_{total} represents the combined resistance (s m^{-1}) of the three-path resistance structure connecting q_s and q^{Tv}_{sat} in Figure A-2.

The top branch of that resistance structure, which we will call r_1, represents resistance to evaporation of a wet leaf surface in the canopy and is described by the equation:

$$r_1 = \frac{r_b}{f_{wet}(L+S)}$$

where r_b is the resistance of the leaf boundary layer (s m^{-1}), f_{wet} is the fraction of the canopy that is wetted, and L and S are the leaf area index (LAI) and steam area index (SAI) respectively. The equation for the leaf boundary layer resistance is:

$$r_b = \frac{1}{C_v}\left(U_{av}/d_{leaf}\right)^{-1/2}$$

where C_v is the turbulent transfer coefficient between the canopy and the canopy air, set to a value of 0.01 m $s^{-1/2}$, and d_{leaf} is the characteristic dimension of the leaves in the direction of wind flow, a PFT-specific parameter (Table A-1).

The second and third branches of the resistance structure between the vegetation and canopy air space (r_2 and r_3) represent transpiration in sunny and shaded conditions respectively. The equations for each are given as:

$$r_2 = \frac{r_b + r_s^{sun}}{(1-f_{wet})L^{sun}}$$

$$r_3 = \frac{r_b + r_s^{sha}}{(1-f_{wet})L^{sha}}$$

where r_s^{sun} and r_s^{sha} are the stomatal resistances under sunny and shaded conditions respectively, and L^{sun} and L^{sha} are the sunny and shaded leaf area indices respectively. The sum of these two indices must always equal the sum of the LAI and SAI. The stomatal resistance is calculated as:

$$\frac{1}{r_s} = m\frac{A_n}{c_s/P_{atm}}h_s + b\beta_t$$

where m is a PFT-dependent parameter (Table A-1), A_n is leaf net photosynthesis of CO_2 (μmol m^{-2} s^{-1}), c_s is the leaf surface CO_2 partial pressure (Pa), P_{atm} is the atmospheric pressure (Pa), h_s is the leaf surface humidity, b is the minimum stomatal conductance (10,000 μmol m^{-2} s^{-1}), and β_t is a soil water stress function ranging from 0 – 1. The only difference between sunny and shaded stomatal resistance is the calculation of net photosynthesis (see Section 8.2 of the Technical Description for more on photosynthesis calculation).

When each of the three resistances in parallel are combined, the equation for r_{total} is as follows:

$$r_{total} = \frac{r_1 r_2 r_3}{r_1 r_2 + r_1 r_3 + r_2 r_3}.$$

Numerical Implementation

The algorithm that the model uses to calculate evaporative fluxes begins by making an estimate of the state variables at the canopy surface height, by averaging temperature and humidity between the ground and atmospheric levels. Next an initial guess at the atmospheric wind velocity is made using an initial value of convective velocity based on an initial stability check. Then an initial guess of the Obukhov length is made based off of the Richardson number. After that, iteration begins on a large system of equations including most of the variables used in the ET module. The system of equations includes equations for: friction velocity, temperature and humidity scales, all aerodynamic resistances, wind velocity incident on leaves, leaf boundary layer

resistance, stomatal resistances, conductances for sensible and latent heat, latent and sensible heat fluxes from the vegetation, vegetation temperature, saturated vapor pressure and humidity at the leaf surface, new values for canopy air temperature and humidity, temperature and specific humidity differences, a new wind speed including convective velocity, and a new Obukhov length. The iteration is stopped after two or more steps if the changes in vegetation temperature and latent heat flux are small enough, or once forty iterations have been completed. Once iteration is complete, the momentum fluxes and sensible and latent heat fluxes from the ground are computed using final parameters. The final value of ET is then obtained by adding together evaporative fluxes from the ground and from the vegetation.

APPENDIX B

MATLAB CODES FOR DATA PROCESSING AND QUALITY CONTROL

Soltis_Data_Plotter_10_04_15_to_10_10_15.m

```
%% Created by Ryan Andrews

clear; clc;

%% User Inputs

%Generic Inputs
days=7; %number of days to plot data for
Month_days=31; %user inputs number of days in starting
month
date_title=' from 10/4/15 to 10/10/15';
startdate='10_04';
concat=0; % =1 if files need to be concatenated, =0 if
already concat
bad_data_plot=0; % =1 if you want plots of all sensors, =0
to not have
% plots skewed by bad data

%Spire Inputs
colspire=19; %number of columns in spire files
Spire_String_1='Soltis_Spire_2015_'; %forms first part of
spire file
Spire_String_2='_0015.dat'; %forms second part of spire
file
Spire_Date_Start=startdate; %user inputs first date of
spire data in str
spire_dpph=288; %user inputs spire data points per hour
Spire_File=strcat(Spire_String_1,Spire_Date_Start,Spire_Str
ing_2); %first
%spire file name
nrad_title=strcat('Net Radiation',date_title); %user inputs
%the title for the net radiation plot
irt_title=strcat('IRT Leaf Temperature',date_title); %user
inputs
%the title for the IRT plot

%UpperData Inputs
```

```
colUD=47; %number of columns in UD files
UD_String_1='Soltis_Upper_2015_'; %forms first part of UD
file
UD_String_2='_0010.dat'; %forms second part of UD file
UD_Date_Start=startdate; %user inputs first date of upper
data in string
UD_dpph=288; %user inputs spire data points per hour
UD_File=strcat(UD_String_1,UD_Date_Start,UD_String_2);
%first
%UD file name
LW_title=strcat('Leaf Wetness',date_title); %user inputs
%the title for the leaf wetness plot
PAR_title=...
    strcat('Photosynthetically Active Radiation
(PAR)',date_title);
%user inputs the title for the PAR plot
AT_title=strcat('Air Temperature',date_title); %user inputs
%the title for the air temp plot
RH_title=strcat('Relative Humidity',date_title); %user
inputs
%the title for the rel humidity plot

%GroundData Inputs
colGD=43; %number of columns in GD files
GD_String_1='Soltis_Ground_2015_'; %forms first part of GD
file
GD_String_2='_0005.dat'; %forms second part of GD file
GD_Date_Start=startdate; %user inputs first date of GD data
in string
GD_dpph=288; %user inputs GD data points per hour
GD_File=strcat(GD_String_1,GD_Date_Start,GD_String_2);
%first
%GD file name
G_title=strcat('Soil Heat Flux',date_title); %user inputs
%the title for the soil heat flux plot
VWC_title=strcat('Volumetric Water Content',date_title);
%user inputs
%the title for the VWC plot
soiltemp_title=strcat('Soil Temperature',date_title); %user
inputs
%the title for the soil temp plot

%George_IntAvg (AP200) Inputs
colAP=71; %number of columns in AP200 files
```

```
AP_String_1='Soltis_George_IntAvg_2015_'; %forms first part
of AP200 file
AP_String_2='_0030.dat'; %forms second part of AP200 file
AP_Date_Start=startdate; %user inputs first date of AP200
data in string
AP_dpph=48; %user inputs AP200 data points per hour
AP_File=strcat(AP_String_1,AP_Date_Start,AP_String_2);
%first
%AP file name
CO2_title=strcat('Carbon Dioxide
Concentration',date_title); %user
%inputs the title for the CO2 plot
H2O_title=strcat('Water Vapor Concentration',date_title);
%user
%inputs the title for the H2O plot
Flow_title=strcat('AP200 Sample Intake
Flowrates',date_title); %user
%inputs the title for the Flow plot
VPD_title=strcat('Vapor Pressure Deficit',date_title);

%Sagui_SF (Sapflow) Inputs
colSF=68; %number of columns in SF files
SF_String_1='Soltis_Sagui_SF_2015_'; %forms first part of
SF file
SF_String_2='_0010.dat'; %forms second part of SF file
SF_Date_Start=startdate; %user inputs first date of SF data
in string
SF_dpph=144; %user inputs SF data points per hour
SF_File=strcat(SF_String_1,SF_Date_Start,SF_String_2);
%first
%SF file name
SF_title=strcat('Sap Flow',date_title); %user
%inputs the title for the SF plot

%Sagui_Soil Inputs
colSoil=7; %number of columns in Soil files
Soil_String_1='Soltis_Sagui_Soil_2015_'; %forms first part
of Soil file
Soil_String_2='_0010.dat'; %forms second part of Soil file
Soil_Date_Start=startdate; %user inputs first date of Soil
data in string
Soil_dpph=144; %user inputs Soil data points per hour
Soil_File=strcat(Soil_String_1,Soil_Date_Start,Soil_String_
2); %first
```

```
%Soil file name
SWP_title=strcat('Soil Water Potential',date_title); %user
%inputs the title for the SWP plot

%Weather Inputs
colWD=30; %number of columns in WD files
WD_String_1='Soltis_Weather_2015_'; %forms first part of WD
file
WD_String_2='_0015.dat'; %forms second part of WD file
WD_Date_Start=startdate; %user inputs first date of WD data
in string
WD_dpph=288; %user inputs WD data points per hour
WD_File=strcat(WD_String_1,WD_Date_Start,WD_String_2);
%first
%WD file name
Precip_title=strcat('Precipitation',date_title); %user
%inputs the title for the precip plot
STemp_title=strcat('Soil Temperature',date_title); %user
%inputs the title for the soil temp plot

%Profile Plot Titles
CO2_Prof_title=strcat('CO2 Concentration Canopy
Profile',date_title);
H2O_Prof_title=strcat('H2O Concentration Canopy
Profile',date_title);
Temp_Prof_title=strcat('Temperature Canopy
Profile',date_title);
PAR_Prof_title=strcat('PAR Canopy Profile',date_title);
LW_Prof_title=strcat('Leaf Wetness Canopy
Profile',date_title);
VPD_Prof_title=strcat('Vapor Pressure Deficit Canopy
Profile',date_title);
ST_Prof_title=strcat('Soil Temperature
Profile',date_title);
VWC_Prof_title=strcat('Volumetric Water Content
Profile',date_title);

%% Concatenate Files


%Concatenator Loop
for j=1:7
    j
    if concat == 1
```

```
        if j==1 %Set local variables equal to spire values
            file1=Spire_File;
            local_start=Spire_Date_Start;
            %assigns local start variable to spire
            len=length(local_start);
            day_string=local_start(1,(len-1):len);
            %creates a string of the current day
            local_date=local_start;
            %give local_date a starting value of
local_start
            local_string_1=Spire_String_1;
            local_string_2=Spire_String_2; %set local str
to spire values
        elseif j==2 %Set local variables equal to UpperData
values
            file1=UD_File;
            local_start=UD_Date_Start;
            %assigns local start variable to UD
            len=length(local_start);
            day_string=local_start(1,(len-1):len);
            %creates a string of the current day
            local_date=local_start;
            %give local_date a starting value of
local_start
            local_string_1=UD_String_1;
            local_string_2=UD_String_2; %set local strings
to UD values
        elseif j==3 %Set local variables equal to
GroundData values
            file1=GD_File;
            local_start=GD_Date_Start;
            %assigns local start variable to GD
            len=length(local_start);
            day_string=local_start(1,(len-1):len);
            %creates a string of the current day
            local_date=local_start;
            %give local_date a starting value of
local_start
            local_string_1=GD_String_1;
            local_string_2=GD_String_2; %set local strings
to GD values
        elseif j==4
            file1=AP_File;
            local_start=AP_Date_Start;
```

```
            %assigns local start variable to AP200
            len=length(local_start);
            day_string=local_start(1,(len-1):len);
            %creates a string of the current day
            local_date=local_start;
            %give local_date a starting value of
local_start
            local_string_1=AP_String_1;
            local_string_2=AP_String_2; %set local strings
to AP200 values
        elseif j==5
            file1=SF_File;
            local_start=SF_Date_Start;
            %assigns local start variable to SF
            len=length(local_start);
            day_string=local_start(1,(len-1):len);
            %creates a string of the current day
            local_date=local_start;
            %give local_date a starting value of
local_start
            local_string_1=SF_String_1;
            local_string_2=SF_String_2; %set local strings
to SF values
        elseif j==6
            file1=Soil_File;
            local_start=Soil_Date_Start;
            %assigns local start variable to Soil
            len=length(local_start);
            day_string=local_start(1,(len-1):len);
            %creates a string of the current day
            local_date=local_start;
            %give local_date a starting value of
local_start
            local_string_1=Soil_String_1;
            local_string_2=Soil_String_2; %set local
strings to Soil values
        else
            file1=WD_File;
            local_start=WD_Date_Start;
            %assigns local start variable to WD
            len=length(local_start);
            day_string=local_start(1,(len-1):len);
            %creates a string of the current day
            local_date=local_start;
```

```
            %give local_date a starting value of
local_start
            local_string_1=WD_String_1;
            local_string_2=WD_String_2; %set local strings
to WD values
        end
        %Loop will concatenate a week of data for a single
data series
        for i=1:(days-1)
            day=str2double(day_string);
            day=day+1;
            if day > Month_days
                day=1;
                month_string=local_start(1,1:2);
                local_month=str2double(month_string);
                local_month=local_month+1;
                if local_month < 10
                    local_month=num2str(local_month);
                    month_string(1,2)=local_month;
                else
                    local_month=num2str(local_month);
                    month_string(1,1:2)=local_month;
                end
                local_date(1,1:2)=month_string;
            else
            end
            if day < 10
                day_string=strcat('0',num2str(day));
            else
                day_string=num2str(day);
            end
            local_date(1,4:5)=day_string;

file2=strcat(local_string_1,local_date,local_string_2);
            data_concatenator(file1,file2,4);
        end
    end
end


%% Extract data from concatenated files and convert to
matrix in MATLAB
dest_path='..\..\Data Organization\NaN filled files\NaN-
filled weekly csv files - unused';
```

```
for j=1:7
    if j==1
        fprintf('Importing and NaN-filling Spire data.\n');
        %Import data from concatonated file
        local_file=Spire_File;

spire_data=importspire(local_file,5,spire_dpph*days+4);
        spire_mat=cell(spire_dpph*7,colspire); %initialize
empty cell
        %array for spire data
        local_data=spire_data;
        %Cut down local data to start at the correct start
time and end at
        %the correct end time
%         local_times=strfind(local_data(:,1),'00:15');
%         empty=1; count=1;
%         while empty==1
%             empty=isempty(local_times(count));
%             if empty ==1
%                 count=count+1;
%             end
%         end
%         local_start_row=count;
        local_mat=spire_mat;
        collocal=colspire;
        spire_gf=nanfill(local_data,spire_dpph*days,15);
%create
        %NaN-filled cell array
        local_gf=spire_gf;
        local_csv=strcat(local_file(:,1:size(local_file,2)-
3),'csv');
        cell2csv(local_csv,local_gf); %export NaN-filled
array to a csv
        % Copy new csv file to directory for master
concatenation
        copyfile(local_csv,dest_path);
        local_gf(cellfun(@ischar,local_gf))={NaN};
        localfinal=cell2mat(local_gf);
    elseif j==2
        fprintf('Importing and NaN-filling Upper data.\n');
        %Import data from concatonated file
        local_file=UD_File;
        UD_data=importupper(local_file,5,UD_dpph*days+4);
```

```
        UD_mat=cell(UD_dpph*7,colUD); %initialize empty
cell array
        %for UD data
        local_data=UD_data;
        local_mat=UD_mat;
        collocal=colUD;
        UD_gf=nanfill(local_data,UD_dpph*days,10); %create
        %NaN-filled cell array
        local_gf=UD_gf;
        local_csv=strcat(local_file(:,1:size(local_file,2)-
3),'csv');
        cell2csv(local_csv,local_gf); %export NaN-filled
array to a csv
        % Copy new csv file to directory for master
concatenation
        copyfile(local_csv,dest_path);
        local_gf(cellfun(@ischar,local_gf))={NaN};
        localfinal=cell2mat(local_gf);
    elseif j==3
        fprintf('Importing and NaN-filling Ground
data.\n');
        %Import data from concatonated file
        local_file=GD_File;
        GD_data=importgnd(local_file,5,GD_dpph*days+4);
        GD_mat=cell(GD_dpph*7,colGD); %initialize empty
cell array
        %for GD data
        local_data=GD_data;
        local_mat=GD_mat;
        collocal=colGD;
        GD_gf=nanfill(local_data,GD_dpph*days,5); %create
        %NaN-filled cell array
        local_gf=GD_gf;
        local_csv=strcat(local_file(:,1:size(local_file,2)-
3),'csv');
        cell2csv(local_csv,local_gf); %export NaN-filled
array to a csv
        % Copy new csv file to directory for master
concatenation
        copyfile(local_csv,dest_path);
        local_gf(cellfun(@ischar,local_gf))={NaN};
        localfinal=cell2mat(local_gf);
        LW_csv_str=local_csv; %stores GD local csv data for
later use in LW
```

```
        %pct string title
    elseif j==4
        fprintf('Importing and NaN-filling AP200 data.\n');
        %Import data from concatonated file
        local_file=AP_File;
        AP_data=importap(local_file,5,AP_dpph*days+4);
        %Import processed EC data here
        ECfile_lower=dir('eddypro_*_Lower_*');
        ECfile_upper=dir('eddypro_*_Upper_*');
        if length(ECfile_lower)==1
            LowerECdata=importec(ECfile_lower.name,4,339);
        else
            LowerECdata=NaN(336,2);
            fprintf('Lower EC data file not found!\n');
        end
        if length(ECfile_upper)==1
            UpperECdata=importec(ECfile_upper.name,4,339);
        else
            UpperECdata=NaN(336,2);
            fprintf('Upper EC data file not found!\n');
        end
        AP_mat=cell(AP_dpph*7,colAP); %initialize empty
cell array
        %for AP200 data
        local_mat=AP_mat;
        collocal=colAP;
        local_data=AP_data;
        AP_gf=nanfill(local_data,AP_dpph*days,30); %create
        %NaN-filled cell array
        %Prepare input VPD data

AP_VPDinputs=[AP_gf(:,7),AP_gf(:,13),AP_gf(:,19),...
            AP_gf(:,25),AP_gf(:,31),AP_gf(:,37),...

AP_gf(:,43),AP_gf(:,49),AP_gf(:,68),AP_gf(:,69),...
            AP_gf(:,70),AP_gf(:,71)];

UD_VPDinputs_raw=[UDfinal(:,10),UDfinal(:,11),UDfinal(:,12)
,...
            UDfinal(:,13)];
        AP_VPDinputs(cellfun(@ischar,AP_VPDinputs))={NaN};
        AP_VPDinputs=cell2mat(AP_VPDinputs);
        UD_VPDinputs=zeros(length(AP_VPDinputs),4);
```

```
        for m=1:length(UD_VPDinputs) %make 30 min averages
of the UD temps
            if m==1

UD_VPDinputs(m,1)=nanmean(UD_VPDinputs_raw(1:5,1));

UD_VPDinputs(m,2)=nanmean(UD_VPDinputs_raw(1:5,2));

UD_VPDinputs(m,3)=nanmean(UD_VPDinputs_raw(1:5,3));

UD_VPDinputs(m,4)=nanmean(UD_VPDinputs_raw(1:5,4));
            else

UD_VPDinputs(m,1)=nanmean(UD_VPDinputs_raw(6*(m-...
                    1):6*m-1,1));

UD_VPDinputs(m,2)=nanmean(UD_VPDinputs_raw(6*(m-...
                    1):6*m-1,2));

UD_VPDinputs(m,3)=nanmean(UD_VPDinputs_raw(6*(m-...
                    1):6*m-1,3));

UD_VPDinputs(m,4)=nanmean(UD_VPDinputs_raw(6*(m-...
                    1):6*m-1,4));
            end
        end

        %Allow for EC pressures to be used when one is
missing
        for i=1:length(UpperECdata)
            if isnan(UpperECdata(i,2))
                if isnan(LowerECdata(i,2))
                else
                    % Upper EC pressure is missing,
subtract 190 from lower
                    UpperECdata(i,2)=LowerECdata(i,2)-190;
                end
            elseif isnan(LowerECdata(i,2))
                % Lower EC pressure is missing, add 190 to
upper
                LowerECdata(i,2)=UpperECdata(i,2)+190;
            end
        end
```

```
        %Use imported data to calculate 8 new columns worth
of VPD data
        VPDfinal=zeros(length(AP_VPDinputs),8);

VPDfinal(:,1)=0.611*exp((17.502*UD_VPDinputs(:,1))./...
            (UD_VPDinputs(:,1)+240.97))-
(AP_VPDinputs(:,1).*...
           UpperECdata(:,2)/10^6);

VPDfinal(:,2)=0.611*exp((17.502*UD_VPDinputs(:,2))./...
            (UD_VPDinputs(:,2)+240.97))-
(AP_VPDinputs(:,2).*...
           UpperECdata(:,2)/10^6);

VPDfinal(:,3)=0.611*exp((17.502*UD_VPDinputs(:,3))./...
            (UD_VPDinputs(:,3)+240.97))-
(AP_VPDinputs(:,3).*...
           UpperECdata(:,2)/10^6);

VPDfinal(:,4)=0.611*exp((17.502*UD_VPDinputs(:,4))./...
            (UD_VPDinputs(:,4)+240.97))-
(AP_VPDinputs(:,4).*...
           ((UpperECdata(:,2)+LowerECdata(:,2))/2)/10^6);

VPDfinal(:,5)=0.611*exp((17.502*AP_VPDinputs(:,9))./...
            (AP_VPDinputs(:,9)+240.97))-
(AP_VPDinputs(:,5).*...
           LowerECdata(:,2)/10^6);

VPDfinal(:,6)=0.611*exp((17.502*AP_VPDinputs(:,10))./...
            (AP_VPDinputs(:,10)+240.97))-
(AP_VPDinputs(:,6).*...
           LowerECdata(:,2)/10^6);

VPDfinal(:,7)=0.611*exp((17.502*AP_VPDinputs(:,11))./...
            (AP_VPDinputs(:,11)+240.97))-
(AP_VPDinputs(:,7).*...
           LowerECdata(:,2)/10^6);

VPDfinal(:,8)=0.611*exp((17.502*AP_VPDinputs(:,12))./...
            (AP_VPDinputs(:,12)+240.97))-
(AP_VPDinputs(:,8).*...
           LowerECdata(:,2)/10^6);
```

```
        %Add the new columns on as part of the AP cell
array and adjust
        %column numbers and other parameters so you can run
thru the
        %nan-filler and have new data outputted to csv
        VPD_gf=num2cell(VPDfinal);
        AP_timestamps=AP_gf(:,1);
        AP_doy=AP_gf(:,3);

VPD_gf=[AP_timestamps,AP_doy,VPD_gf(:,size(VPD_gf,...
            2)-7:size(VPD_gf,2))];
        local_gf=AP_gf;
        local_csv=strcat(local_file(:,1:size(local_file,2)-
3),'csv');
        cell2csv(local_csv,local_gf); %export NaN-filled
array to a csv
        % Copy new csv file to directory for master
concatenation
        copyfile(local_csv,dest_path);
        VPD_cols=cellstr(['TIMESTAMP
';'VPD_A1_L21_38m';...

'VPD_A2_L18_32m';'VPD_A3_L15_27m';'VPD_A4_L12_21m';...
            'VPD_A5_L9_16m ';'VPD_A6_L6_10m ';'VPD_A7_L3_5m
';...
            'VPD_A8_L0_1m  ';'TS            ';'kPa
';...
            'DOY           ';'DDOY          ']);

VPD_cols=[VPD_cols(1,1),VPD_cols(12,1),VPD_cols(2,1),...

VPD_cols(3,1),VPD_cols(4,1),VPD_cols(5,1),VPD_cols(6,1),...
            VPD_cols(7,1),VPD_cols(8,1),VPD_cols(9,1);...

VPD_cols(10,1),VPD_cols(13,1),VPD_cols(11,1),VPD_cols(11,1)
,...

VPD_cols(11,1),VPD_cols(11,1),VPD_cols(11,1),...
            VPD_cols(11,1),VPD_cols(11,1),VPD_cols(11,1)];
        VPD_gf_headings=[VPD_cols;VPD_gf];

VPD_csv=strcat('Soltis_VPD_',local_csv(:,22:size(local_csv,
2)));
```

```
        cell2csv(VPD_csv,VPD_gf_headings); %export VPD data
to its own csv
        local_csv=VPD_csv;
        % Copy new csv file to directory for master
concatenation
        copyfile(local_csv,dest_path);
        local_gf(cellfun(@ischar,local_gf))={NaN};
        localfinal=cell2mat(local_gf);
        VPDfinal=cell2mat(VPD_gf(:,3:10));
    elseif j==5
        fprintf('Importing and NaN-filling Sap Flow
data.\n');
        %Import data from concatonated file
        local_file=SF_File;
        SF_data=importsf(local_file,5,SF_dpph*days+4);
        SF_mat=cell(SF_dpph*7,colSF); %initialize empty
cell array
        %for SF data
        local_data=SF_data;
        local_mat=SF_mat;
        collocal=colSF;
        SF_gf=nanfill(local_data,SF_dpph*days,10); %create
        %NaN-filled cell array
        local_gf=SF_gf;
        local_csv=strcat(local_file(:,1:size(local_file,2)-
3),'csv');
        cell2csv(local_csv,local_gf); %export NaN-filled
array to a csv
        % Copy new csv file to directory for master
concatenation
        copyfile(local_csv,dest_path);
        local_gf(cellfun(@ischar,local_gf))={NaN};
        localfinal=cell2mat(local_gf);
    elseif j==6
        fprintf('Importing and NaN-filling Soil data.\n');
        %Import data from concatonated file
        local_file=Soil_File;

Soil_data=importsoil(local_file,5,Soil_dpph*days+4);
        Soil_mat=cell(Soil_dpph*7,colSoil); %initialize
empty cell array
        %for Soil data
        local_data=Soil_data;
        local_mat=Soil_mat;
```

```
        collocal=colSoil;
        Soil_gf=nanfill(local_data,Soil_dpph*days,10);
%create
        %NaN-filled cell array
        local_gf=Soil_gf;
        local_csv=strcat(local_file(:,1:size(local_file,2)-
3),'csv');
        cell2csv(local_csv,local_gf); %export NaN-filled
array to a csv
        % Copy new csv file to directory for master
concatenation
        copyfile(local_csv,dest_path);
        local_gf(cellfun(@ischar,local_gf))={NaN};
        localfinal=cell2mat(local_gf);
    else
        fprintf('Importing and NaN-filling Weather
data.\n');
        %Import data from concatonated file
        local_file=WD_File;
        WD_data=importwd(local_file,5,WD_dpph*days+4);
        WD_mat=cell(WD_dpph*7,colWD); %initialize empty
cell array
        %for WD data
        local_data=WD_data;
        local_mat=WD_mat;
        collocal=colWD;
        WD_gf=nanfill(local_data,WD_dpph*days,15); %create
        %NaN-filled cell array
        local_gf=WD_gf;
        local_csv=strcat(local_file(:,1:size(local_file,2)-
3),'csv');
        cell2csv(local_csv,local_gf); %export NaN-filled
array to a csv
        % Copy new csv file to directory for master
concatenation
        copyfile(local_csv,dest_path);
        local_gf(cellfun(@ischar,local_gf))={NaN};
        localfinal=cell2mat(local_gf);
    end

    if j==1
        spirefinal=localfinal;
    elseif j==2
        UDfinal=localfinal;
```

```
    elseif j==3
        GDfinal=localfinal;
    elseif j==4
        APfinal=localfinal;
    elseif j==5
        SFfinal=localfinal;
    elseif j==6
        Soilfinal=localfinal;
    else
        WDfinal=localfinal;
    end
end


%% Set up LW percentage data and output to a csv

% Collect all LW mV data into one matrix
LW_mV=[GDfinal(:,42:43),UDfinal(:,18:20)];

%Calculate raw mins and maxes for each LW sensor
LW_mins=[min(LW_mV(:,1)),min(LW_mV(:,2)),min(LW_mV(:,3)),mi
n(LW_mV(:,4)),...
    min(LW_mV(:,5))];
LW_maxs=[max(LW_mV(:,1)),max(LW_mV(:,2)),max(LW_mV(:,3)),ma
x(LW_mV(:,4)),...
    max(LW_mV(:,5))];

%Calculate a cap for what is considered dry/wet in raw
datasets
LW_drymax=LW_mins+0.1*(LW_maxs-LW_mins);
%With 0.15 all averages looked a bit high
LW_wetmin=LW_maxs-0.1*(LW_maxs-LW_mins);

%Collect initial wet/dry datasets for each sensor
LW_L2_logical=LW_mV(:,1) < LW_drymax(1);
LW_L6_logical=LW_mV(:,2) < LW_drymax(2);
LW_L12_logical=LW_mV(:,3) < LW_drymax(3);
LW_L18_logical=LW_mV(:,4) < LW_drymax(4);
LW_L21_logical=LW_mV(:,5) < LW_drymax(5);

temp1=LW_mV(:,1);
LW_L2_dry=temp1(LW_L2_logical);
temp1=LW_mV(:,2);
LW_L6_dry=temp1(LW_L6_logical);
```

```
temp1=LW_mV(:,3);
LW_L12_dry=temp1(LW_L12_logical);
temp1=LW_mV(:,4);
LW_L18_dry=temp1(LW_L18_logical);
temp1=LW_mV(:,5);
LW_L21_dry=temp1(LW_L21_logical);

LW_L2_logical=LW_mV(:,1) > LW_wetmin(1);
LW_L6_logical=LW_mV(:,2) > LW_wetmin(2);
LW_L12_logical=LW_mV(:,3) > LW_wetmin(3);
LW_L18_logical=LW_mV(:,4) > LW_wetmin(4);
LW_L21_logical=LW_mV(:,5) > LW_wetmin(5);

temp1=LW_mV(:,1);
LW_L2_wet=temp1(LW_L2_logical);
temp1=LW_mV(:,2);
LW_L6_wet=temp1(LW_L6_logical);
temp1=LW_mV(:,3);
LW_L12_wet=temp1(LW_L12_logical);
temp1=LW_mV(:,4);
LW_L18_wet=temp1(LW_L18_logical);
temp1=LW_mV(:,5);
LW_L21_wet=temp1(LW_L21_logical);

% Run some statistics on the intial wet/dry datasets
determining a new
% percentage method of representing wetness and dryness
LW_dry_averages=[mean(LW_L2_dry),mean(LW_L6_dry),mean(LW_L1
2_dry),...
    mean(LW_L18_dry),mean(LW_L21_dry)];
LW_dry_stdev=[std(LW_L2_dry),std(LW_L6_dry),std(LW_L12_dry)
,...
    std(LW_L18_dry),std(LW_L21_dry)];
LW_zero_pct=LW_dry_averages+LW_dry_stdev;

LW_wet_averages=[mean(LW_L2_wet),mean(LW_L6_wet),mean(LW_L1
2_wet),...
    mean(LW_L18_wet),mean(LW_L21_wet)];
LW_wet_stdev=[std(LW_L2_wet),std(LW_L6_wet),std(LW_L12_wet)
,...
    std(LW_L18_wet),std(LW_L21_wet)];
LW_100_pct=LW_wet_averages-LW_wet_stdev;

%Account for very dry weeks
```

```
p_all=WDfinal(:,14); p_sum=sum(p_all);
LW_variability=mean(LW_100_pct)-mean(LW_zero_pct);
if p_sum < 0.1 && LW_variability < 120
    LW_zero_pct=[mean(LW_mV(:,1))+std(LW_mV(:,1)),...
        mean(LW_mV(:,2))+std(LW_mV(:,2)),...
        mean(LW_mV(:,3))+std(LW_mV(:,3)),...
        mean(LW_mV(:,4))+std(LW_mV(:,4)),...
        mean(LW_mV(:,5))+std(LW_mV(:,5))];
    LW_100_pct=(LW_maxs-LW_zero_pct)*100/((LW_maxs-
LW_zero_pct)/2)+LW_zero_pct;
    %Sets the percentages such that the max mV value equals
a pct that is
    %2 mV/%pt away from the zero pct
end


LW_percent=zeros(size(LW_mV));
for row=1:length(LW_mV)
    for col=1:size(LW_mV,2)
        LW_percent(row,col)=((LW_mV(row,col)-
LW_zero_pct(col))/...
            (LW_100_pct(col)-LW_zero_pct(col)))*100;
        if LW_percent(row,col)<0
            LW_percent(row,col)=0;
        end
        if LW_percent(row,col)>100
            LW_percent(row,col)=100;
        end
    end
end

%Export LW percentage data to its own csv
LW_cols=cellstr(['TIMESTAMP-ud  ';'TIMESTAMP-gd  ';...

'LW_pct_L21_38m';'LW_pct_L18_33m';'LW_pct_L12_22m';'LW_pct_
L6_11m ';...
    'LW_pct_L2_3m  ';'DOY-ud        ';'TS            ';...
    'pct           ';'DOY-gd        ';'DDOY          ']);
LW_cols=[LW_cols(1,1),LW_cols(8,1),LW_cols(3,1),...

LW_cols(4,1),LW_cols(5,1),LW_cols(2,1),LW_cols(11,1),...
    LW_cols(6,1),LW_cols(7,1);...

LW_cols(9,1),LW_cols(12,1),LW_cols(10,1),LW_cols(10,1),...
```

```
    LW_cols(10,1),LW_cols(9,1),LW_cols(12,1),...
    LW_cols(10,1),LW_cols(10,1)];
LW_gf=num2cell(LW_percent);
LW_gf_headings=[LW_cols;[UD_gf(:,1),UD_gf(:,3),LW_gf(:,5),.
..
    LW_gf(:,4),LW_gf(:,3),GD_gf(:,1),GD_gf(:,3),...
    LW_gf(:,2),LW_gf(:,1)]];
LW_csv=strcat('Soltis_LWpct_',LW_csv_str(:,15:size(LW_csv_s
tr,2)));
cell2csv(LW_csv,LW_gf_headings); %export LWpct data to its
own csv
% Copy new csv file to directory for master concatenation
copyfile(LW_csv,dest_path);

% Delineate wet days from dry days
p_wetday=0.05; %daily precip needs to be 0.05" or more for
wet day status
day1_end=285; %first 3 timestamps cut off of first day
day1=1:day1_end;
day2=(day1_end+1:day1_end+288);
day3=(day2(288)+1:day2(288)+288);
day4=(day3(288)+1:day3(288)+288);
day5=(day4(288)+1:day4(288)+288);
day6=(day5(288)+1:day5(288)+288);
day7=(day6(288)+1:day6(288)+288);
p_daily=[sum(p_all(day1)),sum(p_all(day2)),sum(p_all(day3))
,...

sum(p_all(day4)),sum(p_all(day5)),sum(p_all(day6)),sum(p_al
l(day7))];
wetday_index=p_daily>p_wetday;

%% Set up data for profile plots

%Pull out profile data by data type
CO2Profile=[APfinal(:,6),APfinal(:,12),APfinal(:,18),APfina
l(:,24),...

APfinal(:,30),APfinal(:,36),APfinal(:,42),APfinal(:,48)];
H2OProfile=[APfinal(:,7),APfinal(:,13),APfinal(:,19),APfina
l(:,25),...

APfinal(:,31),APfinal(:,37),APfinal(:,43),APfinal(:,49)];
```

```
TempProfile1=[UDfinal(:,10),UDfinal(:,11),UDfinal(:,12),UDf
inal(:,13)];
TempProfile2=[APfinal(:,68),APfinal(:,69),APfinal(:,70),APf
inal(:,71)];
PARProfile=[UDfinal(:,14),UDfinal(:,15),UDfinal(:,16),UDfin
al(:,17),...
    GDfinal(:,41)];
LWProfile=[UDfinal(:,20),UDfinal(:,19),UDfinal(:,18),GDfina
l(:,43),...
    GDfinal(:,42)];
VPDProfile=VPDfinal;
STProfile=[GDfinal(:,5),GDfinal(:,6),GDfinal(:,7),GDfinal(:
,8),...
    GDfinal(:,9)];
VWCProfile=[GDfinal(:,15),GDfinal(:,16),GDfinal(:,17),GDfin
al(:,18),...
    GDfinal(:,19)];

%Separate each data type into day and night series
CO2_Night=[CO2Profile(1:10,:);CO2Profile(37:58,:);CO2Profil
e(85:106,...

:);CO2Profile(133:154,:);CO2Profile(181:202,:);CO2Profile(2
29:250,...
    :);CO2Profile(277:298,:);CO2Profile(325:336,:)];
CO2_Day=[CO2Profile(11:36,:);CO2Profile(59:84,:);CO2Profile
(107:132,...

:);CO2Profile(155:180,:);CO2Profile(203:228,:);CO2Profile(2
51:276,...
    :);CO2Profile(299:324,:)];
H2O_Night=[H2OProfile(1:10,:);H2OProfile(37:58,:);H2OProfil
e(85:106,...

:);H2OProfile(133:154,:);H2OProfile(181:202,:);H2OProfile(2
29:250,...
    :);H2OProfile(277:298,:);H2OProfile(325:336,:)];
H2O_Day=[H2OProfile(11:36,:);H2OProfile(59:84,:);H2OProfile
(107:132,...

:);H2OProfile(155:180,:);H2OProfile(203:228,:);H2OProfile(2
51:276,...
    :);H2OProfile(299:324,:)];
Temp_Night1=[TempProfile1(1:59,:);TempProfile1(216:347,...
```

```
    :);TempProfile1(504:635,:);TempProfile1(792:923,...
    :);TempProfile1(1080:1211,:);TempProfile1(1368:1499,...

:);TempProfile1(1656:1787,:);TempProfile1(1944:2015,:)];
Temp_Day1=[TempProfile1(60:215,:);TempProfile1(348:503,...
    :);TempProfile1(636:791,:);TempProfile1(924:1079,...
    :);TempProfile1(1212:1367,:);TempProfile1(1500:1655,...
    :);TempProfile1(1788:1943,:)];
Temp_Night2=[TempProfile2(1:10,:);TempProfile2(37:58,...
    :);TempProfile2(85:106,:);TempProfile2(133:154,...
    :);TempProfile2(181:202,:);TempProfile2(229:250,...
    :);TempProfile2(277:298,:);TempProfile2(325:336,:)];
Temp_Day2=[TempProfile2(11:36,:);TempProfile2(59:84,...
    :);TempProfile2(107:132,:);TempProfile2(155:180,...
    :);TempProfile2(203:228,:);TempProfile2(251:276,...
    :);TempProfile2(299:324,:)];
PAR_Night1=[PARProfile(1:59,1:4);PARProfile(216:347,...
    1:4);PARProfile(504:635,1:4);PARProfile(792:923,...
    1:4);PARProfile(1080:1211,1:4);PARProfile(1368:1499,...

1:4);PARProfile(1656:1787,1:4);PARProfile(1944:2015,1:4)];
PAR_Day1=[PARProfile(60:215,1:4);PARProfile(348:503,...
    1:4);PARProfile(636:791,1:4);PARProfile(924:1079,...
    1:4);PARProfile(1212:1367,1:4);PARProfile(1500:1655,...
    1:4);PARProfile(1788:1943,1:4)];
PAR_Night2=[PARProfile(1:60,5);PARProfile(217:348,...
    5);PARProfile(505:636,5);PARProfile(793:924,...
    5);PARProfile(1081:1212,5);PARProfile(1369:1500,...
    5);PARProfile(1657:1788,5);PARProfile(1945:2016,5)];
PAR_Day2=[PARProfile(61:216,5);PARProfile(349:504,...
    5);PARProfile(637:792,5);PARProfile(925:1080,...
    5);PARProfile(1213:1368,5);PARProfile(1501:1656,...
    5);PARProfile(1789:1944,5)];
LW_Night1=[LWProfile(1:59,1:3);LWProfile(216:347,...
    1:3);LWProfile(504:635,1:3);LWProfile(792:923,...
    1:3);LWProfile(1080:1211,1:3);LWProfile(1368:1499,...

1:3);LWProfile(1656:1787,1:3);LWProfile(1944:2015,1:3)];
LW_Day1=[LWProfile(60:215,1:3);LWProfile(348:503,...
    1:3);LWProfile(636:791,1:3);LWProfile(924:1079,...
    1:3);LWProfile(1212:1367,1:3);LWProfile(1500:1655,...
    1:3);LWProfile(1788:1943,1:3)];
LW_Night2=[LWProfile(1:60,4:5);LWProfile(217:348,...
    4:5);LWProfile(505:636,4:5);LWProfile(793:924,...
```

```
    4:5);LWProfile(1081:1212,4:5);LWProfile(1369:1500,...

4:5);LWProfile(1657:1788,4:5);LWProfile(1945:2016,4:5)];
LW_Day2=[LWProfile(61:216,4:5);LWProfile(349:504,...
    4:5);LWProfile(637:792,4:5);LWProfile(925:1080,...
    4:5);LWProfile(1213:1368,4:5);LWProfile(1501:1656,...
    4:5);LWProfile(1789:1944,4:5)];
VPD_Night=[VPDProfile(1:10,:);VPDProfile(37:58,:);VPDProfil
e(85:106,...

:);VPDProfile(133:154,:);VPDProfile(181:202,:);VPDProfile(2
29:250,...
    :);VPDProfile(277:298,:);VPDProfile(325:336,:)];
VPD_Day=[VPDProfile(11:36,:);VPDProfile(59:84,:);VPDProfile
(107:132,...

:);VPDProfile(155:180,:);VPDProfile(203:228,:);VPDProfile(2
51:276,...
    :);VPDProfile(299:324,:)];
ST_Night=[STProfile(1:60,:);STProfile(217:348,...
    :);STProfile(505:636,:);STProfile(793:924,...
    :);STProfile(1081:1212,:);STProfile(1369:1500,...
    :);STProfile(1657:1788,:);STProfile(1945:2016,:)];
ST_Day=[STProfile(61:216,:);STProfile(349:504,...
    :);STProfile(637:792,:);STProfile(925:1080,...
    :);STProfile(1213:1368,:);STProfile(1501:1656,...
    :);STProfile(1789:1944,:)];
VWC_Night=[VWCProfile(1:60,:);VWCProfile(217:348,...
    :);VWCProfile(505:636,:);VWCProfile(793:924,...
    :);VWCProfile(1081:1212,:);VWCProfile(1369:1500,...
    :);VWCProfile(1657:1788,:);VWCProfile(1945:2016,:)];
VWC_Day=[VWCProfile(61:216,:);VWCProfile(349:504,...
    :);VWCProfile(637:792,:);VWCProfile(925:1080,...
    :);VWCProfile(1213:1368,:);VWCProfile(1501:1656,...
    :);VWCProfile(1789:1944,:)];

%Average each column to get each data point
CO2_Night_Profile=[nanmean(CO2_Night(:,1));nanmean(CO2_Nigh
t(:,...
    2));nanmean(CO2_Night(:,3));nanmean(CO2_Night(:,...
    4));nanmean(CO2_Night(:,5));nanmean(CO2_Night(:,...
    6));nanmean(CO2_Night(:,7));nanmean(CO2_Night(:,8))];
CO2_Day_Profile=[nanmean(CO2_Day(:,1));nanmean(CO2_Day(:,..
.
```

```
2));nanmean(CO2_Day(:,3));nanmean(CO2_Day(:,4));nanmean(CO2
_Day(:,...

5));nanmean(CO2_Day(:,6));nanmean(CO2_Day(:,7));nanmean(CO2
_Day(:,...
    8))];
H2O_Night_Profile=[nanmean(H2O_Night(:,1));nanmean(H2O_Nigh
t(:,...
    2));nanmean(H2O_Night(:,3));nanmean(H2O_Night(:,...
    4));nanmean(H2O_Night(:,5));nanmean(H2O_Night(:,...
    6));nanmean(H2O_Night(:,7));nanmean(H2O_Night(:,8))];
H2O_Day_Profile=[nanmean(H2O_Day(:,1));nanmean(H2O_Day(:,..
.

2));nanmean(H2O_Day(:,3));nanmean(H2O_Day(:,4));nanmean(H2O
_Day(:,...

5));nanmean(H2O_Day(:,6));nanmean(H2O_Day(:,7));nanmean(H2O
_Day(:,...
    8))];
Temp_Night_Profile=[nanmean(Temp_Night1(:,1));nanmean(Temp_
Night1(:,...
    2));nanmean(Temp_Night1(:,3));nanmean(Temp_Night1(:,...
    4));nanmean(Temp_Night2(:,1));nanmean(Temp_Night2(:,...

2));nanmean(Temp_Night2(:,3));nanmean(Temp_Night2(:,4))];
Temp_Day_Profile=[nanmean(Temp_Day1(:,1));nanmean(Temp_Day1
(:,...
    2));nanmean(Temp_Day1(:,3));nanmean(Temp_Day1(:,...
    4));nanmean(Temp_Day2(:,1));nanmean(Temp_Day2(:,...
    2));nanmean(Temp_Day2(:,3));nanmean(Temp_Day2(:,4))];
PAR_Night_Profile=[nanmean(PAR_Night1(:,1));nanmean(PAR_Nig
ht1(:,...

2));nanmean(PAR_Night1(:,3));nanmean(PAR_Night1(:,4));...
    nanmean(PAR_Night2(:,1))];
PAR_Day_Profile=[nanmean(PAR_Day1(:,1));nanmean(PAR_Day1(:,
...
    2));nanmean(PAR_Day1(:,3));nanmean(PAR_Day1(:,4));...
    nanmean(PAR_Day2(:,1))];
LW_Night_Profile=[nanmean(LW_Night1(:,1));nanmean(LW_Night1
(:,...
    2));nanmean(LW_Night1(:,3));nanmean(LW_Night2(:,...
```

```
    1));nanmean(LW_Night2(:,2))];
LW_Day_Profile=[nanmean(LW_Day1(:,1));nanmean(LW_Day1(:,...
    2));nanmean(LW_Day1(:,3));nanmean(LW_Day2(:,...
    1));nanmean(LW_Day2(:,2))];
VPD_Night_Profile=[nanmean(VPD_Night(:,1));nanmean(VPD_Nigh
t(:,...
    2));nanmean(VPD_Night(:,3));nanmean(VPD_Night(:,...
    4));nanmean(VPD_Night(:,5));nanmean(VPD_Night(:,...
    6));nanmean(VPD_Night(:,7));nanmean(VPD_Night(:,8))];
VPD_Day_Profile=[nanmean(VPD_Day(:,1));nanmean(VPD_Day(:,..
.

2));nanmean(VPD_Day(:,3));nanmean(VPD_Day(:,4));nanmean(VPD
_Day(:,...

5));nanmean(VPD_Day(:,6));nanmean(VPD_Day(:,7));nanmean(VPD
_Day(:,...
    8))];
ST_Night_Profile=[nanmean(ST_Night(:,1));nanmean(ST_Night(:
,...
    2));nanmean(ST_Night(:,3));nanmean(ST_Night(:,...
    4));nanmean(ST_Night(:,5))];
ST_Day_Profile=[nanmean(ST_Day(:,1));nanmean(ST_Day(:,...
    2));nanmean(ST_Day(:,3));nanmean(ST_Day(:,...
    4));nanmean(ST_Day(:,5))];
VWC_Night_Profile=[nanmean(VWC_Night(:,1));nanmean(VWC_Nigh
t(:,...
    2));nanmean(VWC_Night(:,3));nanmean(VWC_Night(:,...
    4));nanmean(VWC_Night(:,5))];
VWC_Day_Profile=[nanmean(VWC_Day(:,1));nanmean(VWC_Day(:,..
.
    2));nanmean(VWC_Day(:,3));nanmean(VWC_Day(:,...
    4));nanmean(VWC_Day(:,5))];

%%%%%%%%%%%%%%%%%%%%%%%%%%%%
%LW percentage profile setup
%%%%%%%%%%%%%%%%%%%%%%%%%%%%

%Create all the LW profile datasets in percentages
LWProfile_pct=LW_percent;

%Day/Night profiles
LW_Night1_pct=[LWProfile_pct(1:59,3:5);LWProfile_pct(216:34
7,...
```

```
3:5);LWProfile_pct(504:635,3:5);LWProfile_pct(792:923,...

3:5);LWProfile_pct(1080:1211,3:5);LWProfile_pct(1368:1499,.
..

3:5);LWProfile_pct(1656:1787,3:5);LWProfile_pct(1944:2015,3
:5)];
LW_Day1_pct=[LWProfile_pct(60:215,3:5);LWProfile_pct(348:50
3,...

3:5);LWProfile_pct(636:791,3:5);LWProfile_pct(924:1079,...

3:5);LWProfile_pct(1212:1367,3:5);LWProfile_pct(1500:1655,.
..
    3:5);LWProfile_pct(1788:1943,3:5)];
LW_Night2_pct=[LWProfile_pct(1:60,1:2);LWProfile_pct(217:34
8,...

1:2);LWProfile_pct(505:636,1:2);LWProfile_pct(793:924,...

1:2);LWProfile_pct(1081:1212,1:2);LWProfile_pct(1369:1500,.
..

1:2);LWProfile_pct(1657:1788,1:2);LWProfile_pct(1945:2016,1
:2)];
LW_Day2_pct=[LWProfile_pct(61:216,1:2);LWProfile_pct(349:50
4,...

1:2);LWProfile_pct(637:792,1:2);LWProfile_pct(925:1080,...

1:2);LWProfile_pct(1213:1368,1:2);LWProfile_pct(1501:1656,.
..
    1:2);LWProfile_pct(1789:1944,1:2)];

LW_Night_Profile_pct=[nanmean(LW_Night1_pct(:,3));nanmean(L
W_Night1_pct(:,...

2));nanmean(LW_Night1_pct(:,1));nanmean(LW_Night2_pct(:,...
    2));nanmean(LW_Night2_pct(:,1))];
LW_Day_Profile_pct=[nanmean(LW_Day1_pct(:,3));nanmean(LW_Da
y1_pct(:,...
    2));nanmean(LW_Day1_pct(:,1));nanmean(LW_Day2_pct(:,...
    2));nanmean(LW_Day2_pct(:,1))];
```

```
%Wet/Dry profiles

%Adjust day variables to Upper values
day1=1:287;day2=day2+2;day3=day3+2;day4=day4+2;day5=day5+2;
day6=day6+2;day7=day7+2;
%Separate all Upper LW into wet/dry
LW_Dry1=[];
LW_Wet1=[];
for d=1:7
    if d == 1
        loc_day=[day1,nan(1,1)];
    elseif d == 2
        loc_day=day2;
    elseif d == 3
        loc_day=day3;
    elseif d == 4
        loc_day=day4;
    elseif d == 5
        loc_day=day5;
    elseif d == 6
        loc_day=day6;
    else
        loc_day=day7;
    end
    if wetday_index(d) == 1
        loc_length=length(LW_Wet1);

loc_vect=[LW_Wet1;LW_percent(loc_day(1):(loc_day(287)+1),3:
5)];
        LW_Wet1=loc_vect;
    elseif wetday_index(d) ==0
        loc_length=length(LW_Dry1);

loc_vect=[LW_Dry1;LW_percent(loc_day(1):(loc_day(287)+1),3:
5)];
        LW_Dry1=loc_vect;
    end
end

%Adjust day variables to Ground values
day1=1:288;day2=day2+1;day3=day3+1;day4=day4+1;day5=day5+1;
day6=day6+1;day7=day7+1;
%Separate all Upper LW into wet/dry
```

```
LW_Dry2=[];
LW_Wet2=[];
for d=1:7
    if d == 1
        loc_day=day1;
    elseif d == 2
        loc_day=day2;
    elseif d == 3
        loc_day=day3;
    elseif d == 4
        loc_day=day4;
    elseif d == 5
        loc_day=day5;
    elseif d == 6
        loc_day=day6;
    else
        loc_day=day7;
    end
    if wetday_index(d) == 1
        loc_length=length(LW_Wet2);
        loc_vect=[LW_Wet2;LW_percent(loc_day,1:2)];
        LW_Wet2=loc_vect;
    elseif wetday_index(d) ==0
        loc_length=length(LW_Dry2);
        loc_vect=[LW_Dry2;LW_percent(loc_day,1:2)];
        LW_Dry2=loc_vect;
    end
end

%Aggregate LW wet/dry profiles
if isempty(LW_Wet1)
    LW_Wet_Profile=nan(5,1);

LW_Dry_Profile=[nanmean(LW_Dry1(:,3));nanmean(LW_Dry1(:,...
        2));nanmean(LW_Dry1(:,1));nanmean(LW_Dry2(:,...
        2));nanmean(LW_Dry2(:,1))];
elseif isempty(LW_Dry1)

LW_Wet_Profile=[nanmean(LW_Wet1(:,3));nanmean(LW_Wet1(:,...
        2));nanmean(LW_Wet1(:,1));nanmean(LW_Wet2(:,...
        2));nanmean(LW_Wet2(:,1))];
    LW_Dry_Profile=nan(5,1);
else
```

```
LW_Wet_Profile=[nanmean(LW_Wet1(:,3));nanmean(LW_Wet1(:,...
        2));nanmean(LW_Wet1(:,1));nanmean(LW_Wet2(:,...
        2));nanmean(LW_Wet2(:,1))];

LW_Dry_Profile=[nanmean(LW_Dry1(:,3));nanmean(LW_Dry1(:,...
        2));nanmean(LW_Dry1(:,1));nanmean(LW_Dry2(:,...
        2));nanmean(LW_Dry2(:,1))];
end

%Enter instrument heights to be plotted on y axis
CO2_Height=[37.8;32.3;26.8;21.4;16;10.3;5;1.1];
H2O_Height=CO2_Height;
Temp_Height=[38.4;32.8;21.7;16.4;10.7;5.4;1.4];%L15 taken
off (27.3)
PAR_Height=[37.6;32;10.1]; %L15(26.5) and L12(21) taken off
LW_Height=[38.2;32.6;21.8;10.5;3.3];
VPD_Height=[CO2_Height(1:2);CO2_Height(4:8)]; %L15 taken
off
Soil_Depths=[2;9;16;23;30]; %cm

%Remove L15 from Temp and VPD profiles
temp=[Temp_Night_Profile(1:2);Temp_Night_Profile(4:8)];
Temp_Night_Profile=temp;
temp=[Temp_Day_Profile(1:2);Temp_Day_Profile(4:8)];
Temp_Day_Profile=temp;
temp=[VPD_Night_Profile(1:2);VPD_Night_Profile(4:8)];
VPD_Night_Profile=temp;
temp=[VPD_Day_Profile(1:2);VPD_Day_Profile(4:8)];
VPD_Day_Profile=temp;

%Remove bad soil data from profiles also
% temp=[ST_Night_Profile(1:3);ST_Night_Profile(5)];
% ST_Night_Profile=temp;
% temp=[ST_Day_Profile(1:3);ST_Day_Profile(5)];
% ST_Day_Profile=temp;
temp=VWC_Night_Profile(2:5);
VWC_Night_Profile=temp;
temp=VWC_Day_Profile(2:5);
VWC_Day_Profile=temp;

%Remove L12 and L15 PAR also
temp=[PAR_Night_Profile(1:2);PAR_Night_Profile(5)];
PAR_Night_Profile=temp;
```

```
temp=[PAR_Day_Profile(1:2);PAR_Day_Profile(5)];
PAR_Day_Profile=temp;

%Temporary - change -7999 error codes to NaNs
% GDfinal(GDfinal==-7999)=NaN;

%% Make all of the Plots

%Specify domains to be used for each data series
spire_domain=1:length(spirefinal)-2; %domain that will be
used for plots
%including spire data
UD_domain=1:length(UDfinal)-1; %domain that will be used
for plots
%including UD data
GD_domain=1:length(GDfinal); %domain that will be used for
plots
%including GD data
AP_domain=1:length(APfinal); %domain that will be used for
plots
%including AP200 data
SF_domain=1:length(SFfinal); %domain that will be used for
plots
%including SF data
Soil_domain=1:length(Soilfinal); %domain that will be used
for plots
%including Soil data
WD_domain=1:length(WDfinal)-2; %domain that will be used
for plots
%including WD data

%Specify time bounds and steps to be used for each series
ts=3/spire_dpph:1/spire_dpph:7; %spire series
tu=2/UD_dpph:1/UD_dpph:7; %UD series
tg=1/GD_dpph:1/GD_dpph:7; %GD series
ta=1/AP_dpph:1/AP_dpph:7; %AP200 series
tsf=1/SF_dpph:1/SF_dpph:7; %SF series
tsl=1/Soil_dpph:1/Soil_dpph:7; %Soil series
tw=3/WD_dpph:1/WD_dpph:7; %WD series

if bad_data_plot==0 %only plotting good data
    close all
    %Plot 1: Net Radiation
    figure()
```

```
WDfinal(:,size(WDfinal,2)+1)=WDfinal(:,27)+WDfinal(:,29)-
WDfinal(:,...
        28)-WDfinal(:,30); % Calc. net rad from components
    plot(ts,spirefinal(spire_domain,10),tu,...

UDfinal(UD_domain,9),tw,WDfinal(WD_domain,size(WDfinal,2)))
    xlabel('Day'); ylabel('Net Radiation (W/m^2)');
    title(nrad_title);
    legend('Spire','34 m (L19)','Met CNR1','Location',...
        'BestOutside');

    %Plot 2: LW as a percentage
    figure()

plot(tg,LW_percent(GD_domain,1),tg,LW_percent(GD_domain,2),
tu,...

LW_percent(UD_domain,3),tu,LW_percent(UD_domain,4),tu,...
        LW_percent(UD_domain,5));
    xlabel('Day'); ylabel('Percent Wetness');
    title(LW_title);
    legend('3 m (L2)','11 m (L6)','22 m (L12)','33 m
(L18)', '38 m (L21)',...
        'Location','BestOutside');
    axis([0 7 -10 110]);

    %Plot 3: Leaf Wetness
    figure()

plot(tg,GDfinal(GD_domain,42),tg,GDfinal(GD_domain,43),tu,.
..

UDfinal(UD_domain,18),tu,UDfinal(UD_domain,19),tu,...
        UDfinal(UD_domain,20));
    xlabel('Day'); ylabel('Wetness Index (mV)');
    title(LW_title);
    legend('3 m (L2)','11 m (L6)','22 m (L12)','33 m
(L18)', '38 m (L21)',...
        'Location','BestOutside');

    %Plot 4: PAR
    figure()
    plot(tg,GDfinal(GD_domain,41),tu,...
```

```
        UDfinal(UD_domain,15),tu,UDfinal(UD_domain,14));
    xlabel('Day'); ylabel('PAR (umol/m^2/sec)');
    title(PAR_title);
    legend('10 m (L6)','32 m (L18)','38 m (L21)',...
        'Location','BestOutside');

    %Plot 5: Air Temperature
    figure()

plot(tw,WDfinal(WD_domain,6),tw,WDfinal(WD_domain,4),...

tu,UDfinal(UD_domain,10),tu,UDfinal(UD_domain,11),tu,...

UDfinal(UD_domain,13),ta,APfinal(AP_domain,68),ta,...

APfinal(AP_domain,69),ta,APfinal(AP_domain,70),ta,...
        APfinal(AP_domain,71));
    xlabel('Day'); ylabel('Air Temperature (deg C)');
    title(AT_title);
    legend('Met 30','Met 10','38 m (L21)','33 m (L18)','21
m (L12)',...
        '16 m (L9)','11 m (L6)','5 m (L3)','1 m
(L0)','Location',...
        'BestOutside');
    axis([0 7 16 32]);

    %Plot 6: CO2 Concentration
    figure()

plot(ta,APfinal(AP_domain,6),ta,APfinal(AP_domain,12),ta,..
.

APfinal(AP_domain,18),ta,APfinal(AP_domain,24),ta,...

APfinal(AP_domain,30),ta,APfinal(AP_domain,36),ta,...
        APfinal(AP_domain,42),ta,APfinal(AP_domain,48));
    xlabel('Day'); ylabel('Carbon Dioxide Concentration
(ppm)');
    title(CO2_title);
    legend('38 m (L21)','32 m (L18)','27 m (L15)','21 m
(L12)','16 m (L9)',...
        '10 m (L6)','5 m (L3)','1 m
(L0)','Location','BestOutside');
    axis([0 7 350 450]);
```

```
    %Plot 7: H2O Concentration
    figure()

plot(ta,APfinal(AP_domain,7),ta,APfinal(AP_domain,13),ta,..
.

APfinal(AP_domain,19),ta,APfinal(AP_domain,25),ta,...

APfinal(AP_domain,31),ta,APfinal(AP_domain,37),ta,...
        APfinal(AP_domain,43),ta,APfinal(AP_domain,49));
    xlabel('Day'); ylabel('Water Vapor Concentration
(ppt)');
    title(H2O_title);
    legend('38 m (L21)','32 m (L18)','27 m (L15)','21 m
(L12)','16 m (L9)',...
        '10 m (L6)','5 m (L3)','1 m
(L0)','Location','BestOutside');
    axis([0 7 12 38]);

    %Plot 8: Sap Flow
    figure()

plot(tsf,SFfinal(SF_domain,5),tsf,SFfinal(SF_domain,6),...

tsf,SFfinal(SF_domain,7),tsf,SFfinal(SF_domain,8),...

tsf,SFfinal(SF_domain,9),tsf,SFfinal(SF_domain,10),...
        tsf,SFfinal(SF_domain,11),...

tsf,SFfinal(SF_domain,13),tsf,SFfinal(SF_domain,16),...

tsf,SFfinal(SF_domain,17),tsf,SFfinal(SF_domain,18),...

tsf,SFfinal(SF_domain,19),tsf,SFfinal(SF_domain,20),...

tsf,SFfinal(SF_domain,21),tsf,SFfinal(SF_domain,22),...

tsf,SFfinal(SF_domain,23),tsf,SFfinal(SF_domain,24),...
        tsf,SFfinal(SF_domain,38),...

tsf,SFfinal(SF_domain,39),tsf,SFfinal(SF_domain,40),...

tsf,SFfinal(SF_domain,41),tsf,SFfinal(SF_domain,42),...
```

```
tsf,SFfinal(SF_domain,43),tsf,SFfinal(SF_domain,44),...

tsf,SFfinal(SF_domain,45),tsf,SFfinal(SF_domain,46),...

tsf,SFfinal(SF_domain,48),tsf,SFfinal(SF_domain,49),...
        tsf,SFfinal(SF_domain,50));
    xlabel('Day'); ylabel('mV');
    title(SF_title);
    legend('1','2','3','4','5','6','7','9',...
        '12','13','14','15','16','17','18','19','20',...

'34','35','36','37','38','39','40','41','42','44','45','46'
,...
        'Location','BestOutside');

    %Plot 9: Precipitation
    figure()
    plot(tw,WDfinal(WD_domain,14));
    xlabel('Day'); ylabel('Precipitation (in.)');
    title(Precip_title);

    %Plot 10: IRTs
    figure()

plot(ts,spirefinal(spire_domain,13),ts,spirefinal(spire_dom
ain,17));
    xlabel('Day'); ylabel('Leaf Temperature (deg C)');
    title(irt_title);
    legend('IRT 1 (N)','IRT 3 (S)');

    %Plot 11: Flowrates
    figure()

plot(ta,APfinal(AP_domain,10),ta,APfinal(AP_domain,16),ta,.
..

APfinal(AP_domain,22),ta,APfinal(AP_domain,28),ta,...

APfinal(AP_domain,34),ta,APfinal(AP_domain,40),ta,...
        APfinal(AP_domain,46),ta,APfinal(AP_domain,52));
    xlabel('Day'); ylabel('Sample Intake Flow Rate
(mL/min)');
    title(Flow_title);
```

```
    legend('38 m (L21)','32 m (L18)','27 m (L15)','21 m
(L12)','16 m (L9)',...
        '10 m (L6)','5 m (L3)','1 m
(L0)','Location','BestOutside');

    %Plot 12: VPD
    figure()

plot(ta,VPDfinal(AP_domain,1),ta,VPDfinal(AP_domain,2),ta,.
..
        VPDfinal(AP_domain,4),ta,...

VPDfinal(AP_domain,5),ta,VPDfinal(AP_domain,6),ta,...
        VPDfinal(AP_domain,7),ta,VPDfinal(AP_domain,8));
    xlabel('Day'); ylabel('VPD (kPa)');
    title(VPD_title);
    legend('38 m (L21)','32 m (L18)','21 m (L12)','16 m
(L9)',...
        '10 m (L6)','5 m (L3)','1 m
(L0)','Location','BestOutside');
    axis([0 7 0 2]);

    %Plot 13: Soil Heat Flux
    figure()

plot(tg,GDfinal(GD_domain,35),tg,GDfinal(GD_domain,36),tg,.
..

GDfinal(GD_domain,37),tg,GDfinal(GD_domain,38),tg,...
        GDfinal(GD_domain,39),tg,GDfinal(GD_domain,40));
    xlabel('Day'); ylabel('Soil Heat Flux (W/m^2)');
    title(G_title);
    legend('Site A','Site B','Site C','Site D','Site
E','Site F (profile)',...
        'Location','BestOutside');
    axis([0 7 -8 8]);

    %Plot 14: Soil Water Potential
    figure()

plot(tsl,Soilfinal(Soil_domain,5),tsl,Soilfinal(Soil_domain
,6),tsl,...
        Soilfinal(Soil_domain,7));
    xlabel('Day'); ylabel('Soil Water Potential (-kPa)');
```

```
    title(SWP_title);
    legend('25 mm','15 cm','25
cm','Location','BestOutside');
    axis([0 7 27 37]);

    %Plot 15: VWC time series
    figure()
    plot(tg,GDfinal(GD_domain,16),tg,...

GDfinal(GD_domain,17),tg,GDfinal(GD_domain,18),tg,...

GDfinal(GD_domain,19),tg,GDfinal(GD_domain,20),tg,...

GDfinal(GD_domain,21),tg,GDfinal(GD_domain,22),tg,...
        GDfinal(GD_domain,23),tg,GDfinal(GD_domain,24));
    xlabel('Day'); ylabel('Volumetric Water Content
(m^3/m^3)');
    title(VWC_title);
    legend('Profile - 9 cm','Profile - 16 cm',...
        'Profile - 23 cm','Profile - 30 cm','Site A','Site
B',...
        'Site C','Site D','Site
E','Location','BestOutside');

    %Plot 16: Soil temp time series
    figure()

plot(tg,GDfinal(GD_domain,5),tg,GDfinal(GD_domain,6),tg,...
        GDfinal(GD_domain,7),tg,GDfinal(GD_domain,8),tg,...

GDfinal(GD_domain,9),tg,GDfinal(GD_domain,10),tg,...

GDfinal(GD_domain,11),tg,GDfinal(GD_domain,12),tg,...
        GDfinal(GD_domain,13),tg,GDfinal(GD_domain,14));
    xlabel('Day'); ylabel('Soil Temperature (deg C)');
    title(soiltemp_title);
    legend('Profile - 2 cm','Profile - 9 cm','Profile - 16
cm',...
        'Profile - 23 cm','Profile - 30 cm','Site A','Site
B',...
        'Site C','Site D','Site
E','Location','BestOutside');

    %Plot 17: Soil temp profile
```

```
    figure()

plot(ST_Night_Profile,Soil_Depths,ST_Day_Profile,Soil_Depth
s);
    set(gca,'YDir','reverse');
    xlabel('Soil Temperature (deg C)'); ylabel('Depth in
Soil (cm)');
    title(ST_Prof_title);
    legend('Night','Day','Location','Best');

    %Plot 18: VWC profile
    figure()

plot(VWC_Night_Profile,Soil_Depths(2:5),VWC_Day_Profile,...
        Soil_Depths(2:5));
    set(gca,'YDir','reverse');
    xlabel('Volumetric Water Content (m^3/m^3)');
ylabel('Depth in Soil (cm)');
    title(VWC_Prof_title);
    legend('Night','Day','Location','Best');

    %Plot 19: CO2 Profile
    figure()

plot(CO2_Night_Profile,CO2_Height,CO2_Day_Profile,CO2_Heigh
t);
    xlabel('CO2 Concentration (ppm)'); ylabel('Canopy
Height (m)');
    title(CO2_Prof_title);
    legend('Night','Day','Location','Best');

    %Plot 20: H2O Profile
    figure()

plot(H2O_Night_Profile,H2O_Height,H2O_Day_Profile,H2O_Heigh
t);
    xlabel('H2O Concentration (ppm)'); ylabel('Canopy
Height (m)');
    title(H2O_Prof_title);
    legend('Night','Day','Location','Best');

    %Plot 21: Temp Profile
    figure()
```

```
plot(Temp_Night_Profile,Temp_Height,Temp_Day_Profile,Temp_H
eight);
    xlabel('Air Temperature (deg C)'); ylabel('Canopy
Height (m)');
    title(Temp_Prof_title);
    legend('Night','Day','Location','Best');

    %Plot 22: PAR Profile
    figure()

plot(PAR_Night_Profile,PAR_Height,PAR_Day_Profile,PAR_Heigh
t);
    xlabel('PAR (umol/m^2/sec)'); ylabel('Canopy Height
(m)');
    title(PAR_Prof_title);
    legend('Night','Day','Location','Best');

    %Plot 23: LW pct Profile
    figure()

plot(LW_Night_Profile_pct,LW_Height,LW_Day_Profile_pct,LW_H
eight,...
        LW_Wet_Profile,LW_Height,LW_Dry_Profile,LW_Height);
    xlabel('Percent Wetness'); ylabel('Canopy Height (m)');
    title(LW_Prof_title);

legend('Night','Day','Wet','Dry','Location','BestOutside');

    %Plot 24: VPD Profile
    figure()

plot(VPD_Night_Profile,VPD_Height,VPD_Day_Profile,VPD_Heigh
t);
    xlabel('VPD (kPa)'); ylabel('Canopy Height (m)');
    title(VPD_Prof_title);
    legend('Night','Day','Location','Best');

elseif bad_data_plot==1
    close all
    %Plot 1: Net Radiation
    figure()
```

```
WDfinal(:,size(WDfinal,2)+1)=WDfinal(:,27)+WDfinal(:,29)-
WDfinal(:,...
        28)-WDfinal(:,30); % Calc. net rad from components

plot(tw,WDfinal(WD_domain,12),ts,spirefinal(spire_domain,10
),tu,...

UDfinal(UD_domain,9),tw,WDfinal(WD_domain,size(WDfinal,2)))
    xlabel('Day'); ylabel('Net Radiation (W/m^2)');
    title(nrad_title);
    legend('Met Solar Rad','Spire','34 m (L19)','Met
CNR1','Location',...
        'BestOutside');

    %Plot 2: LW as a percentage
    figure()

plot(tg,LW_percent(GD_domain,1),tg,LW_percent(GD_domain,2),
tu,...

LW_percent(UD_domain,3),tu,LW_percent(UD_domain,4),tu,...
        LW_percent(UD_domain,5));
    xlabel('Day'); ylabel('Percent Wetness');
    title(LW_title);
    legend('3 m (L2)','11 m (L6)','22 m (L12)','33 m
(L18)', '38 m (L21)',...
        'Location','BestOutside');

    %Plot 3: Leaf Wetness
    figure()

plot(tg,GDfinal(GD_domain,42),tg,GDfinal(GD_domain,43),tu,.
..

UDfinal(UD_domain,18),tu,UDfinal(UD_domain,19),tu,...
        UDfinal(UD_domain,20));
    xlabel('Day'); ylabel('Wetness Index (mV)');
    title(LW_title);
    legend('3 m (L2)','11 m (L6)','22 m (L12)','33 m
(L18)', '38 m (L21)',...
        'Location','BestOutside');

    %Plot 4: PAR
```

```
    figure()

plot(tg,GDfinal(GD_domain,41),tu,UDfinal(UD_domain,17),tu,...

UDfinal(UD_domain,16),tu,UDfinal(UD_domain,15),tu,...
        UDfinal(UD_domain,14));
    xlabel('Day'); ylabel('PAR (umol/m^2/sec)');
    title(PAR_title);
    legend('10 m (L6)','21 m (L12)','27 m (L15)','32 m
(L18)','38 m (L21)',...
        'Location','BestOutside');

    %Plot 5: Air Temperature
    figure()

plot(tw,WDfinal(WD_domain,6),tw,WDfinal(WD_domain,4),...

tu,UDfinal(UD_domain,10),tu,UDfinal(UD_domain,11),tu,...

UDfinal(UD_domain,12),tu,UDfinal(UD_domain,13),ta,...

APfinal(AP_domain,68),ta,APfinal(AP_domain,69),ta,...
        APfinal(AP_domain,70),ta,APfinal(AP_domain,71));
    xlabel('Day'); ylabel('Air Temperature (deg C)');
    title(AT_title);
    legend('Met 30','Met 10','38 m (L21)','33 m (L18)','27
m (L15)',...
        '21 m (L12)','16 m (L9)','11 m (L6)','5 m (L3)','1
m (L0)',...
        'Location','BestOutside');

    %Plot 6: CO2 Concentration
    figure()

plot(ta,APfinal(AP_domain,6),ta,APfinal(AP_domain,12),ta,...

APfinal(AP_domain,18),ta,APfinal(AP_domain,24),ta,...

APfinal(AP_domain,30),ta,APfinal(AP_domain,36),ta,...
        APfinal(AP_domain,42),ta,APfinal(AP_domain,48));
    xlabel('Day'); ylabel('Carbon Dioxide Concentration
(ppm)');
```

```
    title(CO2_title);
    legend('38 m (L21)','32 m (L18)','27 m (L15)','21 m
(L12)','16 m (L9)',...
        '10 m (L6)','5 m (L3)','1 m
(L0)','Location','BestOutside');

    %Plot 7: H2O Concentration
    figure()

plot(ta,APfinal(AP_domain,7),ta,APfinal(AP_domain,13),ta,..
.

APfinal(AP_domain,19),ta,APfinal(AP_domain,25),ta,...

APfinal(AP_domain,31),ta,APfinal(AP_domain,37),ta,...
        APfinal(AP_domain,43),ta,APfinal(AP_domain,49));
    xlabel('Day'); ylabel('Water Vapor Concentration
(ppt)');
    title(H2O_title);
    legend('38 m (L21)','32 m (L18)','27 m (L15)','21 m
(L12)','16 m (L9)',...
        '10 m (L6)','5 m (L3)','1 m
(L0)','Location','BestOutside');

    %Plot 8: Sap Flow
    figure()

plot(tsf,SFfinal(SF_domain,5),tsf,SFfinal(SF_domain,6),...

tsf,SFfinal(SF_domain,7),tsf,SFfinal(SF_domain,8),...

tsf,SFfinal(SF_domain,9),tsf,SFfinal(SF_domain,10),...
        tsf,SFfinal(SF_domain,11),...

tsf,SFfinal(SF_domain,13),tsf,SFfinal(SF_domain,16),...

tsf,SFfinal(SF_domain,17),tsf,SFfinal(SF_domain,18),...

tsf,SFfinal(SF_domain,19),tsf,SFfinal(SF_domain,20),...

tsf,SFfinal(SF_domain,21),tsf,SFfinal(SF_domain,22),...

tsf,SFfinal(SF_domain,23),tsf,SFfinal(SF_domain,24),...
        tsf,SFfinal(SF_domain,38),...
```

```
tsf,SFfinal(SF_domain,39),tsf,SFfinal(SF_domain,40),...

tsf,SFfinal(SF_domain,41),tsf,SFfinal(SF_domain,42),...

tsf,SFfinal(SF_domain,43),tsf,SFfinal(SF_domain,44),...

tsf,SFfinal(SF_domain,45),tsf,SFfinal(SF_domain,46),...

tsf,SFfinal(SF_domain,48),tsf,SFfinal(SF_domain,49),...
        tsf,SFfinal(SF_domain,50));
    xlabel('Day'); ylabel('mV');
    title(SF_title);
    legend('1','2','3','4','5','6','7','9',...
        '12','13','14','15','16','17','18','19','20',...

'34','35','36','37','38','39','40','41','42','44','45','46'
,...
        'Location','BestOutside');

    %Plot 9: Precipitation
    figure()
    plot(tw,WDfinal(WD_domain,14));
    xlabel('Day'); ylabel('Precipitation (in.)');
    title(Precip_title);

    %Plot 10: IRTs
    figure()

plot(ts,spirefinal(spire_domain,13),ts,spirefinal(spire_dom
ain,15),...

ts,spirefinal(spire_domain,17),ts,spirefinal(spire_domain,1
9));
    xlabel('Day'); ylabel('Leaf Temperature (deg C)');
    title(irt_title);
    legend('IRT 1 (N)','IRT 2 (E)','IRT 3 (S)','IRT 4
(W)');

    %Plot 11: Flowrates
    figure()

plot(ta,APfinal(AP_domain,10),ta,APfinal(AP_domain,16),ta,.
..
```

```
APfinal(AP_domain,22),ta,APfinal(AP_domain,28),ta,...

APfinal(AP_domain,34),ta,APfinal(AP_domain,40),ta,...
        APfinal(AP_domain,46),ta,APfinal(AP_domain,52));
    xlabel('Day'); ylabel('Sample Intake Flow Rate
(mL/min)');
    title(Flow_title);
    legend('38 m (L21)','32 m (L18)','27 m (L15)','21 m
(L12)','16 m (L9)',...
        '10 m (L6)','5 m (L3)','1 m
(L0)','Location','BestOutside');

    %Plot 12: VPD
    figure()

plot(ta,VPDfinal(AP_domain,1),ta,VPDfinal(AP_domain,2),ta,.
..

VPDfinal(AP_domain,3),ta,VPDfinal(AP_domain,4),ta,...

VPDfinal(AP_domain,5),ta,VPDfinal(AP_domain,6),ta,...
        VPDfinal(AP_domain,7),ta,VPDfinal(AP_domain,8));
    xlabel('Day'); ylabel('VPD (kPa)');
    title(VPD_title);
    legend('38 m (L21)','32 m (L18)','27 m (L15)','21 m
(L12)','16 m (L9)',...
        '10 m (L6)','5 m (L3)','1 m
(L0)','Location','BestOutside');

    %Plot 13: Soil Heat Flux
    figure()

plot(tg,GDfinal(GD_domain,35),tg,GDfinal(GD_domain,36),tg,.
..

GDfinal(GD_domain,37),tg,GDfinal(GD_domain,38),tg,...
        GDfinal(GD_domain,39),tg,GDfinal(GD_domain,40));
    xlabel('Day'); ylabel('Soil Heat Flux (W/m^2)');
    title(G_title);
    legend('Site A','Site B','Site C','Site D','Site
E','Site F (profile)',...
        'Location','BestOutside');
```

```
    %Plot 14: Soil Water Potential
    figure()

plot(tsl,Soilfinal(Soil_domain,5),tsl,Soilfinal(Soil_domain
,6),tsl,...
        Soilfinal(Soil_domain,7));
    xlabel('Day'); ylabel('Soil Water Potential (-kPa)');
    title(SWP_title);
    legend('25 mm','15 cm','25
cm','Location','BestOutside');

    %Plot 15: VWC time series
    figure()

plot(tg,GDfinal(GD_domain,15),tg,GDfinal(GD_domain,16),tg,.
..

GDfinal(GD_domain,17),tg,GDfinal(GD_domain,18),tg,...

GDfinal(GD_domain,19),tg,GDfinal(GD_domain,20),tg,...

GDfinal(GD_domain,21),tg,GDfinal(GD_domain,22),tg,...
        GDfinal(GD_domain,23),tg,GDfinal(GD_domain,24));
    xlabel('Day'); ylabel('Volumetric Water Content
(m^3/m^3)');
    title(VWC_title);
    legend('Profile - 2 cm','Profile - 9 cm','Profile - 16
cm',...
        'Profile - 23 cm','Profile - 30 cm','Site A','Site
B',...
        'Site C','Site D','Site
E','Location','BestOutside');

    %Plot 16: Soil temp time series
    figure()

plot(tg,GDfinal(GD_domain,5),tg,GDfinal(GD_domain,6),tg,...
        GDfinal(GD_domain,7),tg,GDfinal(GD_domain,8),tg,...

GDfinal(GD_domain,9),tg,GDfinal(GD_domain,10),tg,...

GDfinal(GD_domain,11),tg,GDfinal(GD_domain,12),tg,...
        GDfinal(GD_domain,13),tg,GDfinal(GD_domain,14));
    xlabel('Day'); ylabel('Soil Temperature (deg C)');
```

```
    title(soiltemp_title);
    legend('Profile - 2 cm','Profile - 9 cm','Profile - 16
cm',...
        'Profile - 23 cm','Profile - 30 cm','Site A','Site
B',...
        'Site C','Site D','Site
E','Location','BestOutside');

    % Add all variables back into profiles
    Temp_Height=[38.4;32.8;27.3;21.7;16.4;10.7;5.4;1.4];
    VPD_Height=CO2_Height;
    PAR_Height=[37.6;32;26.5;21;10.1];


Temp_Night_Profile=[nanmean(Temp_Night1(:,1));nanmean(Temp_
Night1(:,...

2));nanmean(Temp_Night1(:,3));nanmean(Temp_Night1(:,...

4));nanmean(Temp_Night2(:,1));nanmean(Temp_Night2(:,...

2));nanmean(Temp_Night2(:,3));nanmean(Temp_Night2(:,4))];

Temp_Day_Profile=[nanmean(Temp_Day1(:,1));nanmean(Temp_Day1
(:,...
        2));nanmean(Temp_Day1(:,3));nanmean(Temp_Day1(:,...
        4));nanmean(Temp_Day2(:,1));nanmean(Temp_Day2(:,...

2));nanmean(Temp_Day2(:,3));nanmean(Temp_Day2(:,4))];

VPD_Night_Profile=[nanmean(VPD_Night(:,1));nanmean(VPD_Nigh
t(:,...
        2));nanmean(VPD_Night(:,3));nanmean(VPD_Night(:,...
        4));nanmean(VPD_Night(:,5));nanmean(VPD_Night(:,...

6));nanmean(VPD_Night(:,7));nanmean(VPD_Night(:,8))];

VPD_Day_Profile=[nanmean(VPD_Day(:,1));nanmean(VPD_Day(:,..
.

2));nanmean(VPD_Day(:,3));nanmean(VPD_Day(:,4));nanmean(VPD
_Day(:,...
```

```
5));nanmean(VPD_Day(:,6));nanmean(VPD_Day(:,7));nanmean(VPD
_Day(:,...
        8))];

ST_Night_Profile=[nanmean(ST_Night(:,1));nanmean(ST_Night(:
,...
        2));nanmean(ST_Night(:,3));nanmean(ST_Night(:,...
        4));nanmean(ST_Night(:,5))];

ST_Day_Profile=[nanmean(ST_Day(:,1));nanmean(ST_Day(:,...
        2));nanmean(ST_Day(:,3));nanmean(ST_Day(:,...
        4));nanmean(ST_Day(:,5))];

VWC_Night_Profile=[nanmean(VWC_Night(:,1));nanmean(VWC_Nigh
t(:,...
        2));nanmean(VWC_Night(:,3));nanmean(VWC_Night(:,...
        4));nanmean(VWC_Night(:,5))];

VWC_Day_Profile=[nanmean(VWC_Day(:,1));nanmean(VWC_Day(:,..
.
        2));nanmean(VWC_Day(:,3));nanmean(VWC_Day(:,...
        4));nanmean(VWC_Day(:,5))];

PAR_Night_Profile=[nanmean(PAR_Night1(:,1));nanmean(PAR_Nig
ht1(:,...

2));nanmean(PAR_Night1(:,3));nanmean(PAR_Night1(:,4));...
        nanmean(PAR_Night2(:,1))];

PAR_Day_Profile=[nanmean(PAR_Day1(:,1));nanmean(PAR_Day1(:,
...

2));nanmean(PAR_Day1(:,3));nanmean(PAR_Day1(:,4));...
        nanmean(PAR_Day2(:,1))];

    %Plot 17: Soil temp profile
    figure()

plot(ST_Night_Profile,Soil_Depths,ST_Day_Profile,Soil_Depth
s);
    set(gca,'YDir','reverse');
    xlabel('Soil Temperature (deg C)'); ylabel('Depth in
Soil (cm)');
```

```
    title(ST_Prof_title);
    legend('Night','Day','Location','Best');

    %Plot 18: VWC profile
    figure()

plot(VWC_Night_Profile,Soil_Depths,VWC_Day_Profile,Soil_Dep
ths);
    set(gca,'YDir','reverse');
    xlabel('Volumetric Water Content (m^3/m^3)');
ylabel('Depth in Soil (cm)');
    title(VWC_Prof_title);
    legend('Night','Day','Location','Best');

    %Plot 19: CO2 Profile
    figure()

plot(CO2_Night_Profile,CO2_Height,CO2_Day_Profile,CO2_Heigh
t);
    xlabel('CO2 Concentration (ppm)'); ylabel('Canopy
Height (m)');
    title(CO2_Prof_title);
    legend('Night','Day','Location','Best');

    %Plot 20: H2O Profile
    figure()

plot(H2O_Night_Profile,H2O_Height,H2O_Day_Profile,H2O_Heigh
t);
    xlabel('H2O Concentration (ppm)'); ylabel('Canopy
Height (m)');
    title(H2O_Prof_title);
    legend('Night','Day','Location','Best');

    %Plot 21: Temp Profile
    figure()

plot(Temp_Night_Profile,Temp_Height,Temp_Day_Profile,Temp_H
eight);
    xlabel('Air Temperature (deg C)'); ylabel('Canopy
Height (m)');
    title(Temp_Prof_title);
    legend('Night','Day','Location','Best');
```

```
    %Plot 22: PAR Profile
    figure()

plot(PAR_Night_Profile,PAR_Height,PAR_Day_Profile,PAR_Heigh
t);
    xlabel('PAR (umol/m^2/sec)'); ylabel('Canopy Height
(m)');
    title(PAR_Prof_title);
    legend('Night','Day','Location','Best');

    %Plot 23: LW pct Profile
    figure()

plot(LW_Night_Profile_pct,LW_Height,LW_Day_Profile_pct,LW_H
eight,...
        LW_Wet_Profile,LW_Height,LW_Dry_Profile,LW_Height);
    xlabel('Percent Wetness'); ylabel('Canopy Height (m)');
    title(LW_Prof_title);

legend('Night','Day','Wet','Dry','Location','BestOutside');

    %Plot 24: VPD Profile
    figure()

plot(VPD_Night_Profile,VPD_Height,VPD_Day_Profile,VPD_Heigh
t);
    xlabel('VPD (kPa)'); ylabel('Canopy Height (m)');
    title(VPD_Prof_title);
    legend('Night','Day','Location','Best');
end
```